Mathematical Studies on ECM Degradation and Angiogenesis

DHISA MINERVA

SEPTEMBER 2016

Mathematical Studies on ECM Degradation and Angiogenesis

A dissertation submitted to
THE GRADUATE SCHOOL OF ENGINEERING SCIENCE
OSAKA UNIVERSITY
In partial fulfillment of the requirements for the degree of
DOCTOR OF PHILOSOPHY IN SCIENCE

BY

DHISA MINERVA

SEPTEMBER 2016

Abstract

The work presented here is separated into two topics. The first involves the application of a mathematical method for solving a system of nonlinear ordinary differential equations (ODEs) relating to kinetic reaction systems on extracellular matrix degradation associated with cancer invasion. This method is based on the concept of grouping kinetic reactions based on reaction rate constants. The mass conservation law is used to obtain relationships on dependent variables that are involved in these kinetic reactions. Because these relationships are valid at all times during a reaction, they can be used to solve the ODEs explicitly. This method has been successfully applied to kinetic reaction systems on extracellular matrix degradation. The system consists of 12 ODEs that are generated by kinetic reactions of three basic molecules with specific binding rules. Using the presented model, we showed that the difference between initial concentrations of connected molecules controls the behavior of group solutions. The second topic involves a study on the pattern formation of blood vessel networks in angiogenesis. Angiogenesis is a process by which new blood vessels form. The formation of blood vessel networks is driven by chemotactic and haptotactic responses to environmental gradients of vascular endothelial growth factor (VEGF) and fibronectin, respectively. In the absence of haptotaxis, the sprouts grow directly toward the source of the tumor with little lateral movement. By incorporating both chemotaxis and haptotaxis, some of the sprouts grow backward to the parent vessel upon reaching a certain distance from it, so that their growth toward the source of the tumor progresses slowly. This means that the growth of blood vessel networks in tumor angiogenesis is mostly driven by chemotactic responses to the VEGF gradient. The hybrid discrete-continuous technique is used to simulate vessel network formation by tracking the movement of tip cells in response to the environmental gradient.

Table of Contents

CHAPTER 1

INTEGRABILITY OF KINETIC REACTION SYSTEMS REPRESENTING THE EXTRACELULLAR MATRIX DEGRADATION ASSOCIATED WITH CANCER INVASION

In the field of molecular biology, we often deal with molecules that are involved in several molecular biological events. Mathematical equations are often used to model biological networks of kinetic reactions. As the system increases in size, it becomes difficult to solve and analyze them explicitly. Numerical methods are currently the most powerful tools to solve large systems, but specific information such as the monotonicity of solution and important parameter that regulates the network are not certain. In this chapter, we propose a mathematical method to model and analyze kinetic reaction systems using a grouping system and the mass conservation laws. This method enables us to obtain an explicit solution to ordinary differential equations (ODEs) system, which clarifies important parameters that influence the behavior of solutions. To demonstrate this method, we use kinetic reaction systems representing the extracellular matrix (ECM) degradation associated with cancer invasion as an example.

Introduction

The study described in this chapter helps us to understand large systems of kinetic reactions. Kinetic reactions involve a change in concentration due to the consumption and production of components in a system. This can be translated into mathematical equations by using the law of mass action, which results in a system of first-order

nonlinear ODEs. In most cases, such systems are difficult to solve explicitly, thus they are often studied by using numerical simulations.

To overcome this problem, we propose the idea of grouping kinetic reactions based on reaction rate constants. This grouping is performed along the mass conservation laws, meaning that the local balancing relationships of inflow and outflow of relevant variables are determined. Moreover, these relationships can be used to solve the ODE system.

In the next section, we describe the mathematical modeling of an elementary kinetic reaction system and use the mass conservation laws to obtain the explicit solution. The approach in this elementary process is then used to model kinetic reaction systems representing ECM degradation in the next section. The main topic discussed in this section is the mathematical approach to solving the ODE system. Simulation results are also presented. The chapter ends with some concluding remarks.

The Mathematical Expressions of Elementary Kinetic Reaction Systems

In kinetic reactions, many types of reaction involve in a system. They can be reaction between molecules, molecules and complexes, or between complexes. We assume all reactions that is presented in this chapter has repetition of association and dissociation constant with the relevant elementary molecular reaction. Also, we assume the system is closed, meaning that the system is conserved. Below is the mathematical modeling of some elementary kinetic reaction processes. The explicit solution is also presented on each elementary processes.

1.A Reaction of two different molecules, A and B.

Consider the following reaction:

$$A + B \rightleftharpoons AB, \tag{1}$$

with association constant rate k and disassociation constant rate l. The mass action laws for these reaction are

$$\frac{d[A]}{dt} = -k[A][B] + l[AB], \tag{2}$$

$$\frac{d[B]}{dt} = -k[A][B] + l[AB], \tag{3}$$

$$\frac{d[AB]}{dt} = k[A][B] - l[AB], \tag{4}$$

where $[\cdot]$ denotes the concentration. And the mass conservation laws are

$$\frac{d}{dt}([A] + [AB]) = \frac{d}{dt}([B] + [AB]) = 0. \tag{5}$$

Equation (5) shows that the total concentration of molecule A and AB or B and AB remains constant. Moreover,

$$[A](t) + [AB](t) = I_A, \tag{6}$$

$$[B](t) + [AB](t) = I_B, \tag{7}$$

where $0 \leq I_A = [A](0) + [AB](0)$ and $0 \leq I_B = [B](0) + [AB](0)$ denote as total initial concentration of $[A] + [AB]$ and $[B] + [AB]$. Then, using relations (6) and (7), we can rewrite equation (2) as

$$\begin{aligned}\frac{d[A]}{dt} &= -k[A]\big(I_B - (I_A - [A])\big) + l(I_A - [A]) \\ &= -\big\{k[A]^2 - \big(-l + k(I_A - I_B)\big)[A] - lI_A\big\} \\ &= -k([A] - z_1)([A] - z_2), \end{aligned} \tag{8}$$

with

$$z_1, z_2 = \frac{-l + k(I_A - I_B) \pm \sqrt{\left(-l + k(I_A - I_B)\right)^2 + 4klI_A}}{2k}. \tag{9}$$

If the discriminant of (9) is not zero, which can be satisfied if $l \neq 0$ and $I_A - I_B = 0$, we have two equilibrium points, z_1 and z_2. If $z_1 \neq z_2$,

$$\frac{1}{(z_1 - z_2)}\left(\frac{1}{[A] - z_1} - \frac{1}{[A] - z_2}\right)\frac{d[A]}{dt} = -k$$

$$\left(\frac{1}{[A] - z_1} - \frac{1}{[A] - z_2}\right)d[A] = -k(z_1 - z_2)dt$$

$$\ln\frac{[A] - z_1}{[A] - z_2} = -k(z_1 - z_2)t + S$$

$$\frac{[A] - z_1}{[A] - z_2} = Ce^{-k(z_1 - z_2)t}. \tag{10}$$

Hence, the explicit solution of $[A](t)$ is

$$[A](t) = \frac{z_1 - Cz_2e^{-k(z_1 - z_2)t}}{1 - Ce^{-k(z_1 - z_2)t}}$$

$$= \frac{z_1 - z_2 + z_2 - Cz_2e^{-k(z_1 - z_2)t}}{1 - Ce^{-k(z_1 - z_2)t}}$$

$$= \frac{z_1 - z_2 + z_2\left(1 - Ce^{-k(z_1 - z_2)t}\right)}{1 - Ce^{-k(z_1 - z_2)t}}$$

$$= \frac{z_1 - z_2}{1 - Ce^{-k(z_1 - z_2)t}} + z_2, \tag{11}$$

where

$$C = \frac{[A]_0 - z_1}{[A]_0 - z_2}, \tag{12}$$

for $t \geq 0$.

Solution of $[B]$ and $[AB]$ can be obtained using (6) and (7), respectively. That is

$$[B](t) = I_B - I_A + z_2 + \frac{z_1 - z_2}{1 - Ce^{-k(z_1 - z_2)t}}, \tag{13}$$

$$[AB](t) = I_A - z_2 - \frac{z_1 - z_2}{1 - Ce^{-k(z_1 - z_2)t}}. \tag{14}$$

Now, we observe (9). Since

$$\begin{aligned}\left(-l + k(I_A - I_B)\right)^2 + 4klI_A &= l^2 + k^2(I_A - I_B)^2 + 2kl(I_A + I_B) \\ &\geq l^2 + k^2(I_A - I_B)^2 + 2kl(I_A + I_B - 2I_A) \\ &= l^2 + k^2(I_A - I_B)^2 - 2kl(I_A - I_B) \\ &= \left(-l + k(I_A - I_B)\right)^2, \end{aligned} \tag{15}$$

then (9) satisfies $z_1 > 0 > z_2$. Moreover,

$$\begin{aligned} z_1 &= \frac{-l + k(I_A - I_B) + \sqrt{\left(-l + k(I_A - I_B)\right)^2 + 4klI_A}}{2k} \\ &= \frac{-l + k(I_B - I_A) + \sqrt{\left(-l + k(I_A - I_B)\right)^2 + 4klI_A} + 2k(I_A - I_B)}{2k} \\ &\geq \frac{2k(I_A - I_B)}{2k} \\ &= (I_A - I_B). \end{aligned} \tag{16}$$

From the solution of $[A](t)$ in (11), we take the first derivative:

$$\frac{d[A]}{dt} = \frac{-\left(-C\left(-k(z_1 - z_2)\right)e^{-k(z_1 - z_2)t}\right)(z_1 - z_2)}{(1 - Ce^{-k(z_1 - z_2)t})^2} \tag{17}$$

$$= \frac{-Ck(z_1 - z_2)^2 e^{-k(z_1 - z_2)t}}{(1 - Ce^{-k(z_1 - z_2)t})^2}.$$

The sign of right hand side of (17) depends on the sign of C. Since $[A]_0 - z_2 > 0$, the sign of $[A]_0 - z_1$ would determine the sign of right hand side in (17). It is obvious that if $[A]_0 = 0$, $[A]_0 - z_1 < 0$. For $[A]_0 > 0$, we take $[A]_0 - z_1$ as follow:

$$[A]_0 - z_1 = [A]_0 - \frac{-l + k(I_A - I_B) + \sqrt{\left(-l + k(I_A - I_B)\right)^2 + 4klI_A}}{2k}$$

$$= [A]_0 - \frac{-l + k([A]_0 - [B]_0)}{2k}$$

$$- \frac{\sqrt{\left(-l + k([A]_0 - [B]_0)\right)^2 + 4kl([A]_0 + [AB]_0)}}{2k}$$

$$= \frac{l + k([A]_0 + [B]_0)}{2k}$$

$$- \frac{\sqrt{\left(-l + k([A]_0 - [B]_0)\right)^2 + 4kl([A]_0 + [AB]_0)}}{2k}. \qquad (18)$$

From (18), we find that if $[B]_0 = 0$, $[A]_0 - z_1 < 0$. Moreover, $[A]_0 = [B]_0 = 0$ implies $[A]_0 - z_1 \leq 0$. Consider if the case is $[A]_0 \neq 0$, $[B]_0 \neq 0$. To take care of (18), firstly we look at the inside of the root. Let $P = \left(-l + k([A]_0 - [B]_0)\right)^2 + 4kl([A]_0 + [AB]_0)$.

$$P = l^2 + k^2\left([A]_0{}^2 + [B]_0{}^2 - 2[A]_0[B]_0\right) + 2kl([A]_0 + [B]_0)$$

$$+4kl[AB]_0$$

$$= l^2 + k^2\left([A]_0{}^2 + [B]_0{}^2 + \left(\frac{4l[AB]_0}{k} - 2[A]_0[B]_0\right)\right) \qquad (19)$$

$+2kl([A]_0 + [B]_0)$.

Hence, the sign of C depends on the term of $\left(\frac{4l[AB]_0}{k} - 2[A]_0[B]_0\right)$. If

$$\frac{4l[AB]_0}{k} - 2[A]_0[B]_0 < 2[A]_0[B]_0$$

$$\frac{[AB]_0}{[A]_0[B]_0} < \frac{k}{l}, \tag{20}$$

$[A]_0 - z_1 > 0$, meaning that we have negative sign of (17). The inequality (20) can be achieved by taking large initial concentration of A and B and small initial concentration of AB. This condition would promote association reaction of (1), so that the forward reaction would dominate the backward reaction. In fact, $[A](t)$ is monotonically decreasing:

$$[A](0) = [A]_0 \ \searrow \ [A](\infty) = z_1, \tag{21}$$

and is nonnegative. From (13) and (14), we can find that $[B](t)$ and $[AB](t)$ are monotonically decreasing:

$$[B](0) = I_B - I_A + [A]_0 \ \searrow \ [B](\infty) = I_B - I_A + z_1, \tag{22}$$

and increasing:

$$[AB](0) = I_A - [A]_0 \ \nearrow \ [AB](\infty) = I_A - z_1, \tag{23}$$

respectively. Both $[B](t)$ and $[AB](t)$ are nonnegative.

From (19), $[A]_0 - z_1 < 0$ is satisfied if

$$\frac{[AB]_0}{[A]_0[B]_0} > \frac{k}{l}. \tag{24}$$

In contrary to (20), the inequality (24) would promote the dissociation reaction of (1). In fact, $[A](t)$, $[B](t)$ are monotonically increasing:

$$[A](0) = [A]_0 \ \nearrow \ [A](\infty) = z_1, \tag{25}$$

$$[B](0) = \ I_B - I_A + [A]_0 \ \nearrow \ [B](\infty) = I_B - I_A + z_1, \tag{26}$$

and $[AB](t)$ is monotonically decreasing:

$$[AB](0) = \ I_A - [A]_0 \ \searrow \ [AB](\infty) = I_A - z_1. \tag{27}$$

Both $[A](t)$ and $[B](t)$ are obviously nonnegative. Since

$$\begin{aligned}\left(-l + k(I_A - I_B)\right)^2 + 4klI_A &= l^2 + k^2(I_A - I_B)^2 + 2kl(I_A + I_B) \\ &= l^2 + k^2\left({I_A}^2 + {I_B}^2\right) + 2kl(I_A + I_B) \\ &\quad -2k^2 I_A I_B \\ &\leq l^2 + k^2\left({I_A}^2 + {I_B}^2\right) + 2kl(I_A + I_B) \\ &\leq \left(l + k(I_A + I_B)\right)^2. \end{aligned} \tag{28}$$

Hence,

$$\begin{aligned} I_A - z_1 &= I_A - \frac{-l + k(I_A - I_B) + \sqrt{\left(-l + k(I_A - I_B)\right)^2 + 4klI_A}}{2k} \\ &= \frac{l + k(I_A + I_B) - \sqrt{\left(-l + k(I_A - I_B)\right)^2 + 4klI_A}}{2k} \\ &\geq 0, \end{aligned} \tag{29}$$

meaning that $[AB](t)$ is nonnegative.

If the case is

$$\frac{[AB]_0}{[A]_0[B]_0} = k, \tag{30}$$

we have $[A]_0 - z_1 = 0$. This equality means that from the beginning, the reaction reaches the steady state. We can say that no change in concentration of each component in reaction (1) if (30) occurs.

The discriminant of (9) would be zero if $l = 0$ and $I_A - I_B = 0$. This implies (8) can be rewritten as

$$\frac{d[A]}{dt} = -k[A]^2. \tag{31}$$

The solution of (31) is

$$\frac{1}{[A]^2} d[A] = -kdt$$

$$-\frac{1}{[A]} + \frac{1}{[A](0)} = -kt$$

$$[A](t) = \frac{[A](0)}{1 + [A](0)kt}. \tag{32}$$

The solution of $[B](t)$ is

$$[B](t) = I_B - I_A + \frac{[A](0)}{1 + [A](0)kt}, \tag{33}$$

and solution of $[AB](t)$ is

$$[AB](t) = I_A - \frac{[A](0)}{1 + [A](0)kt}, \tag{34}$$

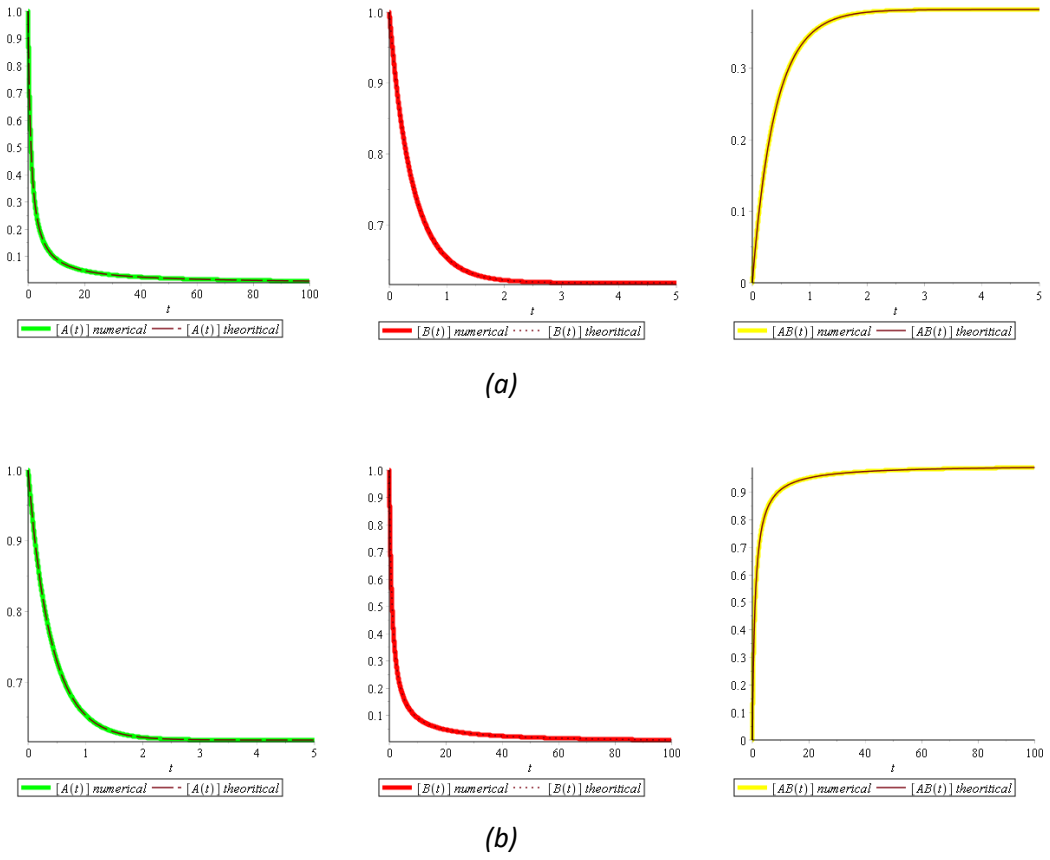

Figure 1. (a) Graph of solution of $[A](t)$, $[B](t)$, $[AB](t)$ with positive discriminant. (b) Graph of solution of $[A](t)$, $[B](t)$, $[AB](t)$ with zero discriminant.

by (6) and (7). Hence, $[A](t)$ now decreases:

$$[A](0) = [A]_0 \;\searrow\; [A](\infty) = 0, \tag{35}$$

with order $O(t^{-1})$, which is slower than in the case if the discriminant of (9) is positive with order $O(e^{-\alpha t})$. Using conservation relations in (6) and (7), we can find that $[B](t)$ is now decreasing:

$$[B](0) = [A]_0 \ \searrow \ [B](\infty) = 0, \tag{36}$$

and $[AB](t)$ is increasing:

$$[AB](0) = \ I_A - [A]_0 \ \nearrow \ [AB](\infty) = I_A, \tag{37}$$

with same order to $[A](t)$, which is $O(t^{-1})$.

Figure 1 shows the solution obtained analytically coincides with the solution obtained numerically for both conditions: positive discriminant and zero discriminant in (9). The graphs also confirm that in comparison to the solution of $[A](t)$ and $[B](t)$ with positive discriminant, the solution with zero discriminant decreases slower.

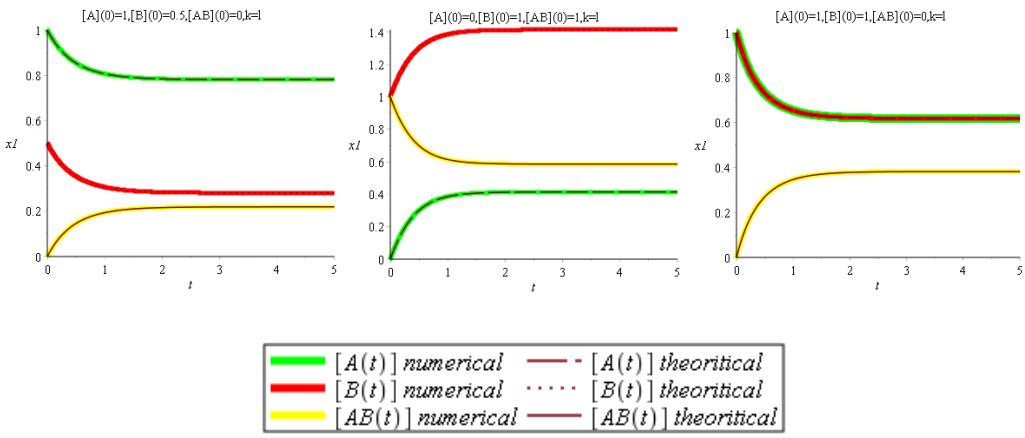

Figure 2. Graph of solutions to reaction system $A + B \rightleftharpoons AB$ obtained numerically and analytically. (left) $[A](0) > z_1$ and $I_B - I_A < 0$. (middle) $[A](0) < z_1$ and $I_B - I_A > 0$. (right) $[A](0) > z_1$ and $I_B - I_A = 0$

From the expression of (9), the initial concentration difference between B and A, $I_B - I_A$ influences the behavior of solution $[A](t)$, $[B](t)$, and $[AB](t)$ and the equilibrium value of $[B](t)$. $I_B - I_A = 0$, $[A](\infty)$ coincides with $[B](\infty)$ at the equilibrium. If $I_B - I_A > 0$, $[B](\infty) > [A](\infty)$. If $I_B - I_A < 0$ $[B](\infty) < [A](\infty)$.

Figure 2 confirms this conclusion and the monotonicity of solutions with two conditions: $[A](0) > z_1$ and $[A](0) < z_1$.

1.B Symmetry reaction.

Let A has two non-identical binding sites. One site can bind to other molecule, let's say B, while the other site can bind to A itself. Consider the following reaction:

$$A + AB \rightharpoonup AAB, \tag{38}$$

with association constant rate k. Free binding site-AB in reaction (38) binds to A with reaction rate $k[A]^2$. However, the following reaction:

$$A + A \rightharpoonup AA, \tag{39}$$

would proceed at $1/2\ k$ rate due to the symmetry of picking reaction pairs. To illustrate this, assume we react certain number of molecules of A, denoted as N_A, in a unit volume. Then, the number of pair collisions between molecules in the system is $\frac{N_A(N_A-1)}{2}$ pairs [Gillespie, 1976]. $\frac{N_A(N_A-1)}{2} \rightarrow \frac{{N_A}^2}{2}$ as $N_A \gg 1$. The half factor explains that reaction (39) occurs at reaction rate $1/2k[A]^2$.

Let the dissociation reaction occurs in (39) with constant rate l. Thus, the mass action laws of reaction (39) are

$$\frac{d[A]}{dt} = -2\left(\frac{1}{2}k[A]^2 + l[AA]\right), \tag{40}$$

$$\frac{d[AA]}{dt} = \frac{1}{2}k[A]^2 - l[AA]. \tag{41}$$

The coefficient 2 on (40) represents the summation of two A's equations. The mass conservation law of reaction (39) is

$$\frac{d}{dt}([A] + 2[AA]) = 0, \tag{42}$$

meaning that

$$[A] + 2[AA] = I_A, \tag{43}$$

where $0 \leq I_A = [A](0) + 2[AA](0)$ as total initial concentration of $[A] + 2[AA]$. Using relation (43), rewrite (40) to

$$\begin{aligned} \frac{d[A]}{dt} &= -\{k[A]^2 + l[A] - lI_A\}. \\ &= -k([A] - m_1)([A] - m_2). \end{aligned} \tag{44}$$

If $m_1 \neq m_2$, we obtain the solution as

$$\begin{aligned} [A](t) &= \frac{m_1 - C_2 m_2 e^{-k(m_1 - m_2)t}}{1 - C_2 e^{-k(m_1 - m_2)t}} \\ &= \frac{m_1 - m_2}{1 - C_2 e^{-k(m_1 - m_2)t}} + m_2 \end{aligned} \tag{45}$$

using similar manner in 1.A, with

$$C_2 = \frac{[A]_0 - m_1}{[A]_0 - m_2}, \tag{46}$$

$$m_1, m_2 = \frac{-l \pm \sqrt{l^2 + 4klI_A}}{k}. \tag{47}$$

Solutions of $[AA](t)$ can be obtained using (43). That is

$$[AA](t) = \frac{1}{2}\left(I_A - m_2 - \frac{m_1 - m_2}{1 - C_2 e^{-k(m_1 - m_2)t}}\right). \quad (48)$$

Since (47) satisfies $m_1 > 0 > m_2$ and the expression of (45) is similar to (11), the same conclusion about positivity, monotonicity and equilibrium values to $[A](t)$ and $[AA](t)$ with reaction in 1.A.

1.C <u>Reaction between complexes with multiplicity.</u>

Suppose that molecule A can bind to molecule B. Then, the following reaction

$$A + BB \rightleftharpoons ABB, \quad (49)$$

would proceed at rate $2k[A][BB]$ and $l[ABB]$ for association and disassociation. This reaction proceeds at double rate because now A has two possibility in choosing where to bind B (Figure 3*:left*). Hence, the mass action laws of reaction (49) are

$$\frac{d[A]}{dt} = -2k[A][BB] + l[ABB], \quad (50)$$

$$\frac{d[B]}{dt} = -2k[A][BB] + l[ABB], \quad (51)$$

$$\frac{d[AB]}{dt} = 2k[A][BB] - l[ABB]. \quad (52)$$

The system (50)-(52) still satisfies (5). Hence, the solution of this system can be obtained in similar manner to (1.A).

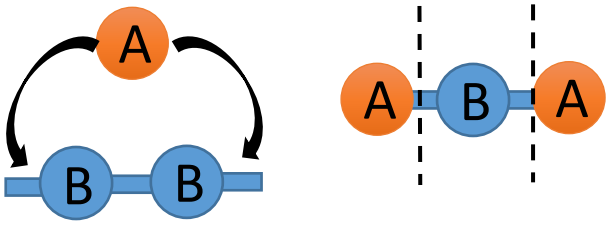

Figure 3. The illustration of attachment and detachment of molecule with two possible choices.

Now, consider the following reaction:

$$A + AB \rightleftharpoons ABA. \tag{53}$$

This reaction now would proceed at rate $k[A][B]$ and $2l[AB]$ for association and disassociation. The double dissociation rate is applied due to two possibility of picking A from detaching A of ABA (Figure 3*:right*). Hence, the mass action laws of reaction (53) are

$$\frac{d[A]}{dt} = -k[A][AB] + 2l[ABA], \tag{54}$$

$$\frac{d[AB]}{dt} = -k[A][AB] + 2l[ABA], \tag{55}$$

$$\frac{d[ABA]}{dt} = k[A][AB] - 2l[ABA]. \tag{56}$$

The system (54)-(56) still satisfies (5). Hence, the solution of this system can be obtained in similar manner to (1.A).

The concept for solving a system of ODEs of elementary kinetic reactions above is using total mass conservation for each molecules. That conservation relations were able to replace the ODE so that the system can be solved analytically.

In the next section, we extend the use of concept to the kinetic reaction systems on ECM degradation associated with cancer invasion. The system involves interaction between three molecules with specific binding rules. Besides mass conservation laws, we use grouping system which is based on kinetic reaction rate.

The Application to The Kinetic Reaction Systems on The ECM Degradation Associated with Cancer Invasion

MT1-MMP, membrane type-matrix metalloproteinase, is believed to play as important molecule in the cancer metastasis, especially in the ECM degradation. MT1-MMP is found highly express on the membrane of small protrusion of cancer cell called invadopodia. Invadopodia helps cancer cell to degrade extracellular matrix. In the beginning process of extracellular matrix degradation, there are several kinetic reactions from interactions between three molecules, MT1-MMP, TIMP2, and MMP2. TIMP2 and MMP2 exist on the extracellular matrix (ECM). Their interaction results in MMP2 activation that leads to the ECM degradation. After that, MT1-MMP begins to degrade the interstitium beyond the ECM.

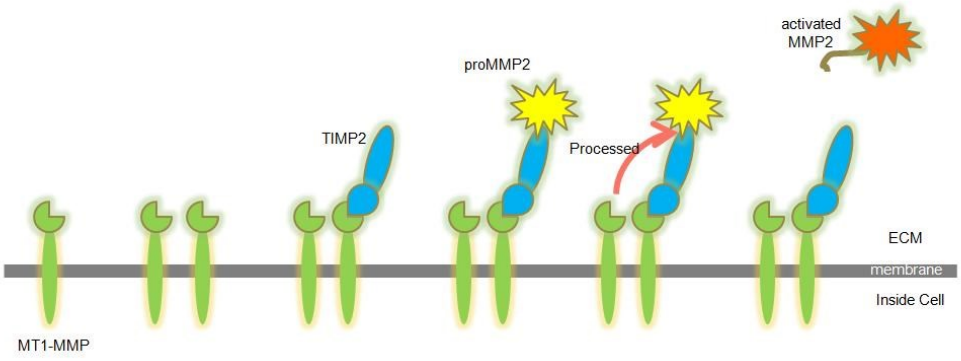

Figure 4. The illustration of MMP2 activation by free TIMP2-MT1-MMP

From that process, we see that the study of MMP2 activation is important for anti-cancer drug development. For simplification, we denote MT1-MMP, TIMP2, and MMP2 as c, b, and a, respectively.

Sato et al. has revealed the mechanism in the MMP2 activation. Below is the scenario (Figure 4):

1. The c penetrates the cell membrane. Once c is on the membrane, c will form the homodimer, cc.
2. The a is associated with cc via b by coupling one site of -cc- with heterodimer ab- or a- with heterotrimer –bcc to produce complex $abcc$.
3. The free site- c process the binding ab by cutting the connection between a and b.
4. The cutted-a is being released and then becomes an activated a.

From this mechanism, we see that the interaction of the three molecules a, b, and c is the key to the MMP2 activation that leads to the ECM degradation. The following binding patterns:

1. c has two non-identical binding sites for b and c itself,
2. b has two non-identical binding sites for a and c,
3. a has one binding sites for b,

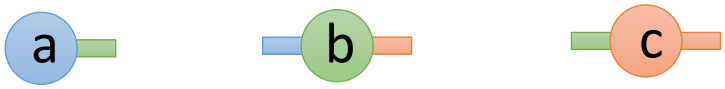

The same color on binding site of a molecule to other molecule indicates one binding pattern. (left) a has one binding site for b. (middle) b has non-identical binding site for a and c. (right) c has non-identical binding site for b and c itself.

Figure 5. The illustration of binding sites of molecule a, b, *and* c

will be assumed in the interaction of molecules a, b, and c (Figure 5). We assume there is no other binding pattern although there is no evidence to ignore other possibility of binding rules.

Using these three binding rules, we can generate nine complexes from monomers a, b, and c as written in the following table:

Table 1

Monomer	a	b	c
Dimer	ab	bc	cc
Trimer	abc	bcc	
Tetramer	$abcc$	$bccb$	
Pentamer	$abccb$		
Hexamer	$abccba$		

The pathway network of kinetic reactions between these twelve complexes are shown in *Figure 6*.

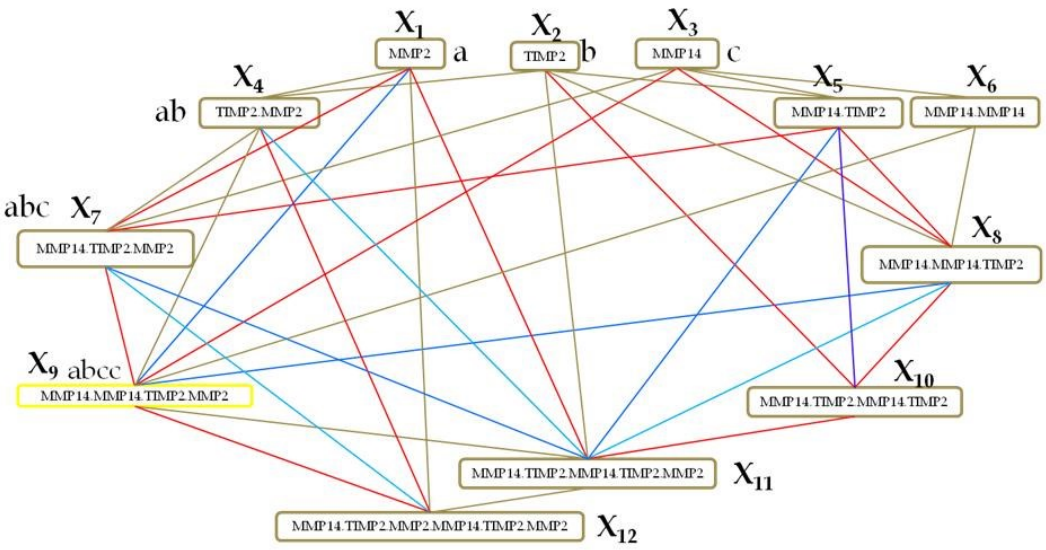

The same color lines toward a component is indicated as one reaction. If only one color, it is dimerization. The bold yellow box in one of the component above indicates the important component in the ECM degradation.

Figure 6. Pathway network of interaction between MT1-MMP, TIMP2, and MMP2

These 12 components with kinetic reactions of three molecules; $a, b, \text{and } c$ and pathway network on *Figure 6* can be used to build a quantitative model of ECM degradation. A first quantitative model was proposed by Karagiannis et al., in which the general interactive behavior of the molecules $a, b, \text{and } c$ was investigated through simulation in the context of type-I collagen proteolysis.

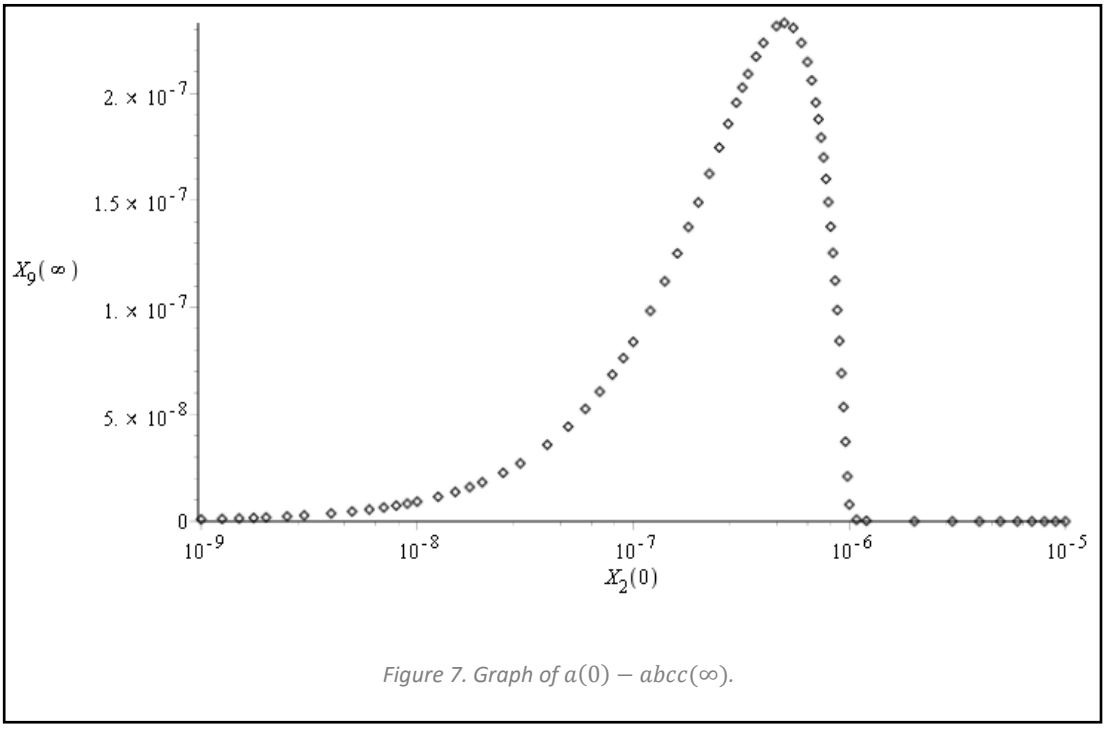

Figure 7. Graph of $a(0) - abcc(\infty)$.

$abcc$ is the important complex in the extracellular matrix degradation. Once these complex is formed, b-free c cuts $a - b$ binding which leads to an activation of a. The activated a degrades the basement membrane and the rest of extracellular matrix degradation will be cone by c.

To form $abcc$ complex, b is sufficiently needed. However, if the existence of b is too much, b-free c on $abcc$ will tend to bind b. As a result, $abccb$ will be formed preferentially to $abcc$ leading to an insignificant of a activation. If the existence of b is too low, $abcc$ will be less formed. This phenomenon can be see in (Figure 7).

Mathematical Expression of Kinetic Reaction Systems on The ECM Degradation Associated with Cancer Invasion

Firstly, denote the concentration of a, b, c, ab, bc, cc, abc, bcc, $abcc$, $bccb$, $abccb$, and $abccba$ as X_1, X_2, X_3, X_4, X_5, X_6, X_7, X_8, X_9, X_{10}, X_{11}, and X_{12}, respectively. To build the mathematical equation of the kinetic reaction systems, we add the following assumptions:

1. The initial concentration of $X_4, X_5, X_6, X_7, X_8, X_9, X_{10}, X_{11}$, and X_{12} are all 0. The initial concentration of X_1, X_2, and X_3 are denoted as $a_0 > 0$, $b_0 > 0$, and $c_0 > 0$, respectively.
2. The complex reaction has repetition rate constant to the relevant monomer reaction.

Due to the assumption on binding rules in previous section (Page 21), we find that the following three group reactions are all reactions that involved in the system:

1. Reaction between monomer a and monomer b or b's compound, written as $b\boldsymbol{B}$, with association rate constant k_1:

$$a + b\boldsymbol{B} \rightharpoonup ab\boldsymbol{B}. \tag{57}$$

2. Reaction between monomer b or $b\boldsymbol{B}$ and monomer c or c's compound, written as $c\boldsymbol{C}$, with association rate constant k_2 and dissociation constant l_2:

$$b\boldsymbol{B} + c\boldsymbol{C} \rightleftharpoons \boldsymbol{B}bc\boldsymbol{C}. \tag{58}$$

3. Reaction between two monomer c or $c\boldsymbol{C}$, which involves symmetry and non-symmetry reactions:

$$c\boldsymbol{C} + c\boldsymbol{C} \rightleftharpoons \boldsymbol{C}cc\boldsymbol{C}. \tag{59}$$

Reaction (59) has association rate constant k_3 and dissociation rate constant l_3 if it is a non-symmetry reaction. If it is symmetry, Reaction (59) has association rate constant $1/2k_3$ and dissociation rate constant l_3.

Based on the three group reactions above, we grouped all reactions that involved in the system into three groups of reaction as written in the following tables:

Table 2

Group 1 $(a + b\boldsymbol{B} \rightharpoonup ab\boldsymbol{B})$				Association constant	dissociation constant
$X_1(a)$	$+ X_2(b)$	$\rightharpoonup$	$X_4(ab)$	k_1	$l_1 = 0$
	$+ X_5(bc)$	$\rightharpoonup$	$X_7(abc)$	k_1	
	$+ X_8(bcc)$	$\rightharpoonup$	$X_9(abcc)$	k_1	
	$+ X_{10}(bccb)$	$\rightharpoonup$	$X_{11}(abccb)$	$2k_1$	
	$+ X_{11}(abccb)$	$\rightharpoonup$	$X_{12}(abccba)$	k_1	

Table 3

Group 2 $(b\boldsymbol{B} + c\boldsymbol{C} \rightleftharpoons \boldsymbol{B}bc\boldsymbol{C})$				Association constant	dissociation constant
$X_2(b)$	$+ X_3(c)$	$\leftrightharpoons$	$X_5(bc)$	k_2	l_2
	$+ X_6(cc)$	$\leftrightharpoons$	$X_8(bcc)$	$2k_2$	l_2
	$+ X_8(bcc)$	$\leftrightharpoons$	$X_{10}(bccb)$	k_2	$2l_2$
	$+ X_9(abcc)$	$\leftrightharpoons$	$X_{11}(abccb)$	k_2	l_2
$X_4(ab)$	$+ X_3(c)$	$\leftrightharpoons$	$X_7(sbc)$	k_2	l_2
	$+ X_6(cc)$	$\leftrightharpoons$	$X_9(abcc)$	$2k_2$	l_2
	$+ X_8(bcc)$	$\leftrightharpoons$	$X_{11}(abccb)$	k_2	l_2
	$+ X_9(abcc)$	$\leftrightharpoons$	$X_{12}(abccba)$	k_2	$2l_2$

Table 4

Group 3 ($c\boldsymbol{C} + c\boldsymbol{C} \rightleftharpoons \boldsymbol{C}cc\boldsymbol{C}$)				Association constant	dissociation constant
$X_3(c)$	$+X_3(c)$	$\rightleftharpoons$	$X_6(cc)$	$1/2k_3$	l_3
	$+X_5(bc)$	$\rightleftharpoons$	$X_8(bcc)$	k_3	l_3
	$+X_7(abc)$	$\rightleftharpoons$	$X_9(abcc)$	k_3	l_3
$X_5(bc)$	$+X_5(bc)$	$\rightleftharpoons$	$X_{10}(bccb)$	$1/2k_3$	l_3
	$+X_7(abc)$	$\rightleftharpoons$	$X_{11}(abccb)$	k_3	l_3
$X_7(abc)$	$+X_7(abc)$	$\rightleftharpoons$	$X_{12}(abccba)$	$1/2k_3$	l_3

From Table 2, Table 3, and Table 4 above, we can write the following 12 nonlinear ODEs system:

$$\frac{dX_1}{dt} = -k_1X_1(X_2 + X_5 + X_8 + 2X_{10} + X_{11}), \tag{60}$$

$$\frac{dX_2}{dt} = -k_1X_1X_2 - k_2X_2(X_3 + 2X_6 + X_8 + X_9) + l_2(X_5 + X_8 + 2X_{10} + X_{11}), \tag{61}$$

$$\frac{dX_3}{dt} = -k_2X_3(X_2 + X_4) - k_3X_3(X_3 + X_5 + X_7) + l_2(X_5 + X_7) + l_3(2X_6 + X_8 + X_9), \tag{62}$$

$$\frac{dX_4}{dt} = k_1X_1X_2 - k_2X_4(X_3 + 2X_6 + X_8 + X_9) + l_2(X_7 + X_9 + X_{11} + 2X_{12}), \tag{63}$$

$$\frac{dX_5}{dt} = -k_1X_1X_5 + k_2X_2X_3 - k_3X_5(X_3 + X_5 + X_7) - l_2X_5 + l_3(X_8 + 2X_{10} + X_{11}), \tag{64}$$

$$\frac{dX_6}{dt} = \frac{1}{2}k_3{X_3}^2 - 2k_2X_6(X_2 + X_4) + l_2(X_8 + X_9) - l_3X_6, \quad (65)$$

$$\frac{dX_7}{dt} = k_1X_1X_5 + k_2X_3X_4 - k_3X_7(X_3 + X_5 + X_7) - l_2X_7 + l_3(X_9 + X_{11} + 2X_{12}), \quad (66)$$

$$\frac{dX_8}{dt} = -k_1X_1X_8 + k_2X_2X_6 - k_2X_8(X_2 + X_4) + k_3X_3X_5 + l_2(-X_8 + 2X_{10} + X_{11}) - l_3X_8, \quad (67)$$

$$\frac{dX_9}{dt} = k_1X_1X_8 - k_2X_9(X_2 + X_4) + 2k_2X_4X_6 + k_3X_3X_7 + l_2(-X_9 + X_{11} + 2X_{12}) - l_3X_9, \quad (68)$$

$$\frac{dX_{10}}{dt} = -2k_1X_1X_{10} + k_2X_2X_8 + \frac{1}{2}k_3{X_5}^2 - 2l_2X_{10} - l_3X_{10}, \quad (69)$$

$$\frac{dX_{11}}{dt} = k_1X_1(2X_{10} - X_{11}) + k_2X_2X_9 + k_2X_4X_8 + k_3X_5X_7 - 2l_2X_{11} - l_3X_{11}, \quad (70)$$

$$\frac{dX_{12}}{dt} = k_1X_1X_{11} + k_2X_4X_9 + \frac{1}{2}k_3{X_7}^2 - 2l_2X_{12} - l_3X_{12}, \quad (71)$$

by using law of mass action as presented in the previous section.

In the next section, the grouping system and mass conservation laws will be presented.

The Grouping System to The ODEs of Kinetic Reaction Systems on The ECM Degradation Associated with Cancer Invasion

From Table 2, all reactions in Group 1 can be summarized as

$$X_1 + (X_2 + X_5 + X_8 + 2X_{10} + X_{11}) \rightharpoonup (X_4 + X_7 + X_9 + X_{11} + 2X_{12}), \qquad (72)$$

with association rate k_1. Coefficient 2 in $X_{10}(bccb)$ indicates $bccb$ has two possible sites for the attachment of a. Coefficient 2 in $X_{12}(abccba)$ indicates that $abccba$ consumes two a molecules unlike others: $X_4(ab)$, $X_7(abc)$, $X_9(abcc)$, and $X_{11}(abccb)$.

Let $\zeta_{2581011} = X_2 + X_5 + X_8 + 2X_{10} + X_{11}$. Using law of mass action, we have the following system to the reaction Group 1:

$$\frac{dX_1}{dt} = -k_1 X_1 \zeta_{2581011}, \qquad (73)$$

$$\frac{d\zeta_{2581011}}{dt} = -k_1 X_1 \zeta_{2581011}. \qquad (74)$$

Observing the ODEs system (60)-(71), the equation (73) is equal to equation (60) and the equation (74) is (61) + (64) + (67) + 2(69) + (70).

Applying mass conservation law to reaction Group 1, we have

$$\frac{d}{dt}(X_1 + X_4 + X_7 + X_9 + X_{11} + 2X_{12}) = 0. \qquad (75)$$

By observing the original ODE system (60)-(71), we find that ODE system (60)-(71) satisfies (75). Thus, equation (75) can be considered as one of mass conservation laws to system (60)-(71). Moreover, equation (75) may be considered as mass conservation law for a_0, since

$$(X_1 + X_4 + X_7 + X_9 + X_{11} + 2X_{12})(t) = a_0. \qquad (76)$$

The other mass conservation to reaction Group 1 is

$$\frac{d}{dt}(\zeta_{2581011} + X_4 + X_7 + X_9 + X_{11} + 2X_{12}) = 0. \tag{77}$$

Again, ODE system (60)-(71) satisfies (77). Equation (77) can be written as

$$(\zeta_{2581011} + X_4 + X_7 + X_9 + X_{11} + 2X_{12})(t) = b_0. \tag{78}$$

We see that equation (78) can be considered as mass conservation law for b_0. Subtracting equation (78) to equation (76), we obtain

$$(\zeta_{2581011} - X_1)(t) = b_0 - a_0. \tag{79}$$

This equation can be considered as mass conservation law for $b_0 - a_0$.

Next, we consider all reactions in Group 2, which can be summarized as

$$\begin{aligned}(X_2 + X_4) + (X_3 + 2X_6 + X_8 + X_9) \leftrightharpoons \\ (X_5 + X_8 + 2X_{10} + X_{11}) + (X_7 + X_9 + X_{11} + 2X_{12}).\end{aligned} \tag{80}$$

with association rate k_2 and dissociation rate l_2. Coefficient 2 in $X_6(cc)$ indicates cc has two possible sites for the attachment of b as in reaction (1C). Coefficient 2 in $X_{10}(bccb)$ and $X_{12}(abccba)$ indicate $bccb$ and $abccba$ consume two b molecules unlike others: $X_5(bc)$, $X_7(abc)$, $X_8(bcc)$, $X_9(abcc)$, and $X_{11}(abccb)$.

Let $\zeta_{24} = X_2 + X_4$ and $\zeta_{3689} = X_3 + 2X_6 + X_8 + X_9$. Using the similar manner to that used in group 1, we have the following system to reaction Group 2:

$$\frac{d\zeta_{24}}{dt} = -k_2\zeta_{24}\zeta_{3689} + l_2(X_5 + X_7 + X_8 + X_9 + 2X_{10} + 2X_{11} + 2X_{12}), \tag{81}$$

$$\frac{d\zeta_{3689}}{dt} = -k_2\zeta_{24}\zeta_{3689} \tag{82}$$

$$+l_2(X_5 + X_7 + X_8 + X_9 + 2X_{10} + 2X_{11} + 2X_{12}).$$

Taking summation of X_2 and X_4 from the ODE system (60)-(71) results equation (81). The similar manner to equation (82). That is, equation (82) is the summation of X_3, $2X_6$, X_8, and X_9: (62)+2(64)+(66)+(67).

The mass conservation to reaction Group 2 other than equation (77) is

$$\frac{d}{dt}(\zeta_{3689} + X_5 + X_7 + X_8 + X_9 + 2X_{10} + 2X_{11} + 2X_{12}) = 0. \tag{83}$$

Again, ODE system (60)-(71) satisfies (83). This equation can be written as

$$(\zeta_{3689} + X_5 + X_7 + X_8 + X_9 + 2X_{10} + 2X_{11} + 2X_{12})(t) = c_0. \tag{84}$$

This equation can be considered as mass conservation law for c_0. Rewrite equation (78) to

$$(\zeta_{24} + X_5 + X_7 + X_8 + X_9 + 2X_{10} + 2X_{11} + 2X_{12})(t) = b_0. \tag{85}$$

By substracting equation (84) to equation (85), we obtain

$$(\zeta_{3689} - \zeta_{24})(t) = c_0 - b_0. \tag{86}$$

This equation can be considered as mass conservation law for $c_0 - b_0$.

The last is reaction of Group 3. All reactions in Group 3 can be summarized as

$$(X_3 + X_5 + X_7) + (X_3 + X_5 + X_7) \leftrightharpoons (X_6 + X_8 + X_9 + X_{10} + X_{11} + X_{12}) \tag{87}$$

with association rate $1/2k_3$ and dissociation rate l_3. Coefficient 2 in all term on the right-hand side of reaction above indicate all components consume two c molecules.

Let $\zeta_{357} = X_3 + X_5 + X_7$. Using law of mass action, we have the following equation:

$$\frac{d\zeta_{357}}{dt} = -k_3{\zeta_{357}}^2 + 2l_3(X_6 + X_8 + X_9 + X_{10} + X_{11} + X_{12}). \tag{88}$$

Again, by summing of X_3, X_7, and X_7 of ODE system (60)-(71), we find that equation (88) is true.

In the next section, we will see how the group ODE system is used to show that the ODE system (60)-(71) is integratable.

The Integrability of ODEs System

By substituting (79), $\zeta_{2581011} = X_1 + b_0 - a_0$, into (73), we have

$$\frac{dX_1}{dt} = -k_1X_1(X_1 + b_0 - a_0). \tag{89}$$

If $b_0 - a_0 = 0$, the solution to (89) would be similar to (32).

Now if the case is $b_0 - a_0 > 0$, the solution to (89) is

$$\left(\frac{1}{X_1} - \frac{1}{X_1 + b_0 - a_0}\right) dX_1 = -k_1(b_0 - a_0)dt \tag{90}$$

$$\ln\frac{X_1}{X_1 + b_0 - a_0} - \ln\frac{a_0}{b_0} = -k_1(b_0 - a_0)t$$

$$\frac{X_1}{X_1 + b_0 - a_0} = \frac{a_0}{b_0} e^{-k_1(b_0 - a_0)t}$$

$$X_1(t) = \frac{a_0(b_0 - a_0)e^{-k_1(b_0 - a_0)t}}{b_0 - a_0 e^{-k_1(b_0 - a_0)t}}.$$

And, if $b_0 - a_0 < 0$, the solution to (89) would be

$$\left(-\frac{1}{X_1} + \frac{1}{X_1 + b_0 - a_0}\right) dX_1 = -k_1(a_0 - b_0)dt$$

$$\ln \frac{X_1 + b_0 - a_0}{X_1} - \ln \frac{b_0}{a_0} = -k_1(a_0 - b_0)t$$

$$\frac{X_1 + b_0 - a_0}{X_1} = \frac{b_0}{a_0} e^{-k_1(a_0 - b_0)t}$$

$$X_1(t) = \frac{a_0(a_0 - b_0)}{a_0 - b_0 e^{-k_1(a_0 - b_0)t}}. \tag{91}$$

In summary, the solution of $X_1(t)$ is expressed as

$$X_1(t) = \begin{cases} \dfrac{a_0}{1 + a_0 k_1 t}, & b_0 - a_0 = 0 \\ \dfrac{a_0(b_0 - a_0)e^{-k_1(b_0 - a_0)t}}{b_0 - a_0 e^{-k_1(b_0 - a_0)t}} & b_0 - a_0 > 0\,, \\ \dfrac{a_0(a_0 - b_0)}{a_0 - b_0 e^{-k_1(a_0 - b_0)t}}, & b_0 - a_0 < 0 \end{cases} \tag{92}$$

By observing (92) at large t, we find that $X_1(t)$ is decreasing monotonically:

$$X_1(0) = a_0 \;\searrow\; X_1(\infty) = \begin{cases} (a_0 - b_0), & b_0 - a_0 < 0 \\ 0, & b_0 - a_0 \geq 0 \end{cases} \tag{93}$$

and is nonnegative.

The solution of $\zeta_{2581011}(t)$ can be obtained using (79). That is

$$\zeta_{2581011}(t) = \begin{cases} \dfrac{a_0}{1 + a_0 k_1 t}, & b_0 - a_0 = 0 \\ \dfrac{b_0(b_0 - a_0)}{b_0 - a_0 e^{-k_1(b_0 - a_0)t}}, & b_0 - a_0 > 0 \\ \dfrac{b_0(a_0 - b_0)e^{-k_1(a_0 - b_0)t}}{a_0 - b_0 e^{-k_1(a_0 - b_0)t}}, & b_0 - a_0 < 0 \end{cases}. \quad (94)$$

Again, by observing (94) at large t, we find that $\zeta_{2581011}(t)$ is decreasing:

$$\zeta_{2581011}(0) = b_0 \ \searrow \ \zeta_{2581011}(\infty) = \begin{cases} (b_0 - a_0), & b_0 - a_0 > 0 \\ 0, & b_0 - a_0 \leq 0 \end{cases}. \quad (95)$$

and is nonnegative.

Next, we consider equation (81). Using relation (85) and (86), we can rewrite equation (81) as follow:

$$\begin{aligned} \frac{d\zeta_{24}}{dt} &= -k_2\zeta_{24}(\zeta_{24} + c_0 - b_0) + l_2(b_0 - \zeta_{24}) \\ &= -\left\{k_2{\zeta_{24}}^2 - \left(-l_2 + k_2(b_0 - c_0)\right)\zeta_{24} - l_2 b_0\right\} \\ &= -k_2(\zeta_{24} - \zeta_{24}^+)(\zeta_{24} - \zeta_{24}^-). \end{aligned} \quad (96)$$

This expression is similar to (8). Hence, the solution to (96) is

$$\zeta_{24}(t) = \frac{\zeta_{24}^+ - \zeta_{24}^-}{1 - C_{24} e^{-k_2(\zeta_{24}^+ - \zeta_{24}^-)t}} + \zeta_{24}^-, \quad (97)$$

where

$$C_{24} = \frac{b_0 - \zeta_{24}^{+}}{b_0 - \zeta_{24}^{-}}, \tag{98}$$

$$\zeta_{24}^{\pm} = \frac{-l_2 + k_2(b_0 - c_0) \pm \sqrt{\left(-l_2 + k_2(b_0 - c_0)\right)^2 + 4k_2 l_2 b_0}}{2k_2}, \tag{99}$$

and $b_0 - c_0 < \zeta_{24}^{+} > 0 > \zeta_{24}^{-}$.

The solution of $\zeta_{3689}(t)$ can be obtained using relation (86). That is,

$$\zeta_{3689}(t) = \frac{\zeta_{24}^{+} - \zeta_{24}^{-}}{1 - C_{24} e^{-k_2(\zeta_{24}^{+} - \zeta_{24}^{-})t}} + \zeta_{24}^{-} + c_0 - b_0. \tag{100}$$

By observing (99) using similar manner in (18) and (19), we find that $b_0 - \zeta_{24}^{+} > 0$. Thus, $\zeta_{24}(t)$ is monotonically decreasing:

$$\zeta_{24}(0) = b_0 \quad \searrow \quad \zeta_{24}(\infty) = \zeta_{24}^{+}. \tag{101}$$

$\zeta_{3689}(t)$ is also decreasing monotonically:

$$\zeta_{3689}(0) = c_0 \quad \searrow \quad \zeta_{3689}(\infty) = \zeta_{24}^{+} + c_0 - b_0. \tag{102}$$

Both $\zeta_{24}(t)$ and $\zeta_{3689}(t)$ are nonnegative for $t \geq 0$.

The analysis result above is for positive discriminant in (99), which can be satisfied if $l_2 \neq 0$, and $b_0 - c_0 \neq 0$. If $l_2 = 0$ and $b_0 - c_0$, (96) now become

$$\frac{d\zeta_{24}}{dt} = -k_2 {\zeta_{24}}^2. \tag{103}$$

Since (103) is similar to (31), the solution to (103) is

$$\zeta_{24}(t) = \frac{b_0}{1 + b_0 k_2 t}, \tag{104}$$

And the solution of $\zeta_{3689}(t)$ is

$$\zeta_{3689}(t) = \frac{b_0}{1 + b_0 k_2 t} + c_0 - b_0. \tag{105}$$

Now, both $\zeta_{24}(t)$ and $\zeta_{3689}(t)$ decrease with $O(t^{-1})$, which is slower than in the case if the discriminant of (99) is positive, with order $O(e^{-\alpha t})$.

To solve equation (61), rewrite equation (61) using relation (86) and definition of $\zeta_{2581011}$ as follow:

$$\begin{aligned} \frac{dX_2}{dt} &= -k_1 X_1(t) X_2 - k_2 X_2 \zeta_{3689}(t) + l_2(\zeta_{2581011}(t) - X_2) \\ &= -X_2(k_1 X_1(t) + k_2 \zeta_{3689}(t) + l_2) + l_2 \zeta_{2581011}(t). \end{aligned} \tag{106}$$

The solution of $X_2(t)$ can be obtained by solving the above equation using method of variation of constant. Thus, the solution of $X_4(t)$ can be obtained by definition of ζ_{24}.

To solve equation (88), first rewrite equation (84) to

$$(\zeta_{357} + 2X_6 + 2X_8 + 2X_9 + 2X_{10} + 2X_{11} + 2X_{12})(t) = c_0. \tag{107}$$

(88) now can be rewritten as follow:

$$\begin{aligned} \frac{d\zeta_{357}}{dt} &= -k_3 {\zeta_{357}}^2 + l_3(c_0 - \zeta_{357}) \\ &= -k_3(\zeta_{357} - \zeta_{357}^+)(\zeta_{357} - \zeta_{357}^-). \end{aligned} \tag{108}$$

Again, the expression of (108) is similar to (8). Hence, the solution of $\zeta_{357}(t)$ is

$$\zeta_{357}(t) = \frac{\zeta_{357}^{+} - \zeta_{357}^{-}}{1 - C_{357}e^{-k_3(\zeta_{357}^{+} - \zeta_{357}^{-})t}} + \zeta_{357}^{-}, \tag{109}$$

where

$$C_{357} = \frac{c_0 - \zeta_{357}^{+}}{c_0 - \zeta_{357}^{-}}, \tag{110}$$

$$\zeta_{357}^{\pm} = \frac{-l_3 \pm \sqrt{{l_3}^2 + 4k_3 l_3 c_0}}{2k_3}. \tag{111}$$

and $\zeta_{357}^{+} > 0 > \zeta_{357}^{-}$. Since $c_0 - \zeta_{357}^{+}$, we find that $\zeta_{357}(t)$ is decreasing monotonically:

$$\zeta_{357}(0) = c_0 \quad \searrow \quad \zeta_{357}(\infty) = \zeta_{357}^{+}, \tag{112}$$

and is nonnegative.

The discriminant of (111) is zero if $l_3 = 0$, leading to the solution of $\zeta_{357}(t)$ is expressed as

$$\zeta_{357}(t) = \frac{c_0}{1 + c_0 k_3 t}. \tag{113}$$

Now, both $\zeta_{357}(t)$ decreases with $O(t^{-1})$, which is slower than in the case of positive discriminant in (111), with order $O(e^{-\alpha t})$.

To solve equation (62), rewrite equation (62) using definition of ζ_{24}, ζ_{3689}, and ζ_{357}:

$$\frac{dX_3}{dt} = -k_2 X_3 \zeta_{24}(t) - k_3 X_3 \zeta_{357}(t) + l_2(\zeta_{357}(t) - X_3) \tag{114}$$

$$+l_3(\zeta_{3689}(t) - X_3)$$

$$= -X_3(k_2\zeta_{24}(t) + k_3\zeta_{357}(t) + l_2 + l_3) + l_2\zeta_{357}(t) + l_3\zeta_{3689}(t).$$

(114) can be solved using method of variation of constant, as well. Then, the solution of $X_5(t)$ can be obtained by similar manner. That is by solving the following equation:

$$\frac{dX_5}{dt} = -k_1X_1(t)X_5 + k_2X_2(t)X_3(t) - k_3X_5\zeta_{357}(t) - l_2X_5$$

$$+l_3(\zeta_{2581011}(t) - X_2(t) + X_5)$$

$$= -X_5(k_1X_1(t) + k_3\zeta_{357}(t) + l_2 + l_3) + k_2X_2(t)X_3(t)$$

$$+l_3\zeta_{2581011}(t). \tag{115}$$

Thus, the solution of $X_7(t)$ can be obtained by definition of ζ_{357}.

The solution of $X_6(t)$, $X_8(t)$, $X_9(t)$, $X_{10}(t)$, $X_{11}(t)$, $X_{12}(t)$ can be obtained by similar manner.

Biological Implication

Cancer invasion is triggered by the production of molecule $abcc$ in the system. Therefore, by controlling the *abcc* production, we may be able to prevent leakage of cancer cells from the primary sites through ECM degradation. From the analysis results in the previous section, we can find the important parameter that regulates the production of molecule $abcc$.

At large t, (106) gives the equilibrium value of X_2, which is written as follows:

$$X_2(\infty) = \frac{l_2\zeta_{2581011}(\infty)}{(k_1X_1(\infty) + k_2X_2\zeta_{3689}(\infty) + l_2)}. \tag{116}$$

Then,

$$X_4(\infty) = \zeta_{24}(\infty) - \frac{l_2\zeta_{2581011}(\infty)}{(k_1X_1(\infty) + k_2X_2\zeta_{3689}(\infty) + l_2)}. \tag{117}$$

At large t, (114) and (115) respectively become

$$X_3(\infty) = \frac{l_2\zeta_{357}(\infty) + l_3\zeta_{3689}(\infty)}{(k_2\zeta_{24}(\infty) + k_3\zeta_{357}(\infty) + l_2 + l_3)}, \tag{118}$$

$$X_5(\infty) = \frac{k_2X_2(\infty)X_3(\infty) + l_3\big(\zeta_{2581011}(\infty) - X_2(\infty)\big)}{(k_1X_1(\infty) + k_3\zeta_{357}(\infty) + l_2 + l_3)}. \tag{119}$$

Then,

$$X_7(\infty) = \zeta_{357}(\infty) - \frac{l_2\zeta_{357}(\infty) + l_3\zeta_{3689}(\infty)}{(k_2\zeta_{24}(\infty) + k_3\zeta_{357}(\infty) + l_2 + l_3)}$$

$$- \frac{k_2X_2(\infty)X_3(\infty) + l_3\big(\zeta_{2581011}(\infty) - X_2(\infty)\big)}{(k_1X_1(\infty) + k_3\zeta_{357}(\infty) + l_2 + l_3)} \tag{120}$$

From (65) and (67), the equilibrium values of $X_6(t)$ and $X_8(t)$ are respectively obtained as follows:

$$X_6(\infty) = \frac{\frac{1}{2}k_3X_3(\infty)^2 + l_2\big(\zeta_{3689}(\infty) - X_3(\infty)\big)}{2k_2\zeta_{24}(\infty) + 2l_2 + l_3}. \tag{121}$$

$$X_8(\infty) = \frac{k_2X_2(\infty)X_6(\infty) + k_3X_3(\infty)X_5(\infty)}{k_1X_1(\infty) + k_2\zeta_{24}(\infty) + 2l_2 + l_3}$$

$$+ \frac{l_2\big(\zeta_{2581011}(\infty) - X_2(\infty) - X_5(\infty)\big)}{k_1X_1(\infty) + k_2\zeta_{24}(\infty) + 2l_2 + l_3}, \tag{122}$$

Hence, the equilibrium value of $X_9(t)$ can be obtained by substituting (101), (116)-(122) into the following equation:

$$X_9(\infty) = \frac{k_1 X_1(\infty) X_8(\infty) + 2k_2 X_4(\infty) X_6(\infty) + k_3 X_3(\infty) X_7(\infty)}{k_2 \zeta_{24}(\infty) + 2l_2 + l_3}$$

$$+ \frac{l_2\big(a_0 - X_1(\infty) - X_4(\infty) - X_7(\infty)\big)}{k_2 \zeta_{24}(\infty) + 2l_2 + l_3}. \qquad (123)$$

Figure 4 shows how the initial concentration of each connected molecule affects the production of $abcc$. Note that *abcc* production is regulated by $[c_o - b_o]$. Specifically, *abcc* is produced when $c_o - b_o > 0$, and is not produced when $c_o - b_o \leq 0$.

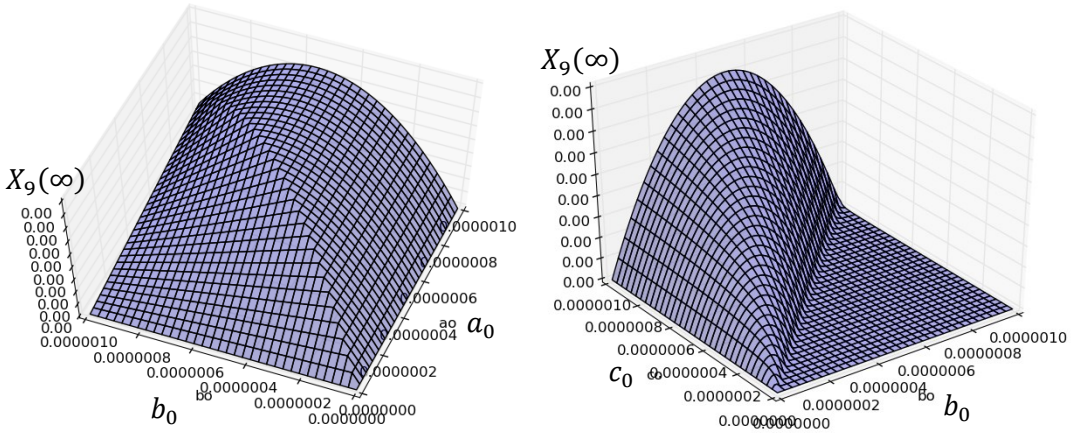

Figure 8. Graph of $X_9(\infty)$ vs $b_o - a_o$ (left) and $c_o - b_o$ (right)

Discussion

From the expressions of the group solutions presented in the previous section, we infer that the initial concentration difference between the connected molecules regulates the behavior of solutions and their equilibrium values. That is

1. $b_0 - a_0$ regulates the solutions and equilibrium values of $X_1(t)$ and $\zeta_{2581011}(t)$. $X_1(t)$ and $\zeta_{2581011}(t)$ decrease at rate $O(t^{-1})$ when $b_0 - a_0 = 0$, and at rate $O(e^{-\alpha t})$ when $b_0 - a_0 \neq 0$,

2. $b_0 - c_0$ regulates the solutions and equilibrium values of $\zeta_{24}(t)$ and $\zeta_{3689}(t)$,

but only one parameter (c_0.) regulates the group solution $\zeta_{357}(t)$.

Here, the nonlinear ODEs system is solved by imposing appropriate doubling rules on the reactions of Group 3. Similarly, Kawasaki et al. imposed doubling rules on a system of mathematical equations to allow an explicit solution. The two approaches apply different concepts to symmetry reactions described in Section 1.B. In their concept, they used full reaction rate to the symmetry reaction and added the following reactions to Reaction group 3:

$$X_3(c) + X_5(bc) \leftrightharpoons X_8(bcc), \tag{124}$$

$$X_3(c) + X_7(abc) \leftrightharpoons X_9(abcc), \tag{125}$$

$$X_5(c) + X_7(bc) \leftrightharpoons X_{11}(bcc), \tag{126}$$

After these manipulations, the ODE of $\zeta_{357}(t)$ can be solved explicitly.

Alternatively, Minerva [2013] omitted reactions (124)-(126), preventing the direct solution of $\zeta_{357}(t)$ from the ODE of $\zeta_{357}(t)$. She reduced the ODE to a Lotka–Volterra system, which is more complicated to solve.

Figure 11 compares the solutions of Kawasaki et al, Minerva [2013] and the present work. The initial concentrations in the simulations were $a_0 = c_0 = 10^{-6}$, $b_0 = 5 \times 10^{-7}$ and rate constants were $k_1 = 2.1 \times 10^7$, $k_2 = 2.74 \times 10^6$, $k_3 = 2 \times 10^6$, $l_2 = 2 \times 10^{-4}$, $l_3 = 10^{-2}$.

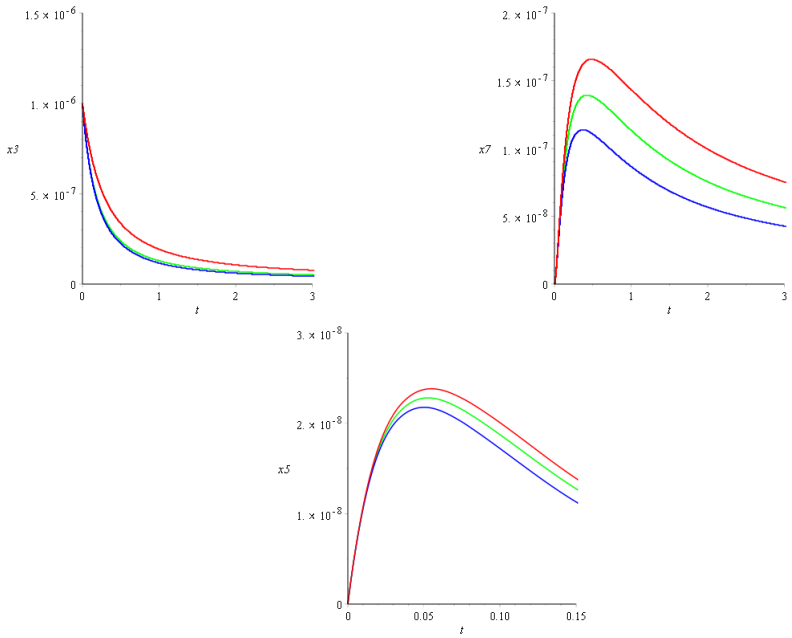

Figure 9. Graph of Solution X_3, X_5, and X_7 in Three Concepts. (Green) First model without doubling rules. (Blue) Method in Kawasaki et al. (Red) Present method.

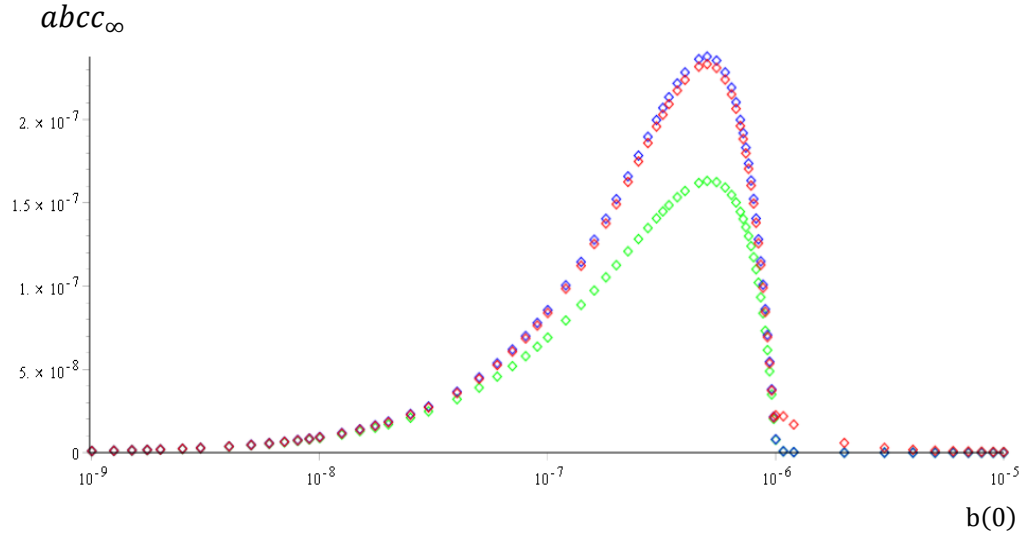

Figure 10. Graph of $b(0) - abcc(\infty)$. (Green) First model without doubling rules. (Blue) Method in Kawasaki et al. (Red) Present method.

As shown in Figure 9., the new concept in the symmetry reaction (red) halves the reaction rate; therefore, the graphical solutions of X_3, X_5, and X_7 reduce more slowly under the new concept than under the previous concepts. The equilibrium is also

higher, implying faster dissociation of the symmetry reactions in Group 3 (as evidenced by the red line of solutions X_6, X_{10}, and X_{12}). Because the present study omits reactions (124)-(126), the solutions of X_8, X_9, and X_{11} are lower in the presented method than in Kawasaki's work. The results of $b_0 - abcc_\infty$ are compared in Figure 11.

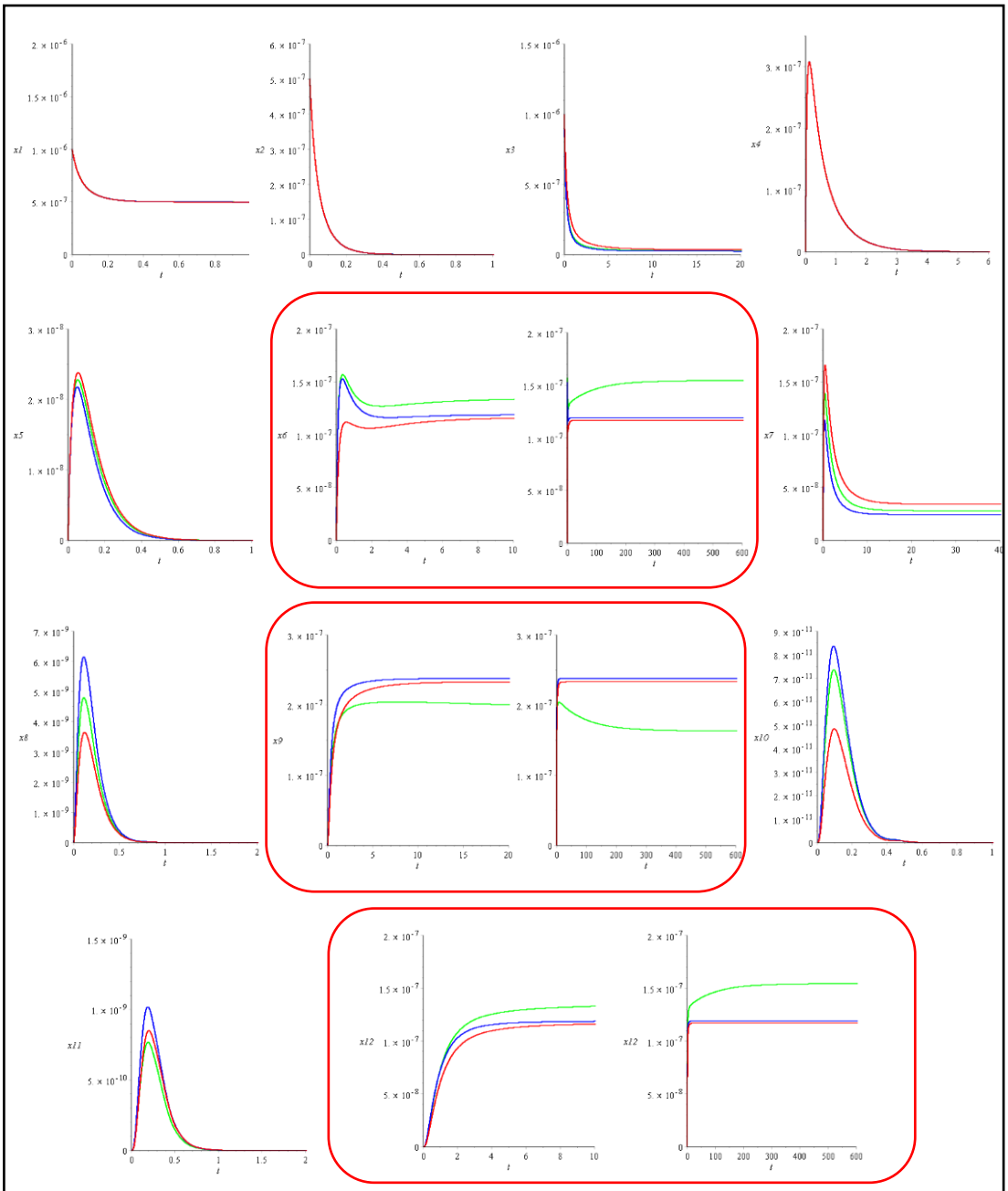

Figure 11. Graph of solution to the ODEs System in Three Concepts. (Green) First model without doubling rules. (Blue) Method in Kawasaki et al. (Red) Present method.

Concluding Remarks

The new concept of the symmetry reaction in Section 1.B allows us to generate an ODE system with appropriate doubling rules. Moreover, the ODEs are completely integratable. This new concept groups the kinetic reactions by their reaction rate constants. The relations between the ODE variables satisfy the mass conservation law and are valid for all $t \geq 0$. The behaviors of the solutions and their equilibrium values are regulated by the concentration differences over the connected molecules.

The approach presented in this chapter is applicable to kinetic reaction systems with n monomers. The system has the following reaction pattern:

$$A_n - A_{n-1} - \cdots - A_2 - A_1 \supset, \tag{127}$$

where $A_1, A_2, \ldots, A_n$ are n distinct molecules, line '$-$' represents the reaction between two connected molecules, and line '$\supset$' represents the dimer reaction. An n-monomer system was successfully treated by Itano and Suzuki. They explicitly solved an n-group ODE system and obtained asymptotically stable solutions that are consistent with the 3-monomer system solved by Itano and Suzuki [2016].

CHAPTER 2

MATHEMATICAL MODELLING AND SIMULATION OF PATTERN FORMATION ON TUMOR-INDUCED ANGIOGENESIS

Angiogenesis, the formation of new blood vessels from pre-existing vessels, is a vital component of many growth processes, including embryogenesis, retinal vasculature, wound healing, tumor growth and numerous vascular diseases. This chapter focuses on angiogenesis in tumor growth, known as tumor-induced angiogenesis. The formation of the blood vessel network is controlled by the movement of endothelial cells, which is driven by chemotactic and haptotactic responses to the gradients of vascular endothelial growth factor (VEGF) and fibronectin, respectively. This chapter investigates the role of VEGF and fibronectin gradients in the growth and patterning of blood vessels. To this end, we vary the parameters in a mathematical model of tumor-induced angiogenesis and present the results of a simulation study. For the simulations, we adopt a hybrid technique that combines discrete and continuous methods.

Introduction

Angiogenesis in tumor growth begins when a tumor cell is deprived of oxygen and nutrients. Once the tumor cell reaches this stage, it releases VEGF into the surrounding tissue [Folkman and Klagsbrun, 1987]. The VEGF diffuses through the extracellular matrix (ECM), establishing a concentration gradient between the tumor cell and the nearby pre-existing vessel. Having reached a nearby vessel, VEGF induces the endothelial cells to degrade the basement membrane that protects them from

the ECM. Consequently, some of the endothelial cells leak from the vessel and begin migrating through the ECM towards the tumor cell. The movement of endothelial cells up the VEGF gradient is called chemotaxis [Sholley et al., 1984]. As the endothelial cells migrate, they recruit other endothelial cells from the parent vessel, forming finger-like sprouts. These sprouts subsequently lengthen under movement of endothelial cells at the leading edge (tip cells).

Cell interaction with fibronectin (a major ECM component) is another important governor of cell movement [Anderson and Chaplain, 1998]. In particular, fibronectin attaches the endothelial cells to the ECM via integrins [Johanson et al., 1987], and stimulates haptotaxis (movement up a concentration gradient) [Carter, 1967]. Therefore, cell movement is driven by both chemotactic response to the up-gradient of VEGF and by haptotactic response to the up-gradient of fibronectin.

As the blood vessel network develops, tip cells meet and fuse with other tip cells or sprouts, eventually forming a loop network (anastomosis) at some distance from the parent vessel [Paweletz, 1989]. Tip cells can also proliferate and form new tip cells. The formation of new sprouts by this process is called sprout branching. As the tip cell approaches the tumor cell, sprout branching accelerates until the tumor cell is penetrated, resulting in vascularization [Muthukkaruppan et al., 1982].

To simulate the formation of the blood vessel network under these biological processes, we employ continuous and discrete mathematical models. The discrete model is obtained by discretizing the continuous model using a finite difference scheme. Instead of solving the finite difference scheme, we take the coefficients in the finite difference scheme as the probabilities of individual cell movements. In this discrete model, a tip cell can choose one of five options; remain still, move left, move right, move down, or move up. The next decision is based on the concentration gradients of VEGF and fibronectin, which are numerically computed by the continuous model. This process outlines our hybrid technique.

In the next section, we present the continuous model of Anderson–Chaplain tumor-induced angiogenesis. Each mathematical term in that model will be clearly explained. In a later section, we will discuss the numerical method and the hybrid technique with branching and anastomosis. The Simulation Results and Discussions section is filled with figures of the blood vessel network simulated under varying initial concentration profiles of VEGF and fibronectin. These results reveal the roles of both molecules in the pattern formation. The final section summarizes the study results.

Tumor-Induced Angiogenesis Anderson-Chaplain Model

We assume the movement of tip cell is influenced by three factors: molecular diffusion, chemotactic response to VEGF gradient, haptotactic response to fibronectin gradient. Then, the total flux of tip cell is given by

$$J_n = J_{\text{diffusion}} + J_{\text{chemotaxis}} + J_{\text{haptotaxis}}. \tag{128}$$

We assume the diffusion flux has form

$$J_{\text{diffusion}} = -D_n \nabla n, \tag{129}$$

where D_n is diffusion constant. For chemotactic response, we assume the tip cell is flowing along the VEGF gradient towards tumor. Thus, we take the chemotaxis flux as

$$J_{\text{chemotaxis}} = \chi_n n \nabla c, \tag{130}$$

where χ_n is the chemotaxis sensitivity of tip cell to the gradient of VEGF (n). χ_n can be assumed to be constant, meaning that the tip cells always respond to the gradient of VEGF, regardless of VEGF concentration. The more realistic χ_n can be written as function of VEGF, that is

$$\chi_n = \frac{\chi_0}{1 + \alpha_n c}, \tag{131}$$

where χ_0 is chemotaxis sensitivity constant and α_n is chemotaxis receptor saturation factor [Lapidus and Schiller, 1976]. The equation (131) means that the tip cells give less response to the high gradient of VEGF.

The haptotactic response of tip cell to the gradient of fibronectin (f) is assumed to have the form

$$J_{\text{haptotaxis}} = \rho_n n \nabla f, \tag{132}$$

where ρ_n is the haptotaxis sensitivity constant. Because our purpose is to track the movement of tip cell, we omit the cell proliferation and degradation. Thus, we have the following mass conservation of tip cell density:

$$\frac{\partial n}{\partial t} + \nabla \cdot J_n = 0, \tag{133}$$

and hence the partial differential equation of tip cell density is written as follow:

$$\begin{aligned} \frac{\partial n}{\partial t} &= -\nabla \cdot \left(J_{\text{diffusion}} + J_{\text{chemotaxis}} + J_{\text{haptotaxis}}\right) \\ &= -\nabla \cdot (-D_n \nabla n + \chi_n n \nabla c + \rho_n n \nabla f) \\ &= D_n \Delta n - \nabla \cdot (\chi_n n \nabla c + \rho_n n \nabla f). \end{aligned} \tag{134}$$

To construct the mathematical equation of VEGF, we assume VEGF reached the steady state and established the concentration gradient. As the tip cell flows through ECM in response to the VEGF gradient, the tip cell binds to VEGF with the uptake rate constant η_c. Then, at the steady state, VEGF concentration is assumed to have the following form:

$$\frac{\partial c}{\partial t} = \eta_c nc. \tag{135}$$

Now, we assume the tip cells secrete fibronectin with secretion rate constant β_f, in addition to the pre-existing fibronectin concentration on the tissue. As the tip cell migrate through ECM, fibronectin gives an adhesion bound for tip cell to the ECM. We assume the adhesion bound of tip cell to the ECM is formed as an uptake of tip cell to fibronectin with rate constant η_f. Hence, we have the following partial differential equation of fibronectin:

$$\frac{\partial f}{\partial t} = \beta_f n - \eta_f nf. \tag{136}$$

For the boundary condition, we assume the growth of sprout remains in the inside of the domain, regardless the shape of domain. Thus, the system (134)-(136) satisfies the following no-flux boundary condition:

$$\upsilon \cdot (-D_n \nabla n + \chi_n n \nabla c + \rho_n n \nabla f) = 0, \tag{137}$$

with υ is normal vector of the boundary. Hence, the complete system of interaction between tip cells, VEGF, and fibronectin is written as

$$\begin{cases} \dfrac{\partial n}{\partial t} = D_n \Delta n - \nabla \cdot (\chi_n n \nabla c + \rho_n n \nabla f), & \text{in } \Omega \times (0,T) \\ \dfrac{\partial c}{\partial t} = \eta_c nc, & \text{in } \Omega \times (0,T) \\ \dfrac{\partial f}{\partial t} = \beta_f n - \eta_f nf, & \text{in } \Omega \times (0,T) \\ \upsilon \cdot (-D_n \nabla n + \chi_n n \nabla c + \rho_n n \nabla f) = 0, & \text{on } \partial\Omega \times (0,T) \end{cases} . \tag{138}$$

Non-Dimensional System

To nondimensionalize the system (138), first we take the domain as $\Omega = (0, L) \times (0, L)$. Set

$$\tilde{n} = \frac{n}{n_0}, \quad \tilde{c} = \frac{c}{c_0}, \quad \tilde{f} = \frac{f}{f_0}, \quad \tilde{x} = \frac{x}{L}, \quad \tilde{y} = \frac{y}{L}, \quad \tilde{t} = \frac{t}{T} \tag{139}$$

where n_0 is the initial tip cell density, c_0 and f_0 are the initial VEGF and fibronectin concentration in which the tip cell responds in chemotactic and haptotactic manner, respectively. Thus,

$$\frac{n_0}{T}\frac{\partial \tilde{n}}{\partial t} = \frac{1}{L^2} D_n n_0 \Delta \tilde{n} - \frac{1}{L} \nabla \cdot \left(\chi_n n_0 \tilde{n} \frac{c_0}{L} \nabla \tilde{c} + \rho_n n_0 \tilde{n} \frac{f_0}{L} \nabla \tilde{f} \right)$$

$$\frac{\partial \tilde{n}}{\partial t} = \frac{D_n T}{L^2} \Delta \tilde{n} - \nabla \cdot \left(\frac{\chi_n c_0 T}{L^2} \tilde{n} \nabla \tilde{c} + \frac{\rho_n f_0 T}{L^2} \tilde{n} \nabla \tilde{f} \right), \tag{140}$$

$$\frac{c_0}{T}\frac{\partial \tilde{c}}{\partial t} = \eta_c n_0 \tilde{n} c_0 \tilde{c}$$

$$\frac{\partial \tilde{c}}{\partial t} = \eta_c n_0 T \tilde{n} \tilde{c}, \tag{141}$$

$$\frac{f_0}{T}\frac{\partial \tilde{f}}{\partial t} = \beta_f n_0 \tilde{n} - \eta_f n_0 \tilde{n} f_0 \tilde{f}$$

$$\frac{\partial \tilde{f}}{\partial t} = \beta_f n_0 T \tilde{n} - \eta_f n_0 T \tilde{n} \tilde{f}. \tag{142}$$

Hence, the system (138) is now written as

$$\begin{cases} \dfrac{\partial n}{\partial t} = D_1 \Delta n - \nabla \cdot (\chi_1 n \nabla c + \rho_1 n \nabla f), & \text{in } \Omega \times (0,T) \\ \dfrac{\partial c}{\partial t} = \eta_1 nc, & \text{in } \Omega \times (0,T) \\ \dfrac{\partial f}{\partial t} = \beta_1 n - \eta_2 nf, & \text{in } \Omega \times (0,T) \\ v \cdot (-D_1 \nabla n + \chi_1 n \nabla c + \rho_1 n \nabla f) = 0, & \text{on } \partial\Omega \times (0,T) \end{cases}, \qquad (143)$$

with

$$D_1 = \frac{D_n T}{L^2}, \quad \chi_1 = \frac{\chi_n c_0 T}{L^2}, \quad \rho_1 = \frac{\rho_n f_0 T}{L^2}, \quad \eta_1 = \eta_c n_0 T,$$
$$\beta_1 = \beta_f n_0 T, \quad \eta_2 = \eta_f n_0 T. \qquad (144)$$

We remove the tildes for refinement.

Parameter Values

Parameter values are estimated from available experimental data. The distance of tumor cell from nearby parent vessel is assumed to be taken with lengthscale $L = 2\,mm$. T =1.5 days $= 1.296 \times 10^5 s$. χ_0, c_0 are assumed to be taken at maximum chemotactic response that was measured in concentration VEGF at around $c_0 = 10^{-10} M$. That is $\chi_0 = 2.6 \times 10^{-1} mm^2 s^{-1} M^{-1}$[Stokes, 1990]. For diffusion constant, we take $D_n = 10^{-14} mm^2 s^{-1}$. These parameter values now give non-dimensional constants as

$$D_1 = \frac{10^{-14} mm^2 s^{-1} 1.296 \times 10^5 s}{4mm^2}$$
$$= 3.5 \times 10^{-4},$$
$$\chi_1 = \frac{2.6 \times 10^{-1} mm^2 s^{-1} M^{-1} 10^{-10} M 1.296 \times 10^5 s}{4mm^2} \qquad (145)$$

$= 0.38.$

For $\alpha_n, \rho_1, \eta_1, \beta_1$, and η_2, we take

$$\alpha_n = 0.6 \quad , \rho_1 = 0.3, \quad \eta_1 = 0.1, \quad \beta_1 = 0.07, \quad \eta_2 = 0.1. \tag{146}$$

Numerical Method

To solve system (143), firstly we define

$$\begin{aligned} \boldsymbol{u} &= \nabla c, \\ \boldsymbol{v} &= \nabla f, \\ \boldsymbol{F} &= n\boldsymbol{G}, \end{aligned} \tag{147}$$

where

$$\boldsymbol{G} = \chi_1 \boldsymbol{u} + \rho_1 \boldsymbol{v}. \tag{148}$$

Then, the first equation of the system (143) is now written as

$$\frac{\partial n}{\partial t} = D_1 \Delta n - \nabla \cdot \boldsymbol{F}. \tag{149}$$

(147) describes the total chemotactic and haptotactic flux of tip cell with velocity $\boldsymbol{G}$ flow. So, the equation (149) can be regarded as convection-diffusion equation. To solve these type of equation, we use an adaptive scheme in which the scheme is updated based on the flow direction. For the diffusion term, we use center space finite difference scheme.

Setting

To implement the adaptive scheme, firstly we introduce main and sub nodes (*Figure 12*:left) which is defined as

$$\left(x_i, y_j, t_k\right) = \left((i-0.5)h, (j-0.5)h, k\tau\right), \qquad (i,j = 1, \dots, N), \tag{150}$$

$$\left(\hat{x}_i, \hat{y}_j, \hat{t}_k\right) = (ih, jh, k\tau), \qquad (i,j = 0,1, \dots, N), \tag{151}$$

respectively, where $N \geq 1$ as the number of spatial partition with $h = L/N$, and $\tau = T/M$, $M \geq 1$ as the number of time partition.

We assume n, $\boldsymbol{u}$, $\boldsymbol{v}$, $\boldsymbol{G}$ are defined on main nodes which is denoted as

$$n\left(x_i, y_j, t_k\right) = n_{i,j}^k, \tag{152}$$

$$\boldsymbol{u}\left(x_i, y_j, t_k\right) = \boldsymbol{u}_{i,j}^k, \tag{153}$$

$$\boldsymbol{v}\left(x_i, y_j, t_k\right) = \boldsymbol{v}_{i,j}^k, \tag{154}$$

$$\boldsymbol{G}\left(x_i, y_j, t_k\right) = \boldsymbol{G}_{i,j}^k, \tag{155}$$

respectively.

c, f, $\boldsymbol{F}$ are assumed to be defined on sub nodes which is denoted as

$$c\left(\hat{x}_i, \hat{y}_j, \hat{t}_k\right) = c_{i,j}^k, \tag{156}$$

$$f\left(\hat{x}_i, \hat{y}_j, \hat{t}_k\right) = f_{i,j}^k, \tag{157}$$

$$\boldsymbol{F}\left(\hat{x}_i, \hat{y}_j, \hat{t}_k\right) = \boldsymbol{F}_{i,j}^k, \tag{158}$$

respectively.

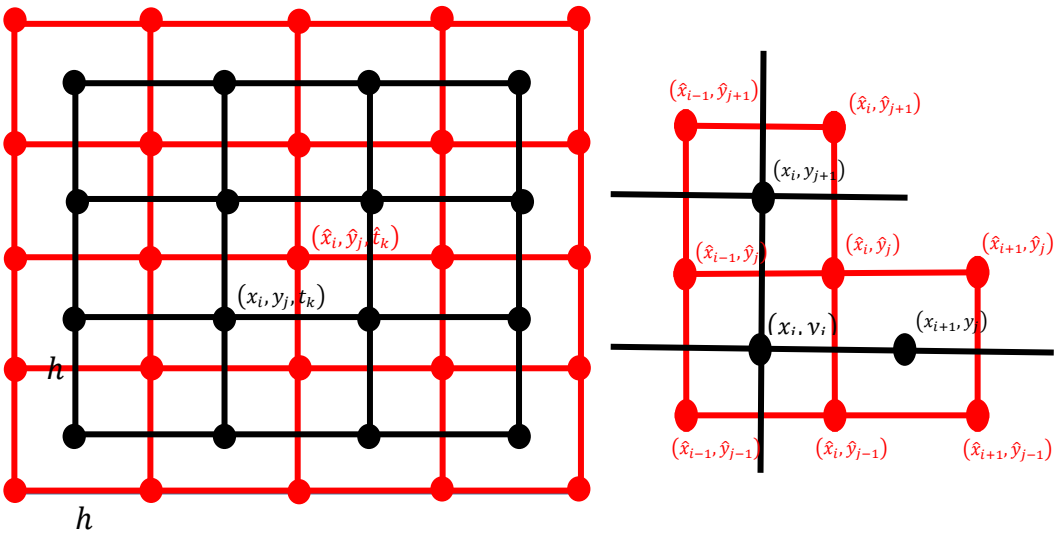

Figure 12. (left) main and sub nodes on square domain. (right) nodes that are used in adaptive scheme.

Adaptive Scheme for Tip Cell Density and Forward Time Scheme for VEGF and Fibronectin concentration

Firstly, we consider equations (153) and (154). Each main nodes is surrounded by four sub nodes and so that the equations (153) and (154) are defined as

$$\begin{aligned}\boldsymbol{u}_{i,j}^k &= \left(u_{i,j,1}^k, u_{i,j,2}^k\right) \\ &= \left(\frac{1}{2}\left(\frac{c_{i,j}^k - c_{i-1,j}^k}{h} + \frac{c_{i,j-1}^k - c_{i-1,j-1}^k}{h}\right), \frac{1}{2}\left(\frac{c_{i,j}^k - c_{i,j-1}^k}{h} + \frac{c_{i-1,j}^k - c_{i-1,j-1}^k}{h}\right)\right),\end{aligned} \tag{159}$$

$$\begin{aligned}\boldsymbol{v}_{i,j}^k &= \left(v_{i,j,1}^k, v_{i,j,2}^k\right) \\ &= \left(\frac{1}{2}\left(\frac{f_{i,j}^k - f_{i-1,j}^k}{h} + \frac{f_{i,j-1}^k - f_{i-1,j-1}^k}{h}\right), \frac{1}{2}\left(\frac{f_{i,j}^k - f_{i,j-1}^k}{h} + \frac{f_{i-1,j}^k - f_{i-1,j-1}^k}{h}\right)\right),\end{aligned} \tag{160}$$

respectively.

Define

$$u_{i,j,1}^{k,\pm} = max\{\pm u_{i,j,1}^{k}, 0\}, \quad u_{i,j,2}^{k,\pm} = max\{\pm u_{i,j,2}^{k}, 0\}, \tag{161}$$

$$v_{i,j,1}^{k,\pm} = max\{\pm v_{i,j,1}^{k}, 0\}, \quad v_{i,j,2}^{k,\pm} = max\{\pm v_{i,j,2}^{k}, 0\}. \tag{162}$$

Then, equation (155) is written as

$$\begin{aligned} \boldsymbol{G}_{i,j}^{k} &= \left(G_{i,j,1}^{k}, G_{i,j,2}^{k}\right) \\ &= \left(\chi_1 u_{i,j,1}^{k} + \rho_1 v_{i,j,1}^{k}, \chi_1 u_{i,j,2}^{k} + \rho_1 v_{i,j,2}^{k}\right), \end{aligned} \tag{163}$$

where

$$G_{i,j,1}^{k,\pm} = \chi_1 u_{i,j,1}^{k,\pm} + \rho_1 v_{i,j,1}^{k,\pm}, \quad G_{i,j,2}^{k,\pm} = m\chi_1 u_{i,j,2}^{k,\pm} + \rho_1 v_{i,j,2}^{k,\pm}. \tag{164}$$

Now, we consider the sub-node where $\boldsymbol{F}_{i,j}^{k}$ is defined. On the x-axis direction, we may assume that $n_{i,j}^{k}$ and $n_{i+1,j}^{k}$ is brought to $\boldsymbol{F}_{i,j}^{k}$ by the flow $G_{i,j,1}^{k,+}$ and $G_{i+1,j,1}^{k,-}$, respectively, and on the y-axis direction, we also may assume that $n_{i,j}^{k}$ and $n_{i,j+1}^{k}$ are brought to $\boldsymbol{F}_{i,j}^{k}$ by the flow $G_{i,j,2}^{k,+}$ and $G_{i,j+1,2}^{k,-}$, respectively. That is

$$\boldsymbol{F}_{i,j}^{k} = \left(F_{i,j,1}^{k}, F_{i,j,2}^{k}\right), \tag{165}$$

where

$$F_{i,j,1}^{k} = n_{i,j}^{k} G_{i,j,1}^{k,+} - n_{i+1,j}^{k} G_{i+1,j,1}^{k,-}, \tag{166}$$

$$F_{i,j,2}^{k} = n_{i,j}^{k} G_{i,j,2}^{k,+} - n_{i,j+1}^{k} G_{i,j+1,2}^{k,-}. \tag{167}$$

Hence, the numerical scheme for $n_{i,j}^{k}$ is written as

$$\frac{n_{i,j}^{k+1}-n_{i,j}^{k}}{\tau}=D_1\left(\frac{n_{i+1,j}^{k}-2n_{i,j}^{k}+n_{i-1,j}^{k}}{h^2}+\frac{n_{i,j+1}^{k}-2n_{i,j}^{k}+n_{i,j-1}^{k}}{h^2}\right)$$

$$-\left(\frac{F_{i,j,1}^{k}-F_{i-1,j,1}^{k}}{h}+\frac{F_{i,j,2}^{k}-F_{i,j-1,2}^{k}}{h}\right). \tag{168}$$

For c and f, we use forward time scheme which is written as

$$\frac{c_{i,j}^{k+1}-c_{i,j}^{k}}{\tau}=\eta_1 n_{i,j}^{k}c_{i,j}^{k}, \tag{169}$$

$$\frac{f_{i,j}^{k+1}-f_{i,j}^{k}}{\tau}=\beta_1 n_{i,j}^{k}-\eta_2 n_{i,j}^{k}f_{i,j}^{k}, \tag{170}$$

respectively.

Hybrid Discrete-Continuous Technique

To simulate the pattern formation of blood vessel network, we assume the stalk cells are recruited from the pre-existing vessel and follow the tip cell as it moves so that the vessel network is generated due to the movement of tip cell. To track the movement of tip cell, we rewrite scheme (168) as

$$\begin{aligned}n_{i,j}^{k+1}&=n_{i,j}^{k}+\frac{\tau D_n}{h^2}\left(n_{i+1,j}^{k}+n_{i-1,j}^{k}+n_{i,j+1}^{k}+n_{i,j-1}^{k}-4n_{i,j}^{k}\right)\\&\quad-\frac{\tau}{h}\left(n_{i,j}^{k}G_{i,j,1}^{k,+}-n_{i+1,j}^{k}G_{i+1,j,1}^{k,-}-n_{i-1,j}^{k}G_{i-1,j,1}^{k,+}+n_{i,j}^{k}G_{i,j,1}^{k,-}\right.\\&\quad\left.+n_{i,j}^{k}G_{i,j,2}^{k,+}-n_{i,j+1}^{k}G_{i,j+1,2}^{k,-}-n_{i,j-1}^{k}G_{i,j-1,2}^{k,+}+n_{i,j}^{k}G_{i,j,2}^{k,-}\right).\\&=n_{i,j}^{k}P_{i,j}^{k,0}+n_{i+1,j}^{k}P_{i+1,j}^{k,1}+n_{i-1,j}^{k}P_{i-1,j}^{k,2}+n_{i,j+1}^{k}P_{i,j+1}^{k,3}\\&\quad+n_{i,j-1}^{k}P_{i,j-1}^{k,4}\end{aligned} \tag{171}$$

by substituting (166) and (167). $P_{i,j}^{k,0}$, $P_{i+1,j}^{k,1}$, $P_{i-1,j}^{k,2}$, $P_{i,j+1}^{k,3}$ are written as

$$P_{i,j}^{k,0} = 1 - 4\frac{\tau D_1}{h^2} - \frac{\tau}{h}\left(G_{i,j,1}^{k,+} + G_{i,j,1}^{k,-} + G_{i,j,2}^{k,+} + G_{i,j,2}^{k,-}\right), \quad (172)$$

$$P_{i+1,j}^{k,1} = \frac{\tau D_1}{h^2} + \frac{\tau}{h} G_{i+1,j,1}^{k,-}, \quad (173)$$

$$P_{i-1,j}^{k,2} = \frac{\tau D_1}{h^2} + \frac{\tau}{h} G_{i-1,j,1}^{k,+}, \quad (174)$$

$$P_{i,j+1}^{k,3} = \frac{\tau D_1}{h^2} + \frac{\tau}{h} G_{i,j+1,2}^{k,-}, \quad (175)$$

$$P_{i,j-1}^{k,4} = \frac{\tau D_1}{h^2} + \frac{\tau}{h} G_{i,j-1,2}^{k,+}. \quad (176)$$

The last expression of (171) means that to get the information of n on the main node (i,j) at time step $k+1$, we need the information on four its neighbor main nodes $(i+1,j)$, $(i-1,j)$, $(i,j+1)$, and $(i,j-1)$ and main node (i,j) at previous time step, k. These information are proportional to the value of n and some weight values $P_{i,j}^{k,0}$, $P_{i+1,j}^{k,1}$, $P_{i-1,j}^{k,2}$, $P_{i,j+1}^{k,3}$, and $P_{i,j-1}^{k,4}$. We might assume the weight values are probability of a tip cell to stay at, jump from right, left, upper, and down to main node (i,j) (Figure 13:left). Then,

$$\begin{aligned} P_{i,j}^{k,0} &= 1 - 4\frac{\tau D_1}{h^2} - \frac{\tau}{h}\left(G_{i,j,1}^{k,+} + G_{i,j,1}^{k,-} + G_{i,j,2}^{k,+} + G_{i,j,2}^{k,-}\right) \\ &= 1 - \left(P_{i,j}^{k,1} + P_{i,j}^{k,2} + P_{i,j}^{k,3} + P_{i,j}^{k,4}\right) \end{aligned} \quad (177)$$

$$P_{i,j}^{k,1} = \frac{\tau D_1}{h^2} + \frac{\tau}{h} G_{i,j,1}^{k,-}, \quad (178)$$

$$P_{i,j}^{k,2} = \frac{\tau D_1}{h^2} + \frac{\tau}{h} G_{i,j,1}^{k,+}, \quad (179)$$

$$P_{i,j}^{k,3} = \frac{\tau D_1}{h^2} + \frac{\tau}{h} G_{i,j,2}^{k,-}, \quad (180)$$

$$P_{i,j}^{k,4} = \frac{\tau D_1}{h^2} + \frac{\tau}{h} G_{i,j,2}^{k,+}, \tag{181}$$

can be regarded as probability of tip cell to stay at, move to left, right, down, and upper from main node (i,j), respectively (Figure 13:right). On the boundary, we set

$$\begin{aligned} P_{i,j}^{k,1} &= 0, \quad i = 1, \forall j, \\ P_{i,j}^{k,2} &= 0, \quad i = N, \forall j, \\ P_{i,j}^{k,3} &= 0, \quad j = 1, \forall i, \\ P_{i,j}^{k,4} &= 0, \quad j = N, \forall i. \end{aligned} \tag{182}$$

Hence, we can use (177)-(181) as the movement probability of tip cells at every time step.

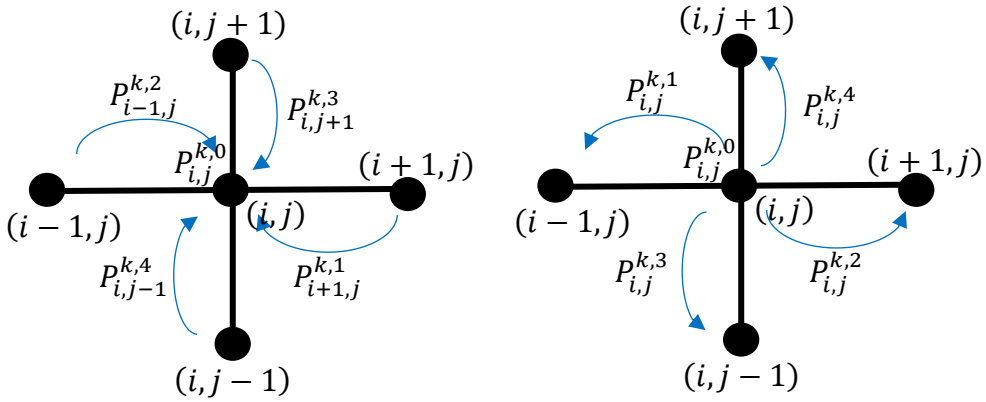

Figure 13. (left) Information nodes to calculate n at node (i,j). (right) P can be thought as jump probability of a component from (i,j) to any 4 nodes.

To track the movement of tip cells and form the blood vessel network, we use Boolean value (1 or 0) for tip cell, denoted as n_*, to indicate the presence of tip cell at given node. By this method, the scheme (169)-(170) now are written as

$$\frac{c_{i,j}^{k+1} - c_{i,j}^{k}}{\tau} = \eta_1 (\widehat{n_*})_{i,j}^{k} c_{i,j}^{k}, \tag{183}$$

$$\frac{f_{i,j}^{k+1} - f_{i,j}^{k}}{\tau} = \beta_1 (\widehat{n_*})_{i,j}^{k} - \eta_2 (n_*)_{i,j}^{k} f_{i,j}^{k}, \tag{184}$$

with

$$(\widehat{n_*})_{i,j}^{k} = \begin{cases} 1, & (n_*)_{i,j}^{k} + (n_*)_{i+1,j}^{k} + (n_*)_{i,j+1}^{k} + (n_*)_{i+1,j+1}^{k} \geq 1, \\ 0, & \text{otherwise} \end{cases}. \tag{185}$$

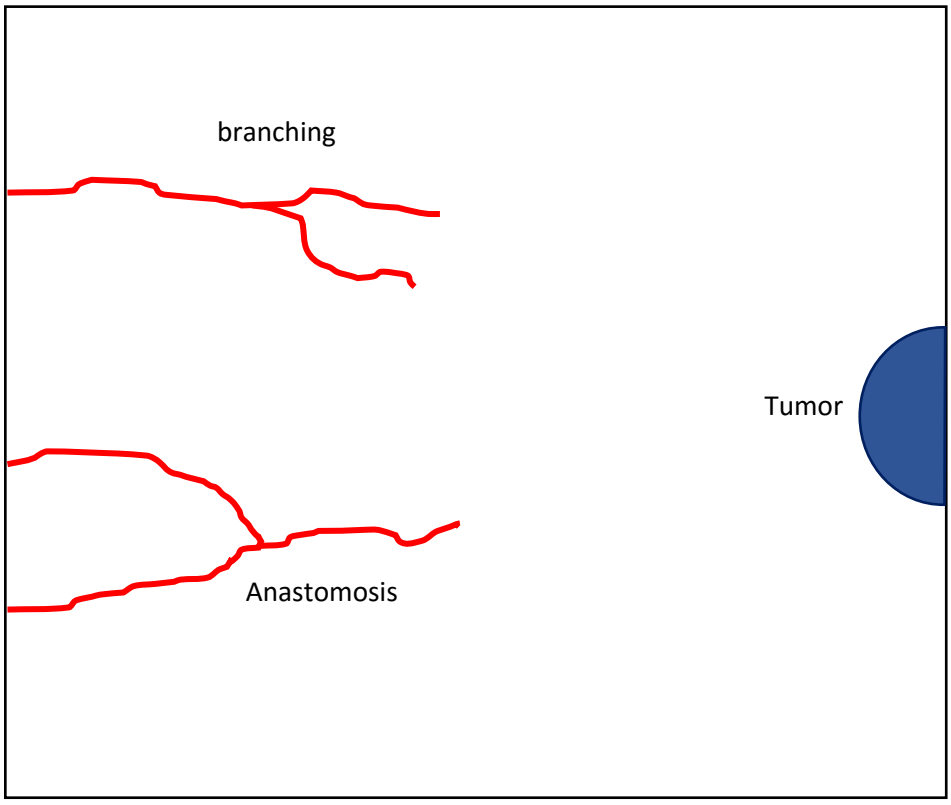

Figure 14. An illustration of branching and anastomosis schematic.

Branching and Anastomosis Rules

Figure 14 gives us an illustration to the rule of branching (tip cell proliferation) and anastomosis (loop formation). Assume that the probability of generating new sprouts (branching) from the existing sprouts is proportional to the concentration of VEGF and is formulated as

$$P_{branching} = \begin{cases} 0, & 0 \le c < 0.25 \\ 0.3, & 0.25 \le c < 0.45 \\ 0.4, & 0.45 \le c < 0.60. \\ 0.5, & 0.60 \le c < 0.70 \\ 1, & 0.70 \le c < 1.00 \end{cases} \quad (186)$$

We also assume the life time of tip cell must exceed the threshold age before branching. We use $T_{branching} = 0.25$. We assume only one of original sprouts continue to grow if anastomosis occurs.

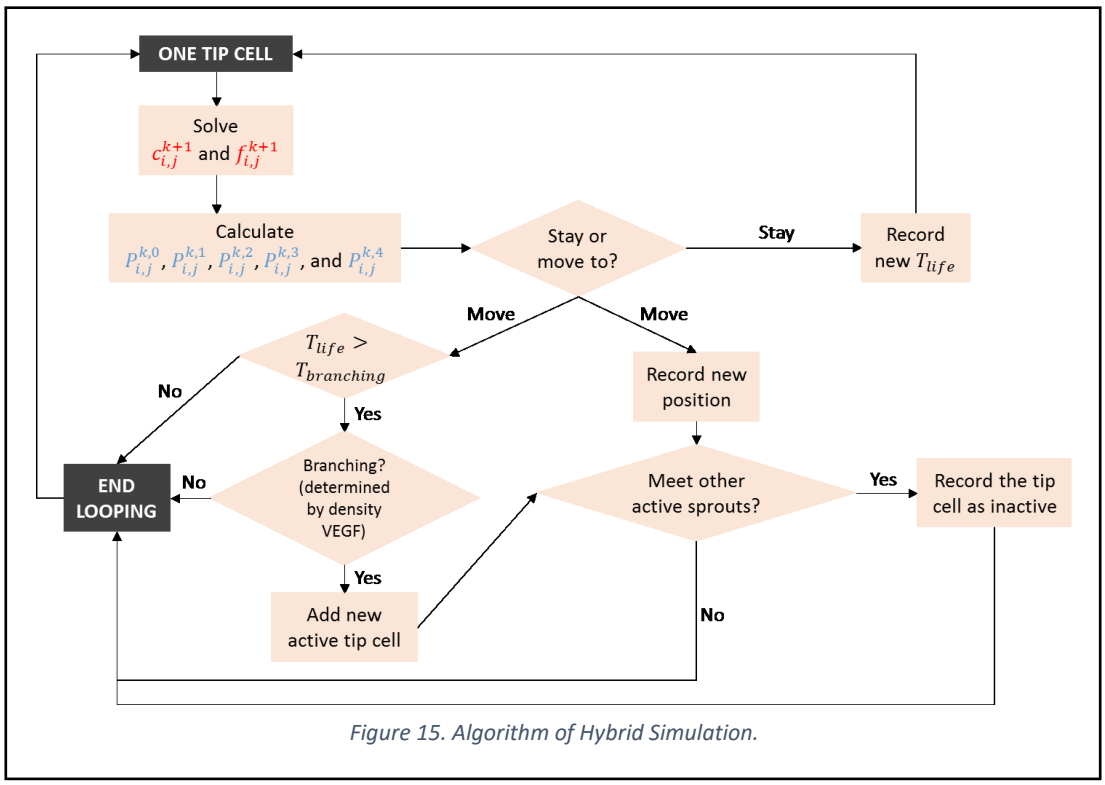

Figure 15. Algorithm of Hybrid Simulation.

Figure 15 shows the flow of the algorithm of hybrid simulation. These flow is done for every time step and one tip cell. The following is the detail of steps in hybrid technique algorithm:

Suppose the position of tip cell and the value of $c_{i,j}$ and $f_{i,j}$ at time step k are determined. Then, at time step $k+1$, we do the following step:

1. Solve the scheme (183) and (184) to obtain the value of $c_{i,j}$ and $f_{i,j}$ on every sub nodes of the domain.
2. Calculate the movement probability (177)-(181).
3. Set a sequence of integers:

$$A = \left\{ q \in \mathbb{Z} | 0 \leq q < S, \qquad S \geq \frac{1}{\min\limits_{w=0,1,2,3,4} P_{i,j}^{w}} \right\} \tag{187}$$

4. For each probability (177)-(181), set independent sub sequence $B_i \subseteq A$, $B_i \ni q \notin B_j, i \neq j$ by choosing randomly $SP_{i,j}^{w}$ numbers.
5. Choose randomly an element of A, $z \in A$.
6. If $z \in B_0$ or $z \in B_1$ or $z \in B_2$ or $z \in B_3$ or $z \in B_4$ then set the movement as staying or moving to left or right or down or upper, respectively.
7. If the decision is 'stay', record new life time and do from step 2 for next tip cell.
8. If the tip cell meets an active sprout. Record the tip cell as inactive sprout.
9. Check the life time of tip cell. If it is greater than $T_{branching}$, check the possibility of branching using (186) by the similar technique in step 3 to 5. If the decision is said to be branching, add new tip cell and check the anastomosis of new tip cell.
10. Do step 1 to 9 for other tip cells.

Simulation Result and Discussion

The parent vessel is assumed to lie on $x = 0$, and a tumor is placed on $x = 1$. We set five initial tip cells as the leading edges of five sprouts. We also require the initial concentration of fibronectin. VEGF stimulation of endothelial cells leads to degradation of their basal lamina; consequently, fibronectin leaks from the blood and diffuses into the surrounding tissue [Hynes, 1990]. The fibronectin bound to the ECM creates a high initial concentration of fibronectin in and around the parent vessel [Clark et al, 1983]. Therefore, we take the initial concentration of fibronectin as follows:

$$f(x, y, 0) = e^{-\frac{x^2}{0.45}}. \tag{188}$$

This initial profile is named F2. In later simulations, we also assume a uniform concentration of the pre-existing fibronectin on the ECM. This profile is called F1.

The initial VEGEF concentration was modeled by two initial profiles based on the source of the tumor. We assume that VEGF has reached steady-state and sets the gradient concentration on the domain. If the tumor source is a line, the initial VEGF concentration is given by:

$$c(x, y, 0) = e^{-\frac{(1-x)^2}{0.45}}. \tag{189}$$

This initial profile is called C1. If the tumor is centered on the point $(1,1/2)$, the initial VEGF concentration is given by:

$$c(x, y, 0) = \begin{cases} 1 & , \quad 0 \le r \le 0.1 \\ \dfrac{(v - r)^2}{(v - 0.1)^2} & , \quad 0.1 < r \le 0.1 \end{cases}, \tag{190}$$

with

$$v = \frac{\left(\sqrt{5} - 0.1\right)}{\left(\sqrt{5} - 1\right)}, \tag{191}$$

$$r = \sqrt{(x-1)^2 + \left(x - \frac{1}{2}\right)^2}. \tag{192}$$

This profile is called C2. The initial profiles of VEGF and fibronectin are presented in Figure 16 and Figure 17.

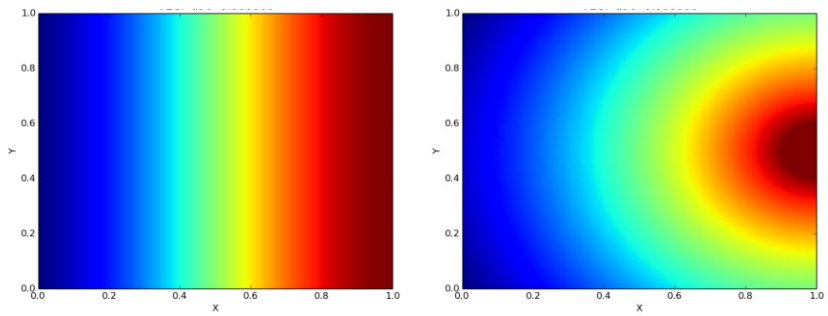

Figure 16. Initial Profile of VEGF. (left) C1 profile. (right) C2 profile

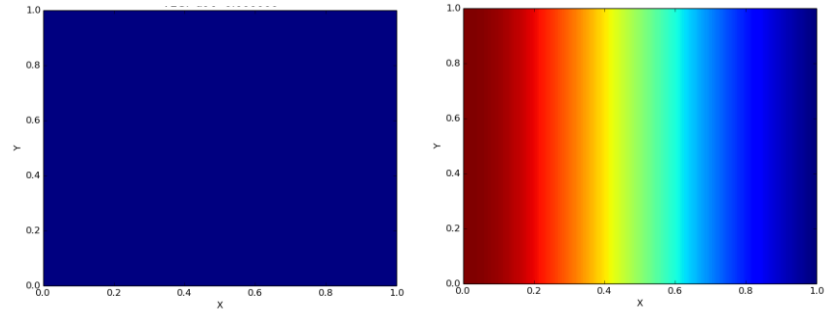

Figure 17. Initial Profile of Fibronectin. (left) F1 profile. (right) F2 profile

Initially, we observe the role of VEGF in the absence of haptotaxis. First, we assume the C1 profile and compare the simulation results for two chemotaxis saturation factors of VEGF; $\alpha_n = 0.6$ (Figure 19) and $\alpha_n = 0$ (Figure 18). At $t = 1$, the vessel

growths are identical in both simulations. Faster growth in Figure 18 than in Figure 19 becomes obvious from $t = 2$. Most of the sprouts reached the tumor at $t = 3$ in Figure 18, and at $t = 4$ in Figure 19. The growth of the vessel network is identical under profiles C1 and C2 up to $t = 4$. At this time, some of the sprouts reached the tumors under the C2 profile (compare Figure 23 with Figure 22). In the absence of a chemotaxis saturation factor for VEGF, the vessels rapidly penetrated and grow inside the tumor. This indicates that when VEGE inhibits the chemotaxis sensitivity, it inhibits the growth of the vessel network. Later, we will investigate the influence of α_n in the growth of vessel networks with both chemotaxis and haptotaxis.

For now, we consider the VEGF-uptake rate constant as a parameter. Setting $\eta_1 = 0$ and assuming the C1 profile (Figure 20), most of the sprouts reached the tumor at $t = 6$. At this stage, the tip cells tended to remain on the line source of the tumor. In contrast, a large η_1 induced a much faster approach of the sprouts to the tumor. Having reached the tumor, the tip cells tended to move backward from the tumor, forming a dense network. The same behavior emerged from the C2 profile. In Figure 24, several of the sprouts maintained their growth inside the penetrated tumor. On the C2 profile with a large η_1, a similar dense network formed after the tip cells penetrated the tumor. These phenomena can be explained by the VEGF gradient. A high η_1 reduces the VEGF concentration at the tip cells, increasing the probability of movement as the tension encourages the tip cells to move. This also confirms that the VEGF gradient drives the cells toward the tumor source.

We now incorporate both chemotaxis and haptotaxis into the simulation model. We first assume F1 as the initial fibronectin profile, and C1 and C2 as the initial VEGF profiles. Figure 26 and Figure 28 show the growth of the vessel network under a uniform initial distribution of fibronectin, i.e., $f(x, y, 0) = 0.5, \forall x, y \in [0,1] \times [0,1]$. Figure 27 and Figure 29 show the fibronectin concentration as the residue of fibronectin uptake and production rate, respectively. Comparing Figure 26 and Figure 28 with Figure 19 and Figure 23, respectively, the formation of vessel network is

similar in all cases. This shows that in the absence of a fibronectin gradient, the growth of the vessel network is unaffected by the haptotactic response.

Next, we assume F2 as the initial fibronectin profile, and C1 and C2 as the VEGF profiles. The formation of the vessel network reached steady state at $t = 3$ on position $x = 0.2$ (Figure 30 - Figure 31). At this position, the tip cells moved backward toward the parent vessel, driven by haptotactic response to the up-gradient of fibronectin. The sprouts never reached the tumor, even over an extended timeframe. With $\alpha_n = 0$, the sprouts reached steady state at $x = 0.9$ and $x = 0.2$ on profiles C1 and C2, respectively (Figure 38 - Figure 39). Some of the sprouts reached the tumor cell on profile C1, indicating that when α_n is high, the tip cells become desensitized at low VEGF, leading to steady state formation.

Setting $\beta_1 = 0$ (no fibronectin production by the tip cells) or $\eta_2 = 0$ (zero fibronectin uptake rate by the tip cells) produces no significant effect on the growth and formation of the vessel network. The simulation results under various β_1 and η_2 on both C1 and C2 profiles are presented in Figure 32 - Figure 37.

Simulation Results with chemotaxis on VEGF gradient concentration C1 profile. Some alterations on chemotaxis saturation factor and VEGF uptake rate by tip cell are performed.

Refer to Figure 16:left for C1 profile.

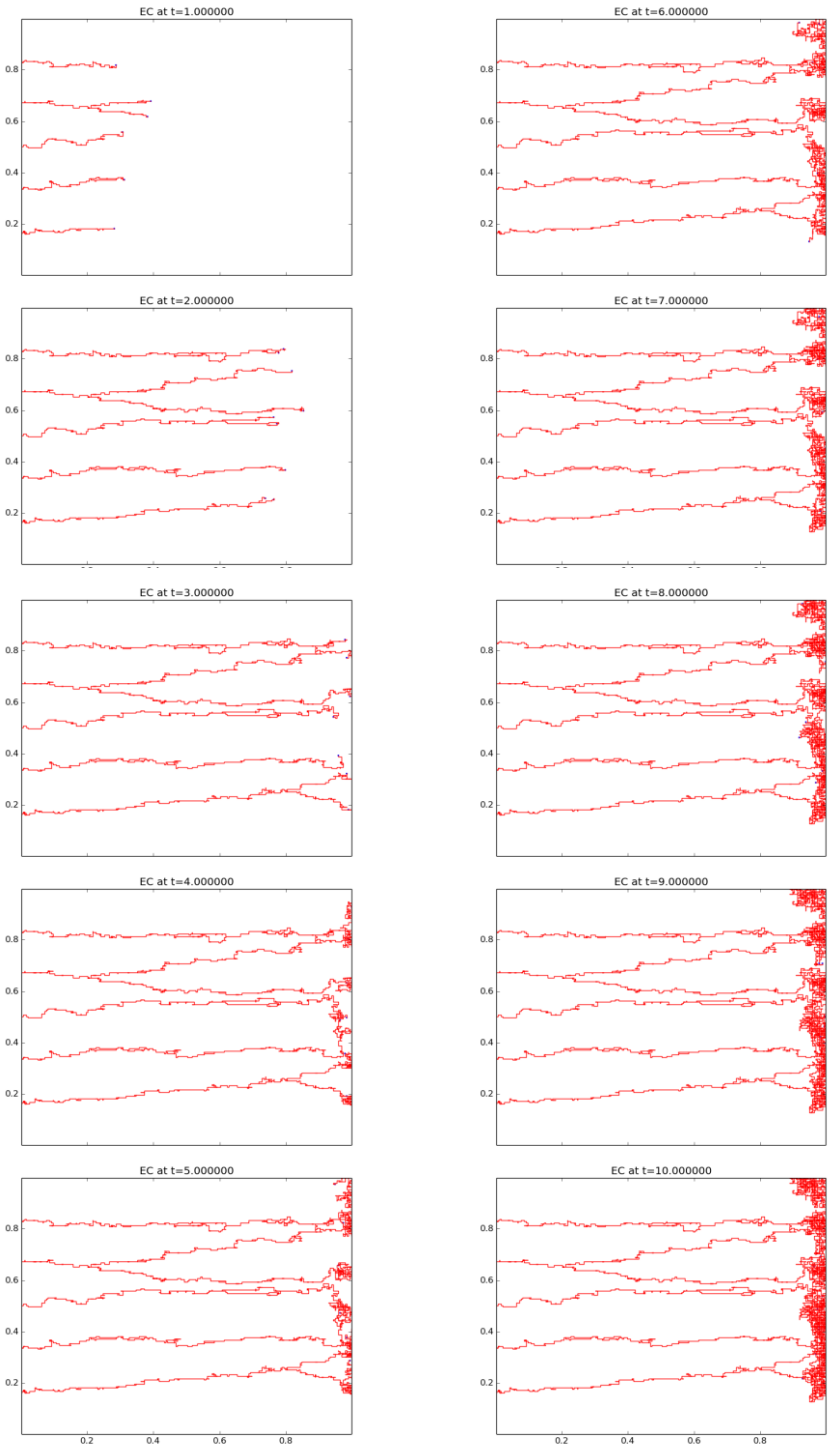

Figure 18. Growth of blood vessel network on C1 profile in the absence of haptotaxis ($\rho_1 = 0$) and chemotaxis saturation factor ($\alpha_n = 0$).

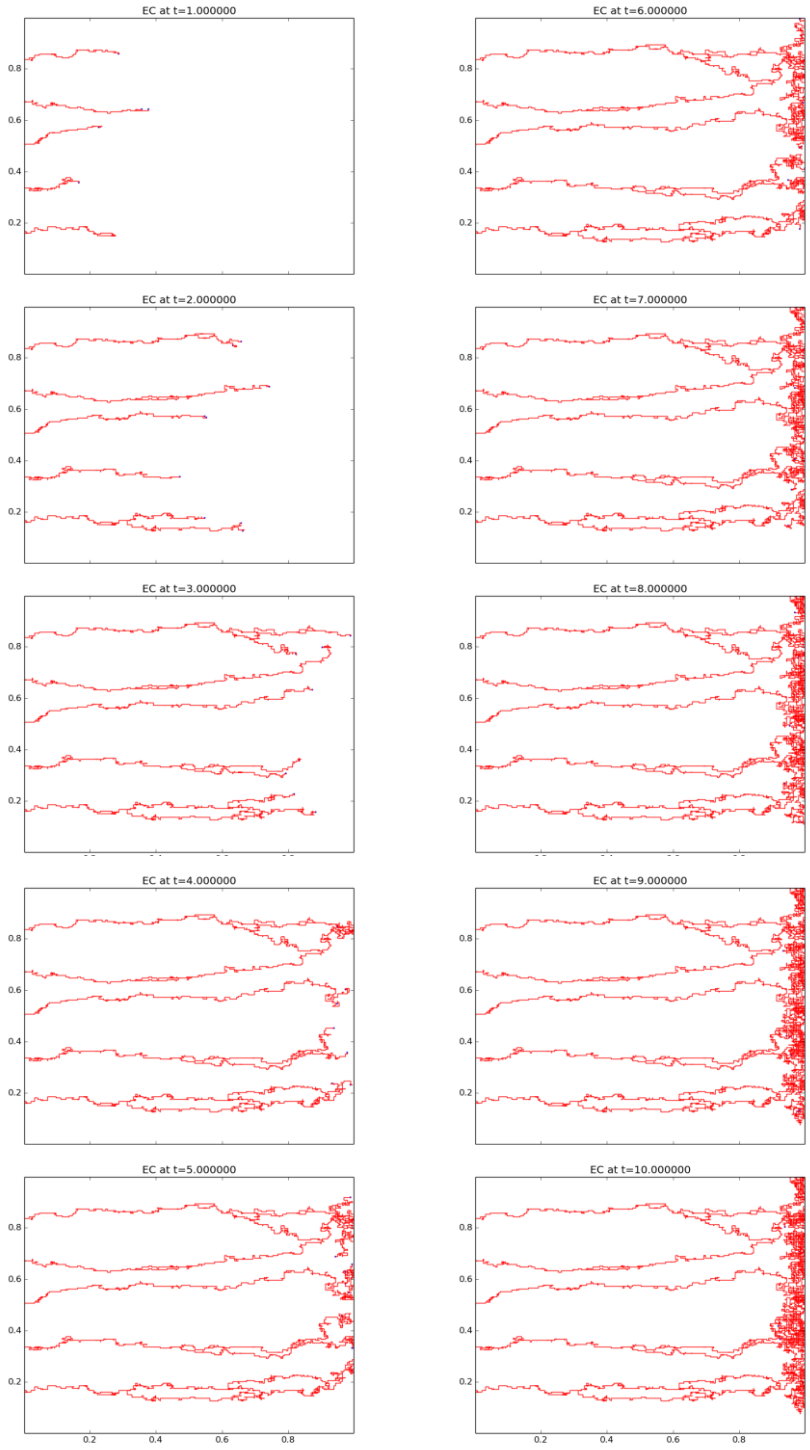

Figure 19. Growth of blood vessel network on C1 profile in the absence of haptotaxis ($\rho_1 = 0$).

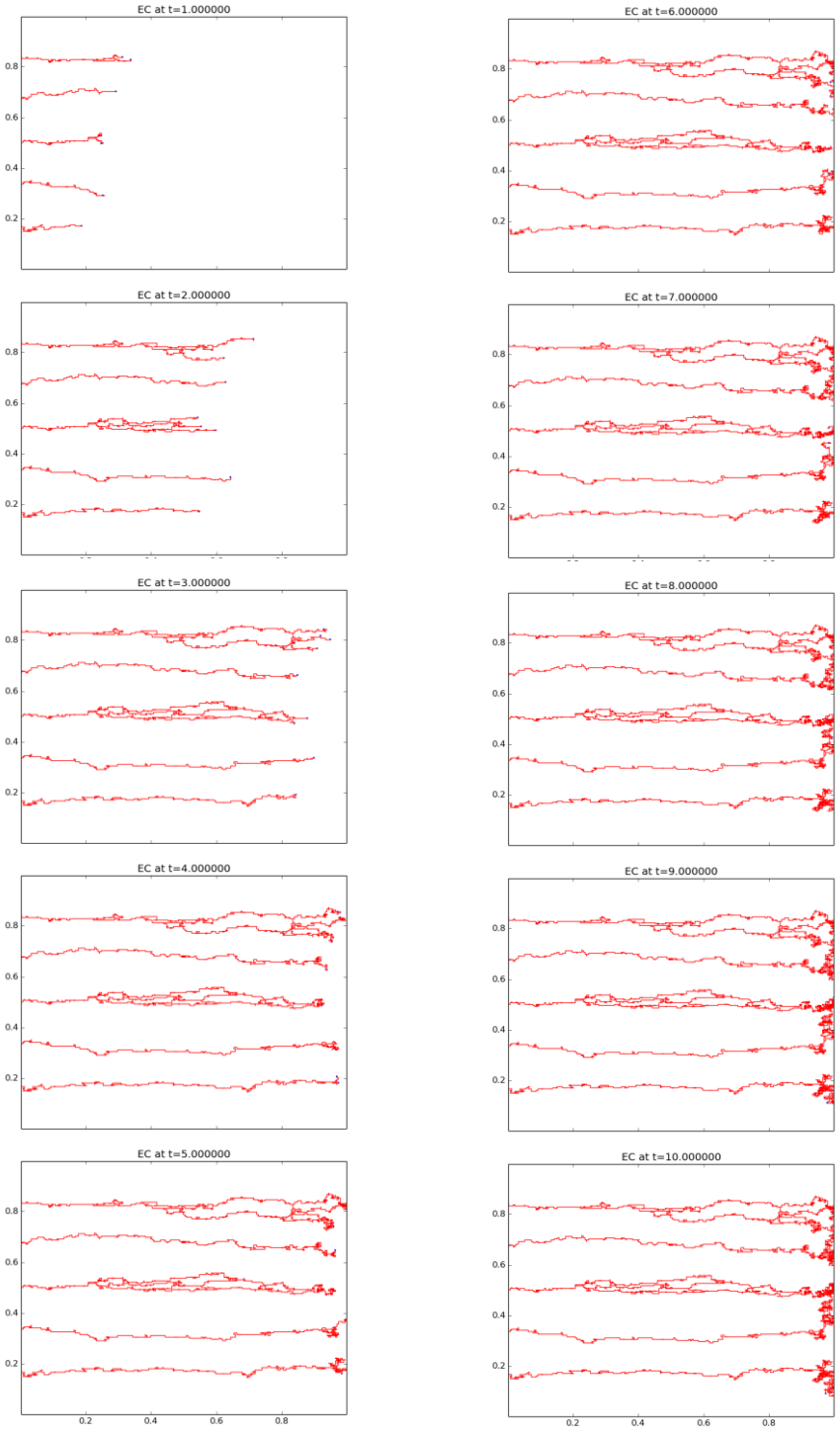

Figure 20. Growth of blood vessel network on C1 profile in the absence of haptotaxis ($\rho_1 = 0$) and uptake rate of VEGF by tip cell ($\eta_1 = 0$).

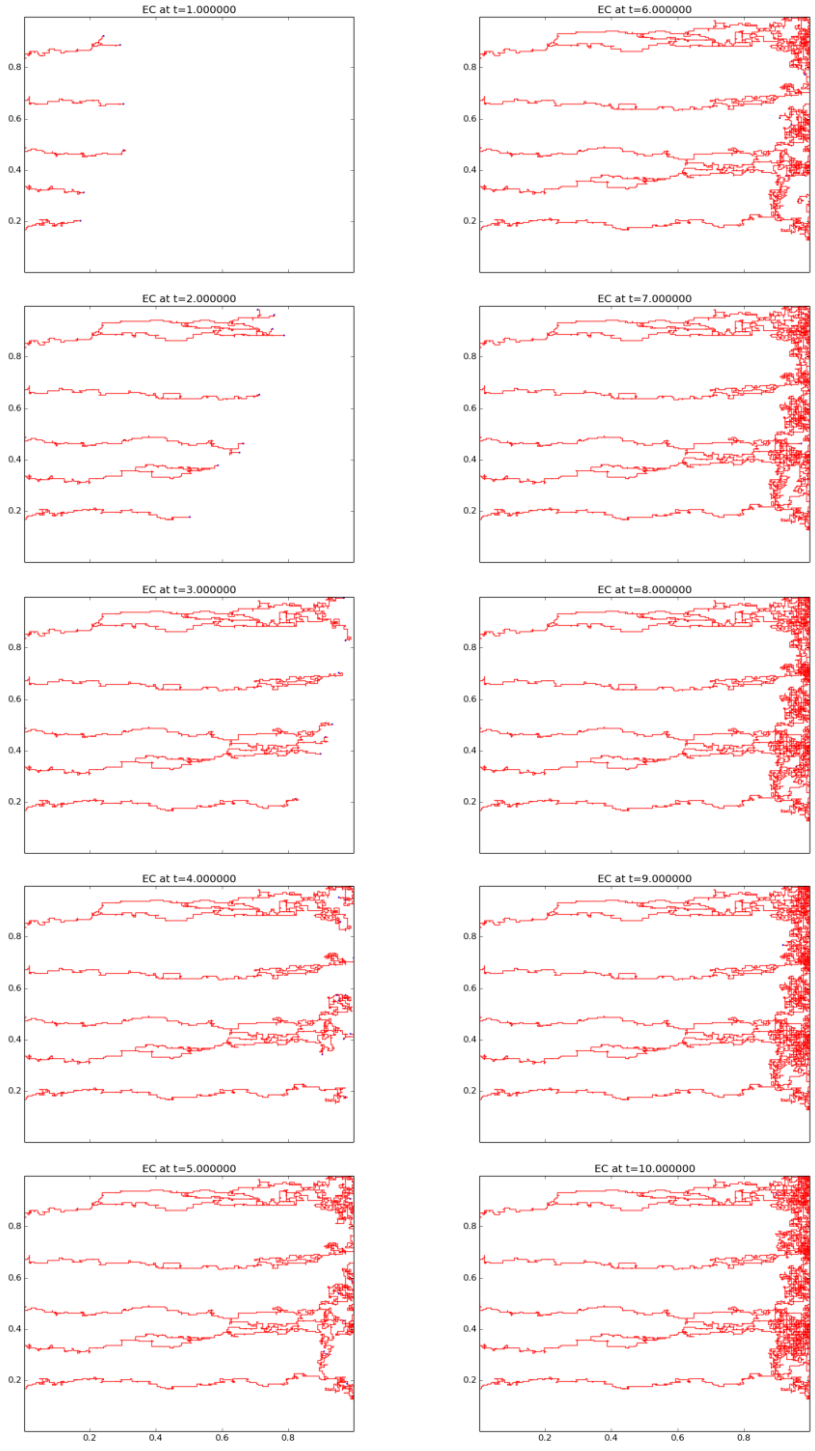

Figure 21. Growth of blood vessel network on C1 profile in the absence of haptotaxis ($\rho_1 = 0$). The uptake rate of VEGF by tip cell is increased three times ($\eta_1 = 0.3$).

Simulation Results with
chemotaxis on VEGF gradient concentration C2 profile. Some alterations on chemotaxis saturation factor and VEGF uptake rate by tip cell are performed.

Refer to Figure 16:right for C2 profile.

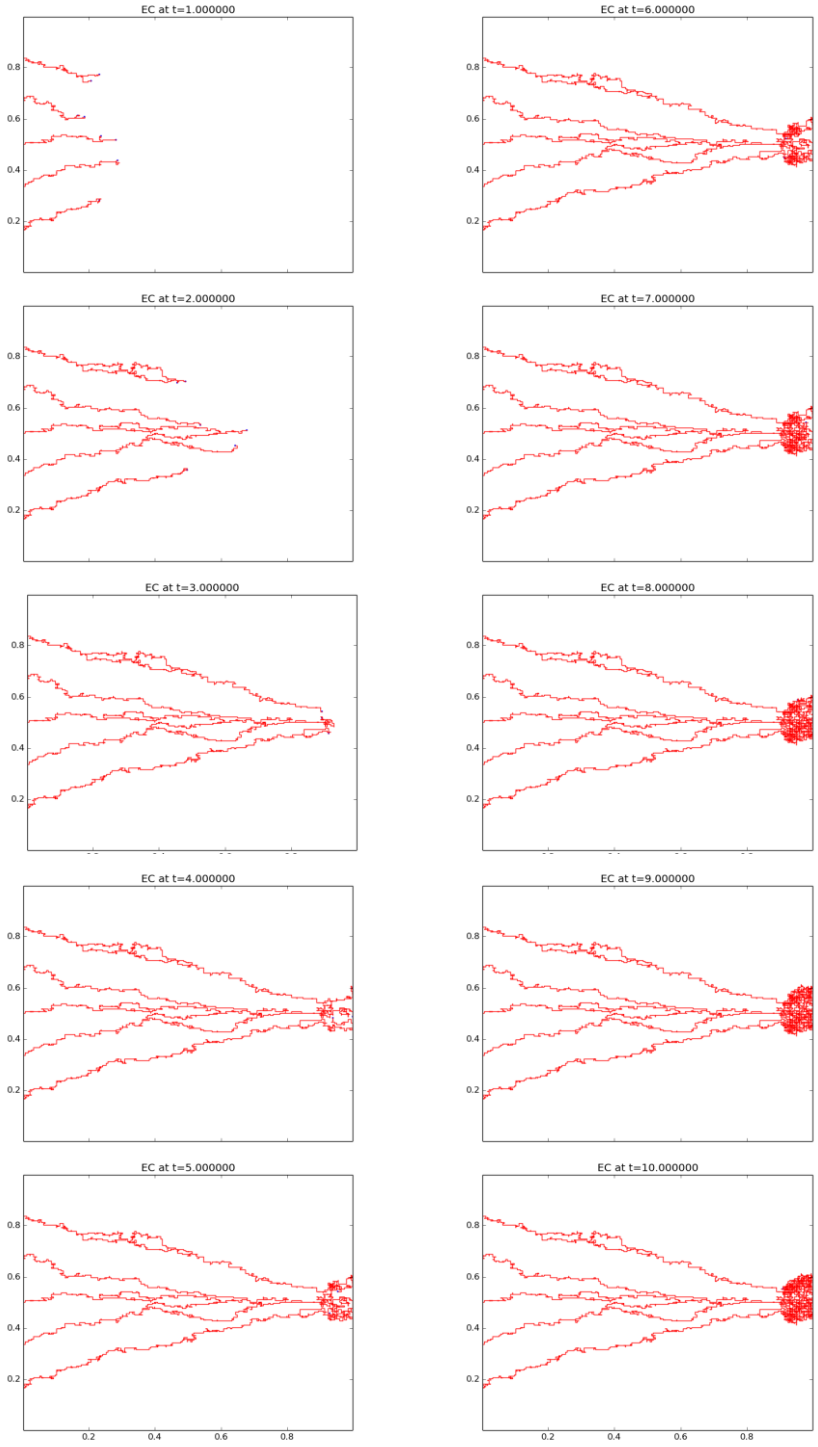

Figure 22. Growth of blood vessel network on C2 profile in the absence of haptotaxis ($\rho_1 = 0$) and chemotaxis saturation factor ($\alpha_n = 0$).

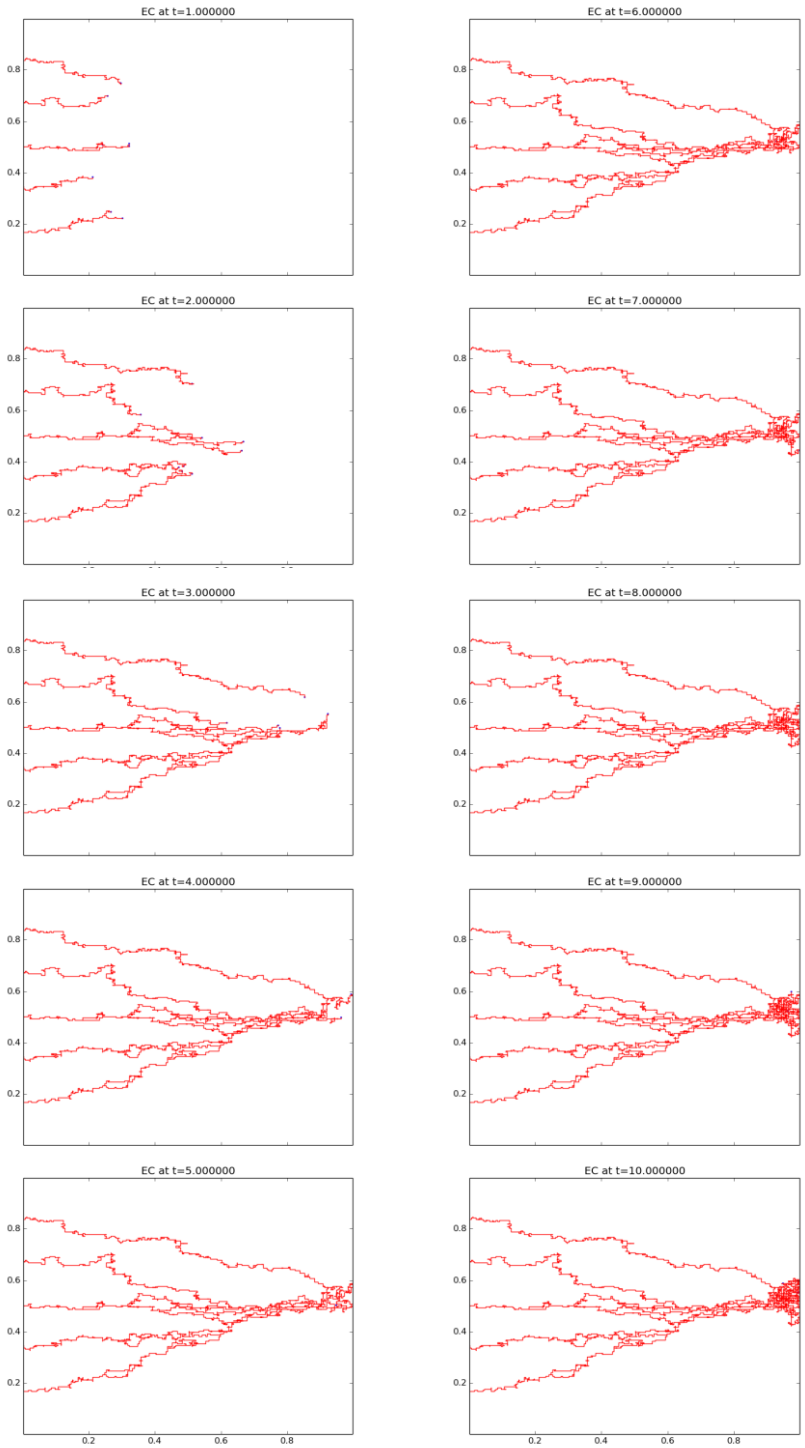

Figure 23. Growth of blood vessel network on C2 profile in the absence of haptotaxis ($\rho_1 = 0$).

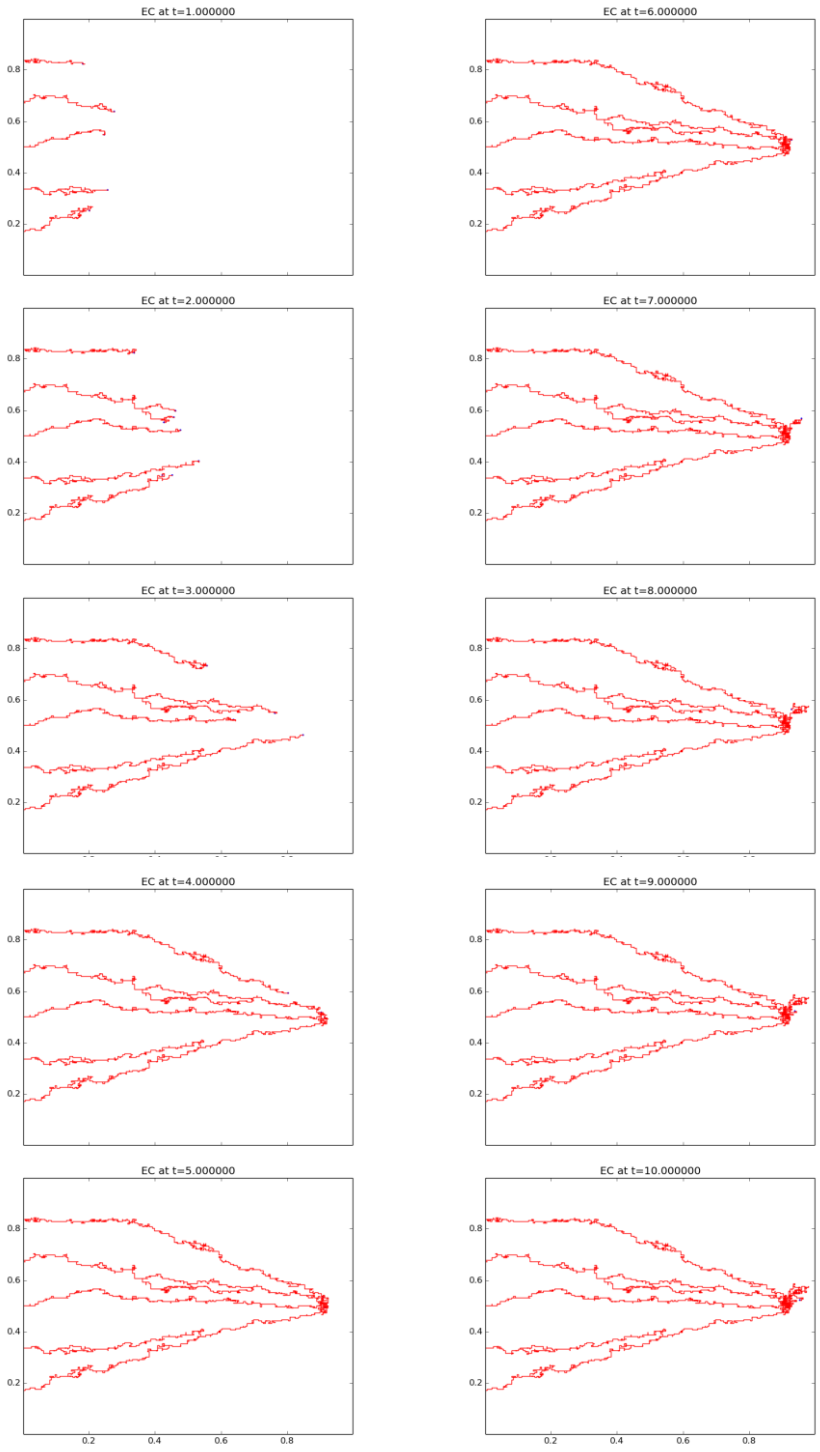

Figure 24. Growth of blood vessel network on C2 profile in the absence of haptotaxis ($\rho_1 = 0$) and uptake rate of VEGF by tip cell ($\eta_1 = 0$).

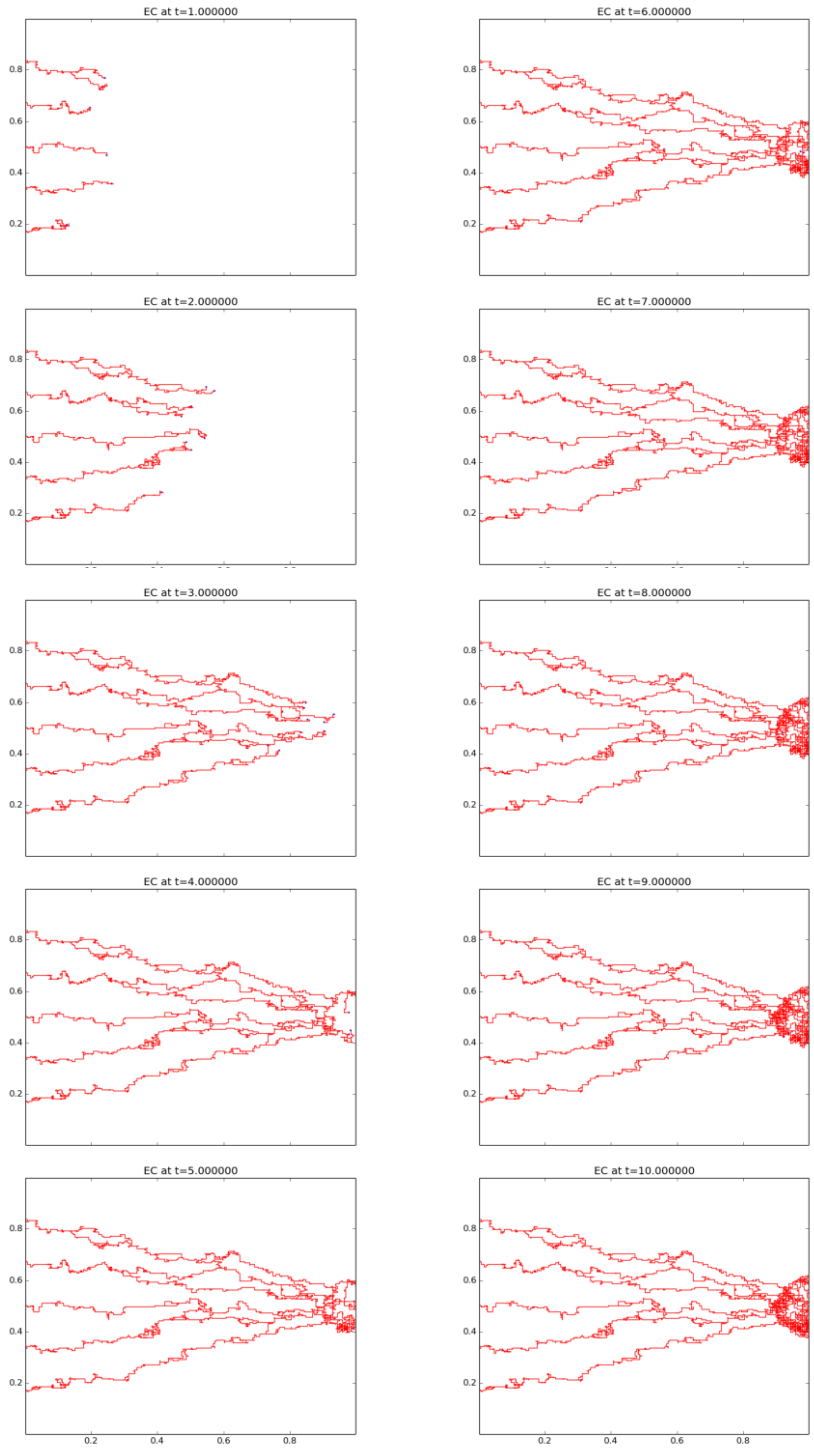

Figure 25. Growth of blood vessel network on C1 profile in the absence of haptotaxis ($\rho_1 = 0$). The uptake rate of VEGF by tip cell is increased three times ($\eta_1 = 0.3$).

Simulation Results with chemotaxis on C1 and C2 profile and haptotaxis on fibronectin concentration F1 profile, respectively. No alteration on parameters is performed.

Refer to Figure 16 for C1 and C2 profile, Figure 17:left for F1 profile, and Figure 19 and Figure 23 for comparison.

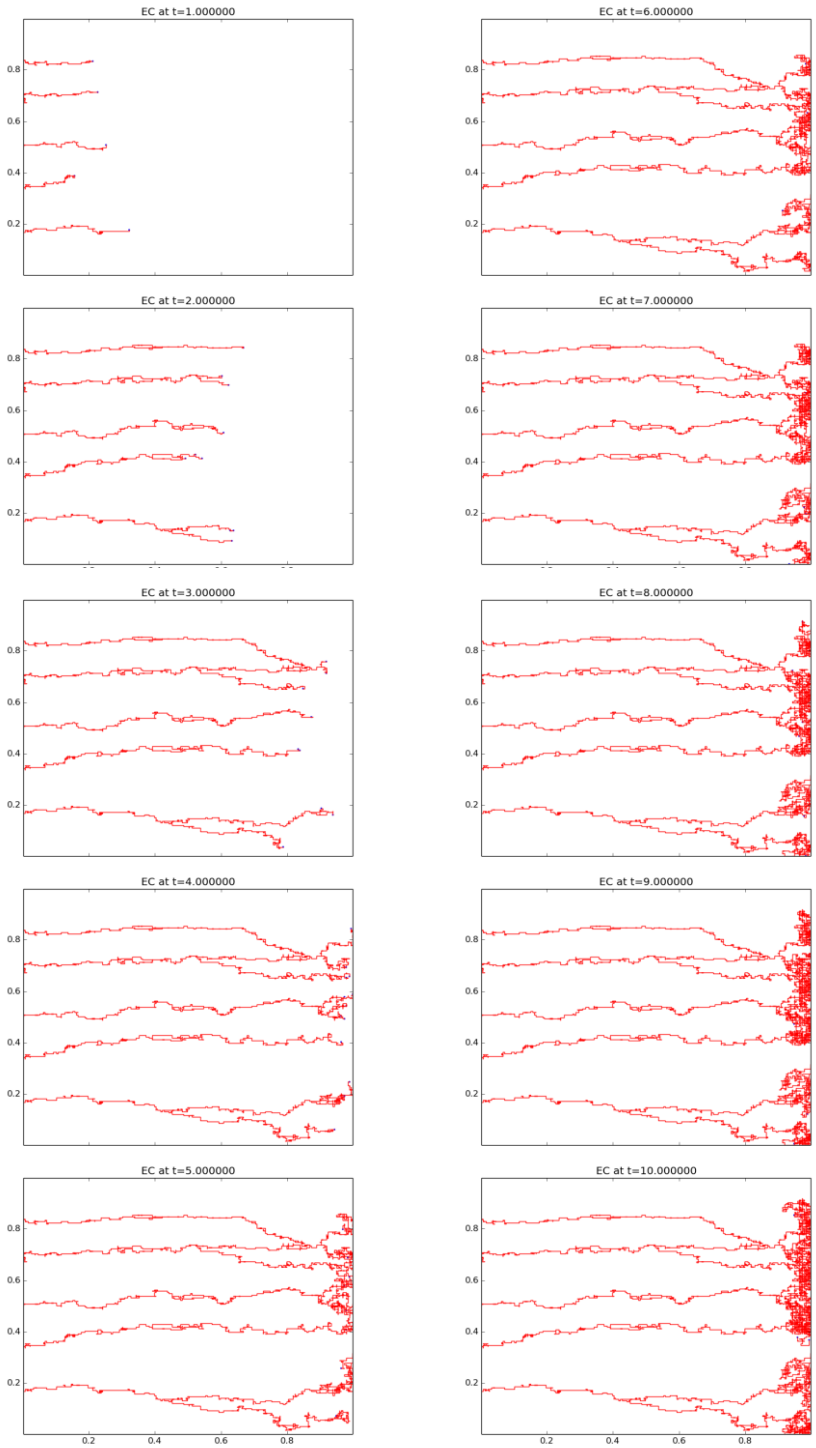

Figure 26. Growth of blood vessel network on C1 and F1 profile with both chemotaxis and haptotaxis.

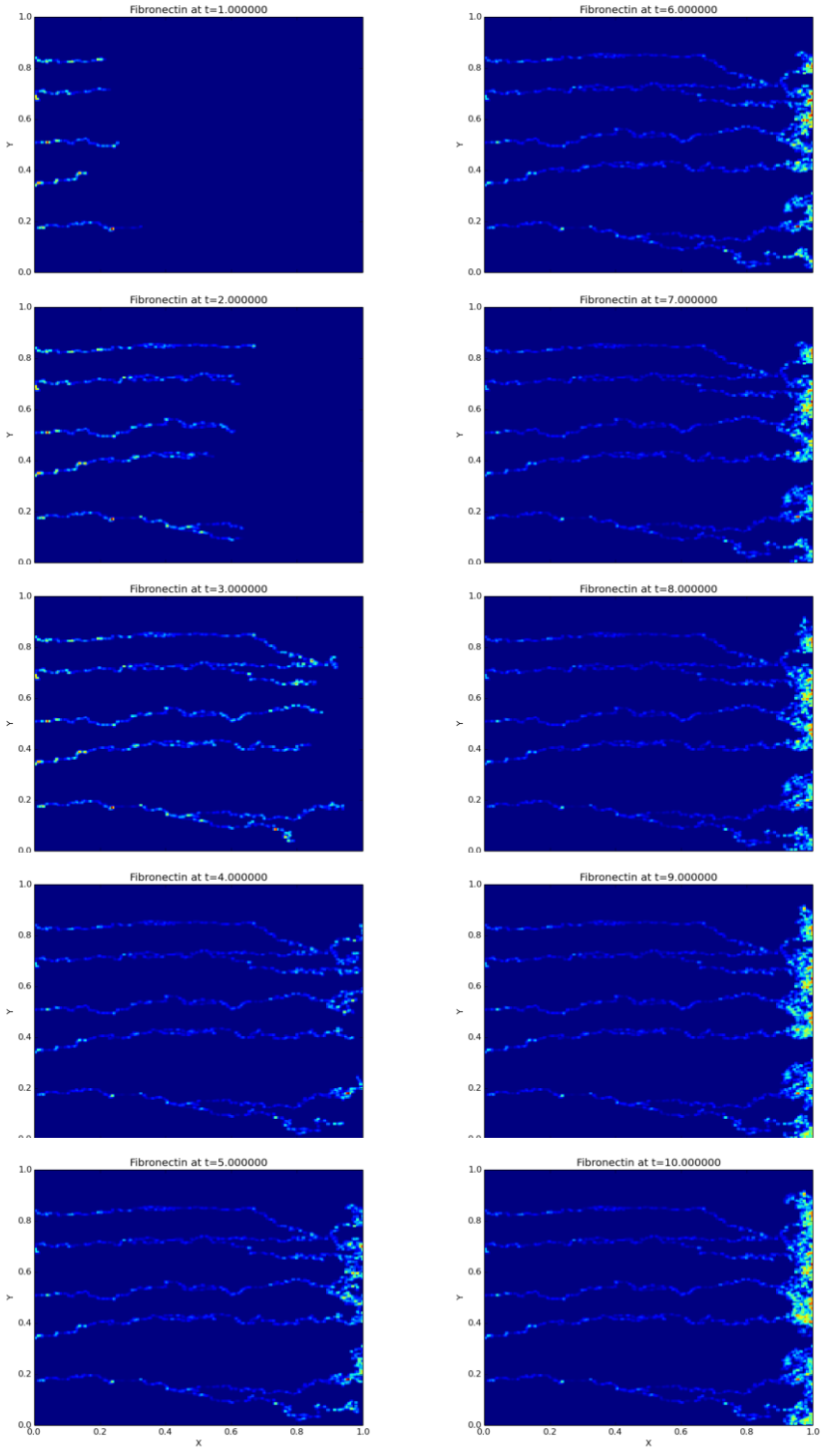

Figure 27. Density of fibronectin on the domain (along the simulation of growth vessel network in Figure 26.

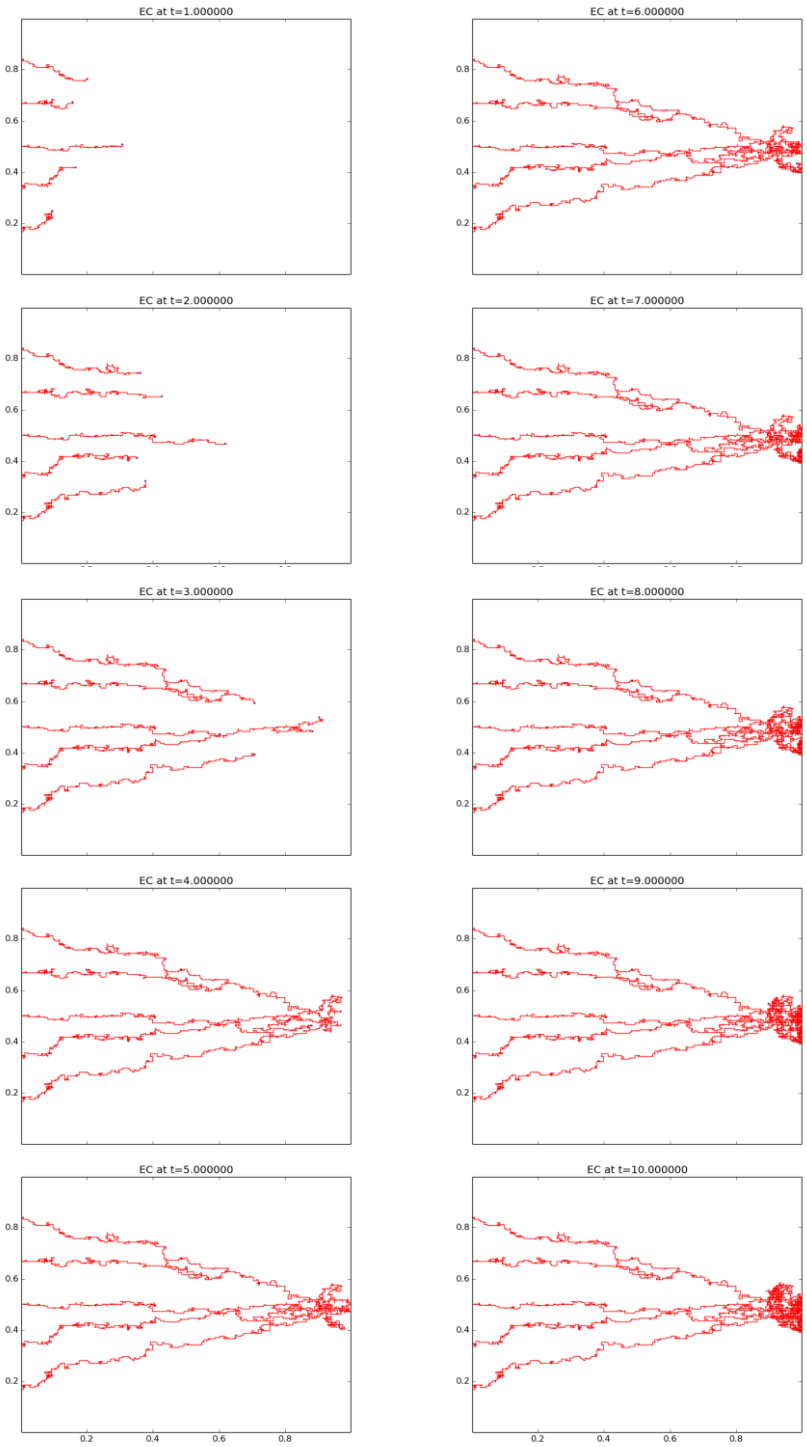

Figure 28. Growth of blood vessel network on C2 and F1 profile with both chemotaxis and haptotaxis.

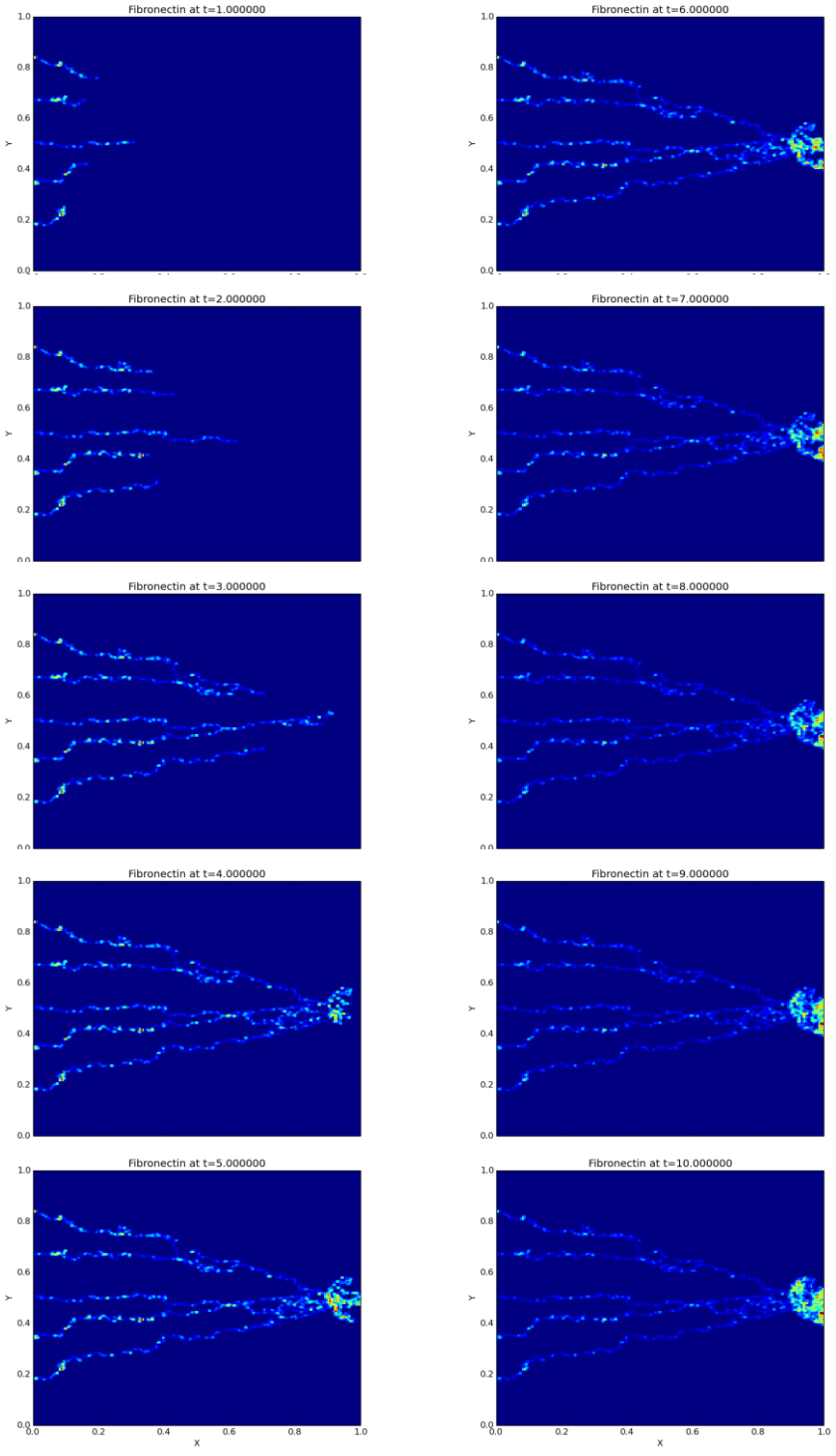

Figure 29. Density of fibronectin on the domain (along the simulation of growth vessel network in Figure 28.

Simulation Results with chemotaxis on C1 and C2 profile and haptotaxis on F2 profile.

Refer to Figure 16 for C1 and C2 profile, Figure 17:right for F2 profile, and Figure 19 and Figure 23 for comparison

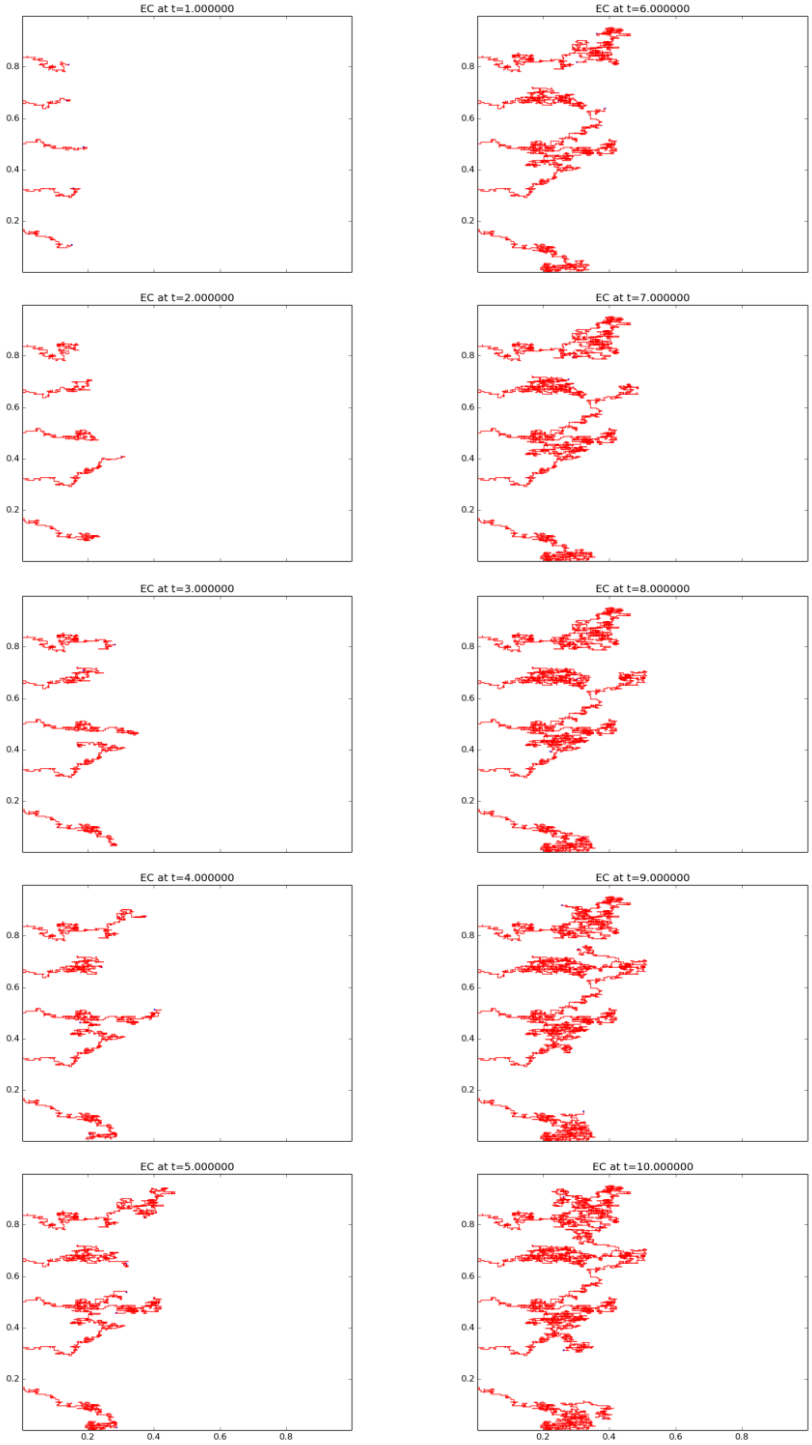

Continue to next page.

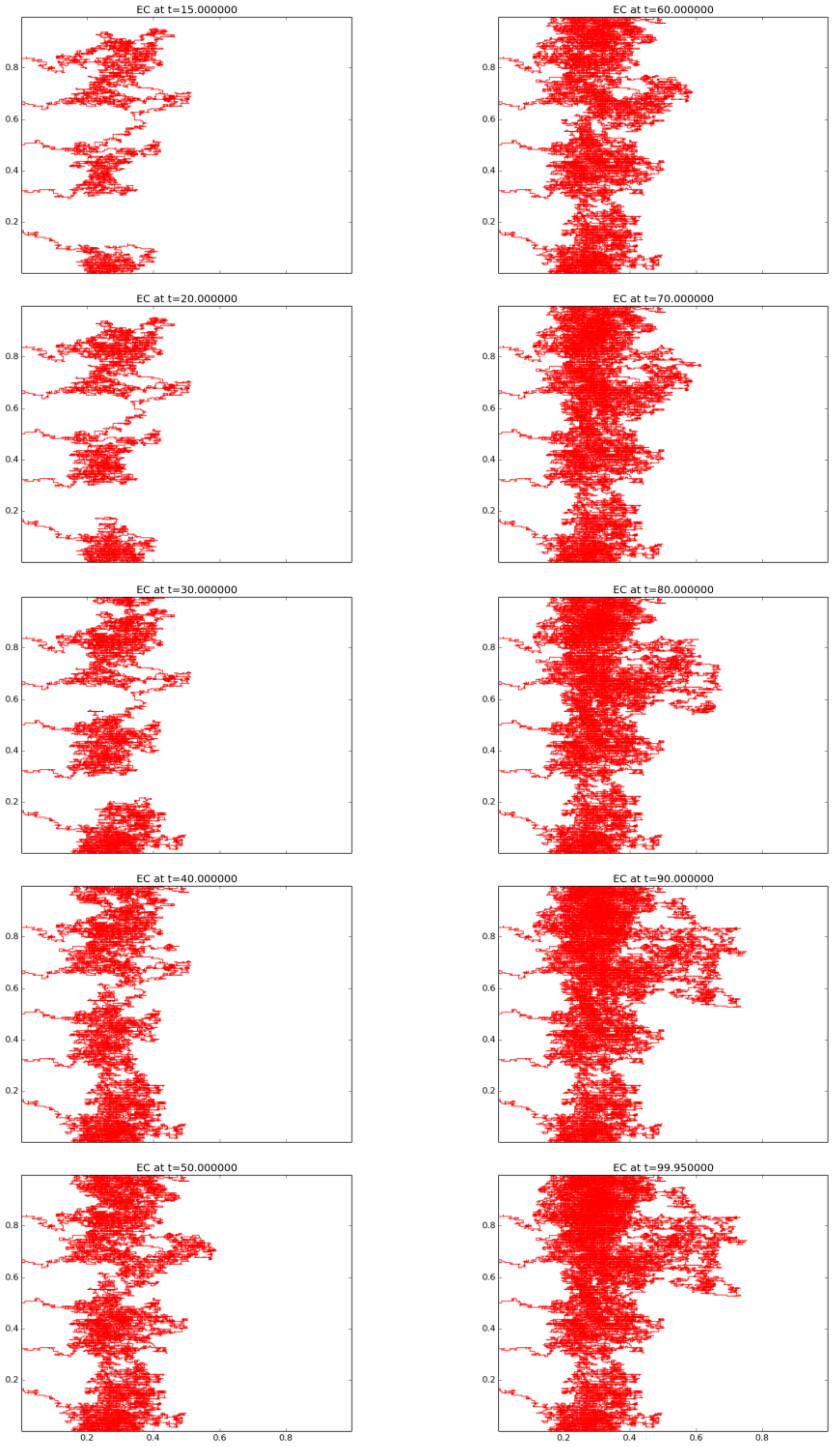

Figure 30. Growth of blood vessel network on C1 and F2 initial profile with both chemotaxis and haptotaxis.

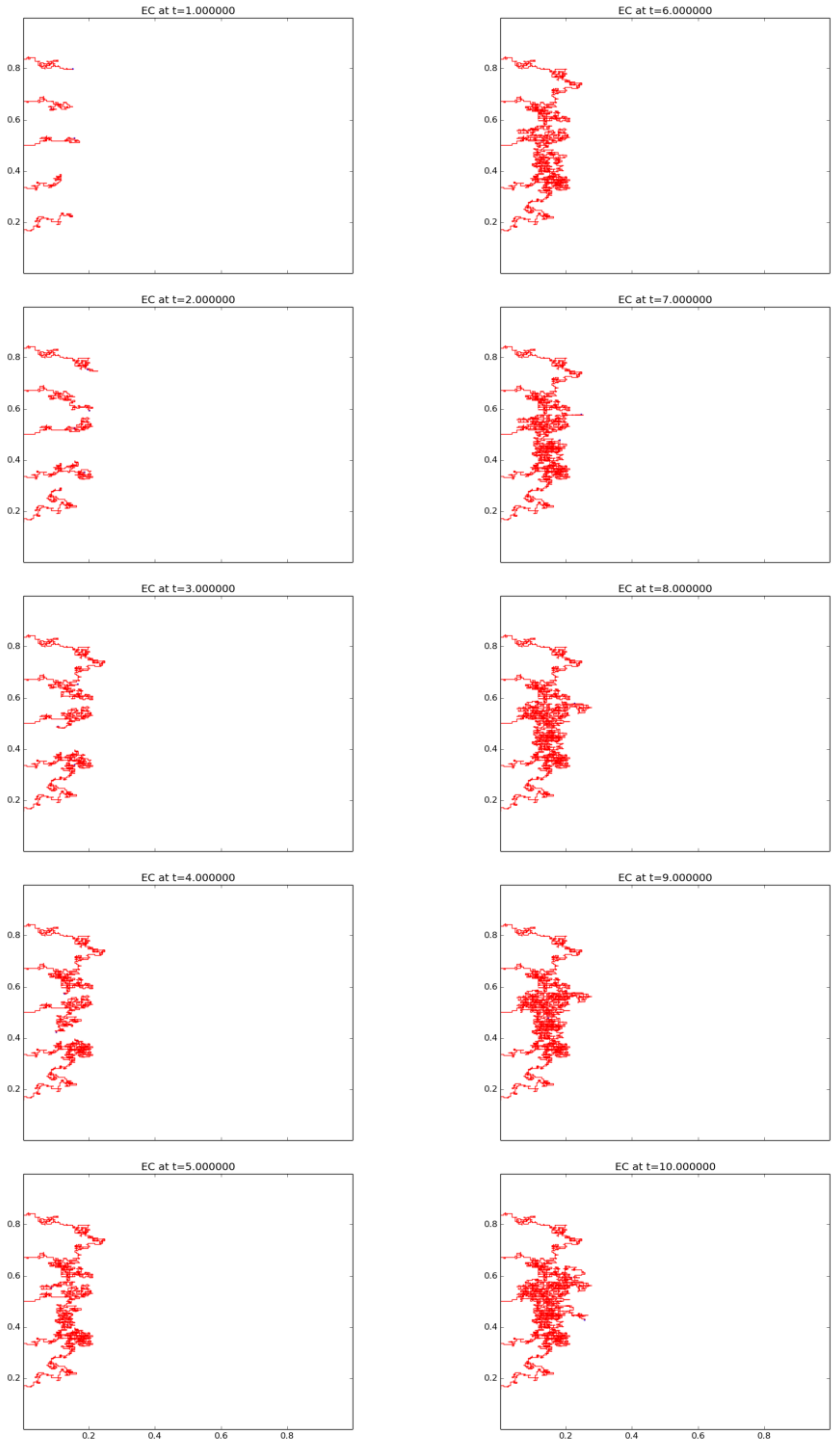

Continue to next page.

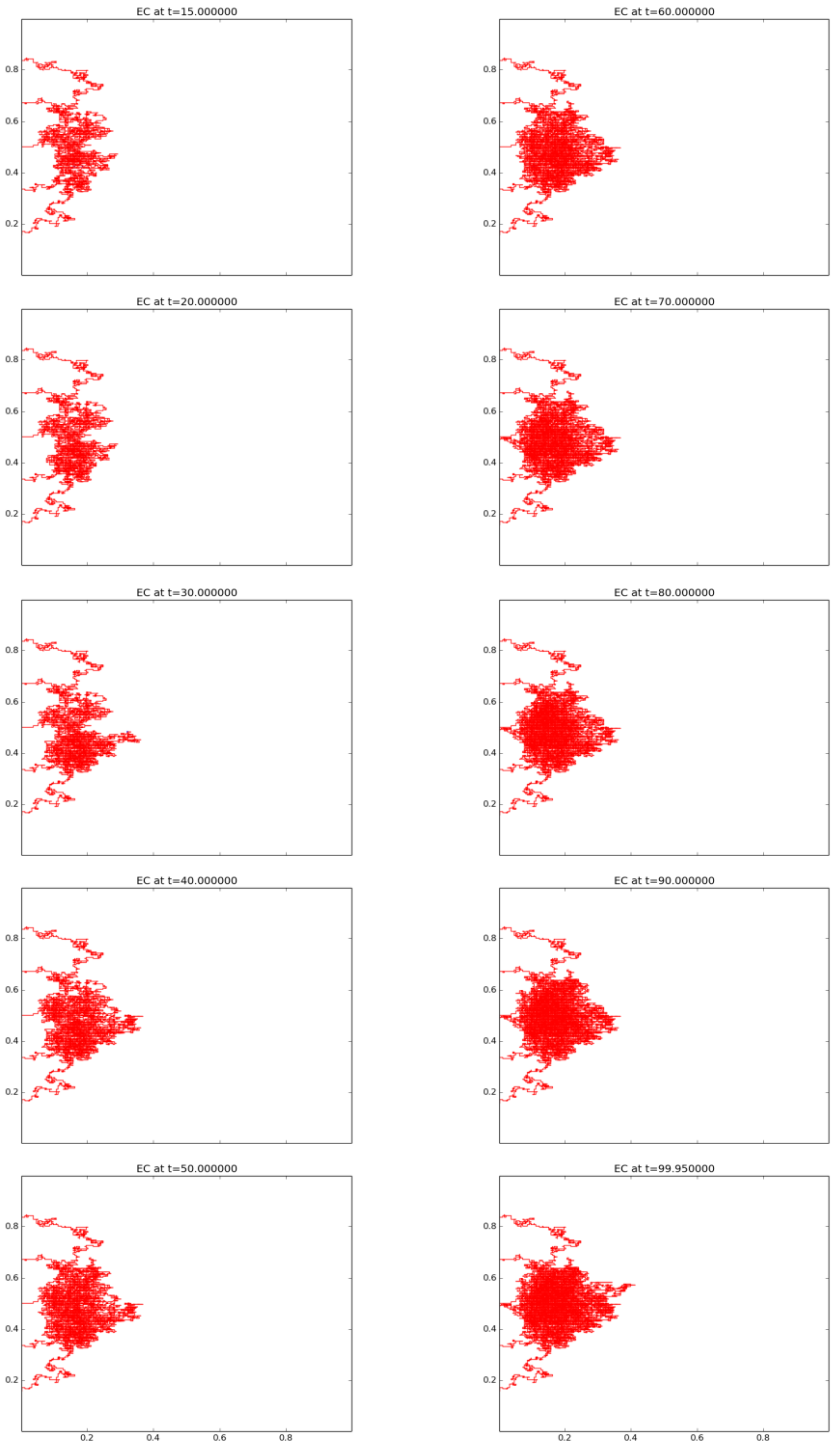

Figure 31. Growth of blood vessel network on C2 and F2 initial profile with both chemotaxis and haptotaxis.

Simulation Results with chemotaxis on C1 and C2 profile and haptotaxis on F2 profile in change of fibronectin production (β_1), uptake rate by tip cell (η_2), and VEGF uptake rate by tip cell (η_2).

Refer to Figure 30 and Figure 31 as for comparison.

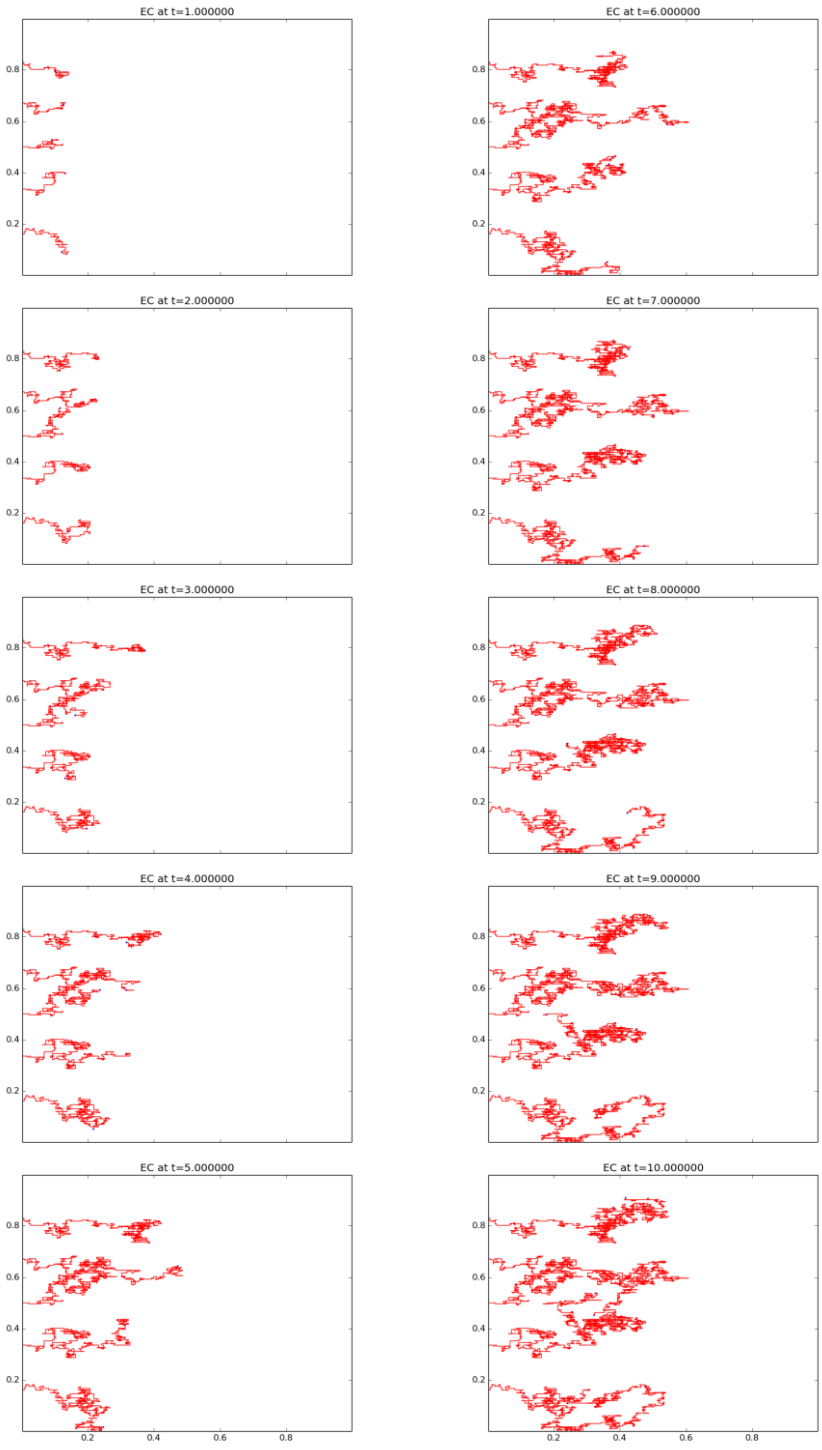

Continue to next page.

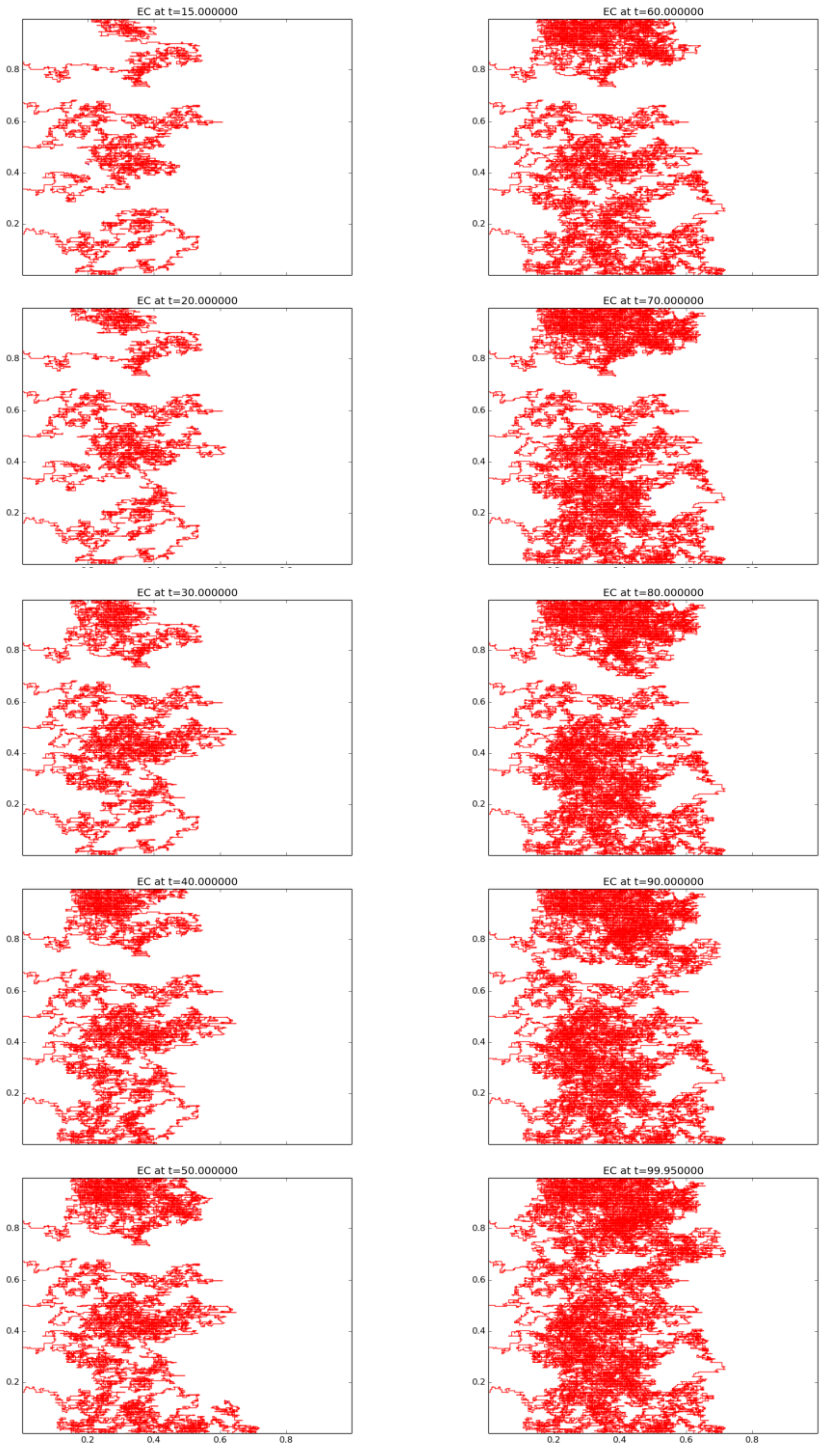

Figure 32. Growth of blood vessel network on C1 and F2 initial profile with both chemotaxis and haptotaxis and in the absence of fibronectin production rate by tip cell ($\beta_1 = 0$).

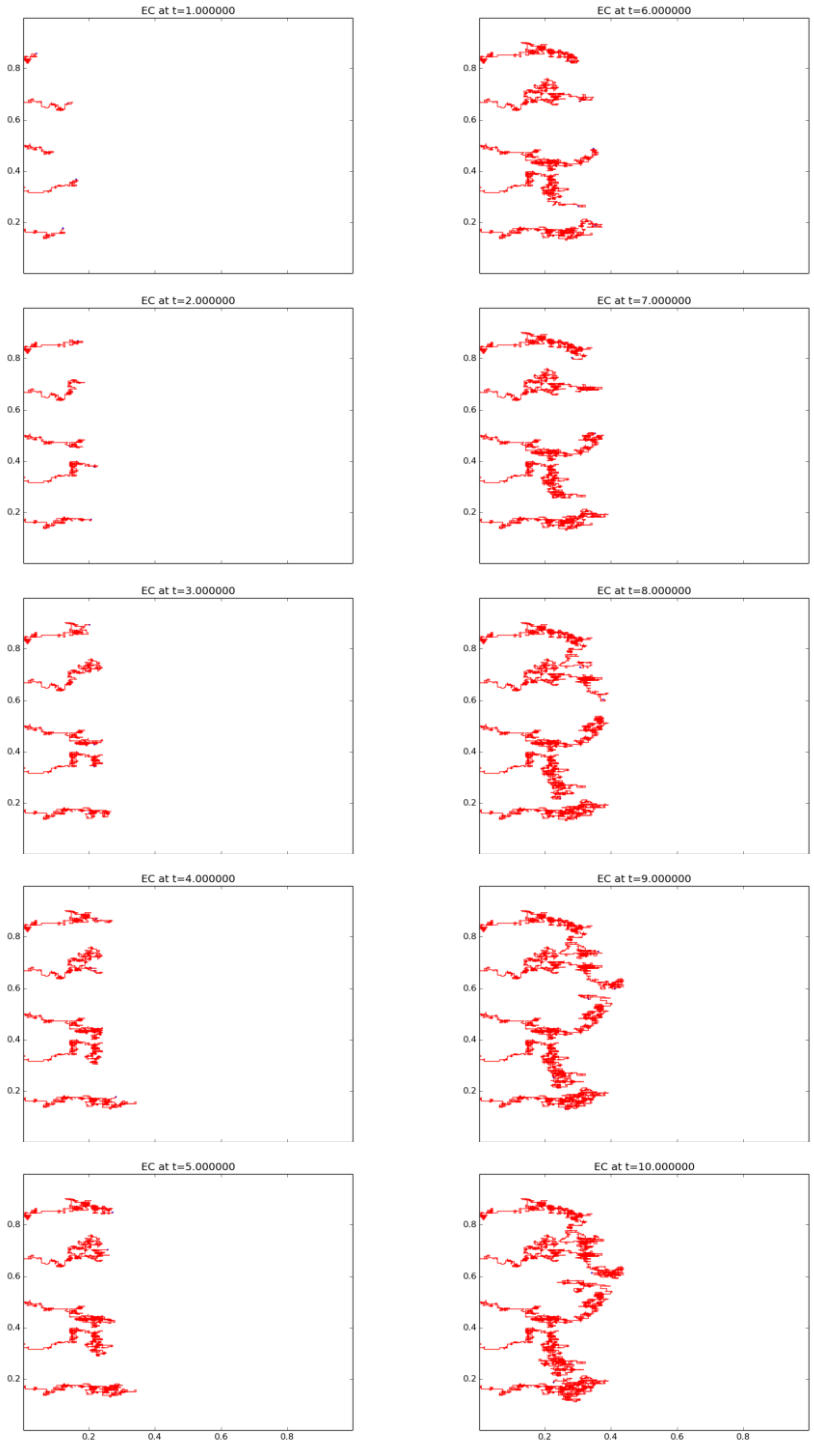

Figure 33. Growth of blood vessel network on C1 and F2 initial profile with both chemotaxis and haptotaxis and in the absence of fibronectin uptake rate by tip cell ($\eta_2 = 0$).

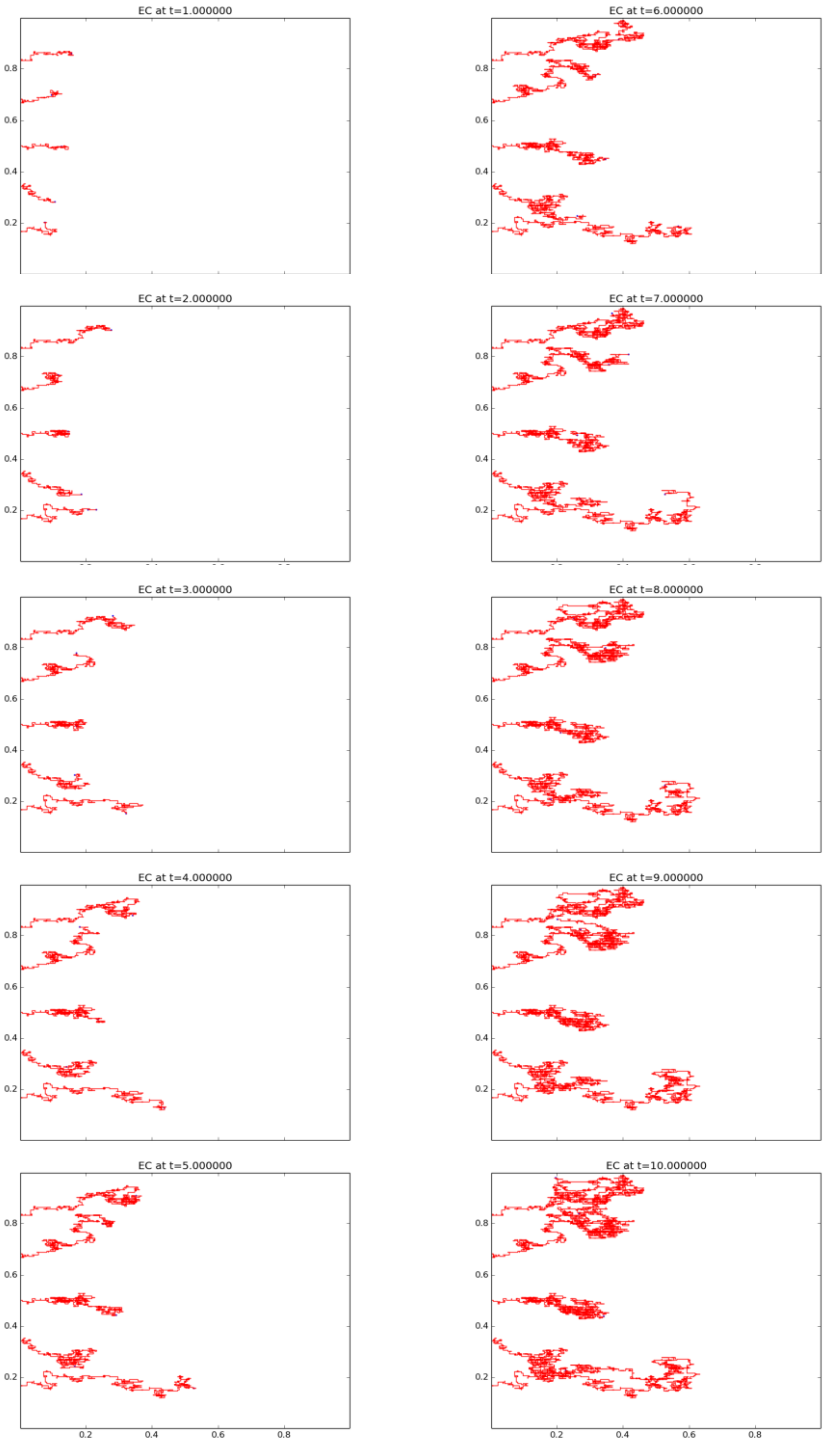

Continue to next page.

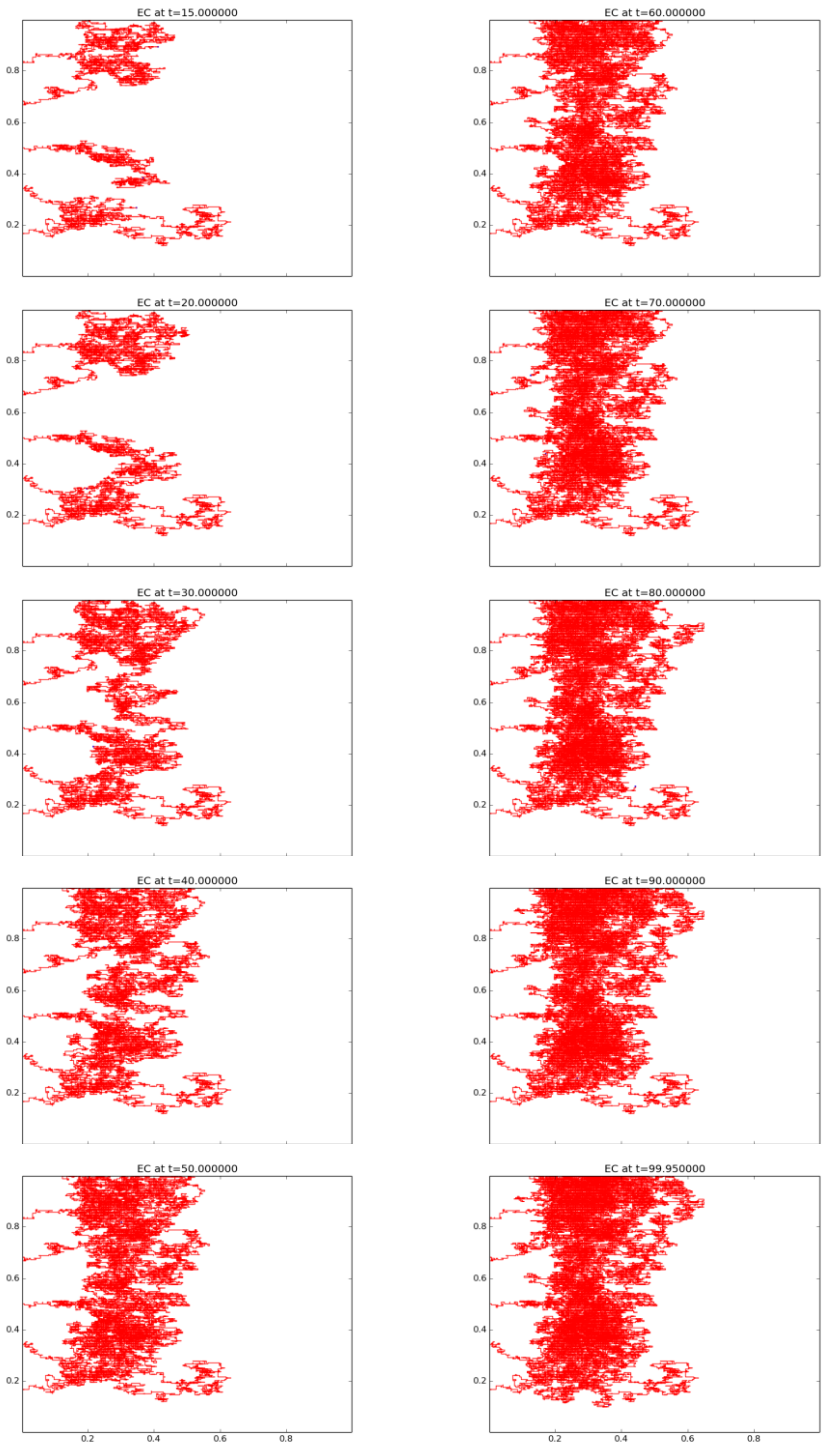

Figure 34. Growth of blood vessel network on C1 and F2 initial profile with both chemotaxis and haptotaxis and in the absence of fibronectin uptake rate by tip cell ($\eta_2 = 0$) and fibronectin production by tip cell ($\beta_1 = 0$).

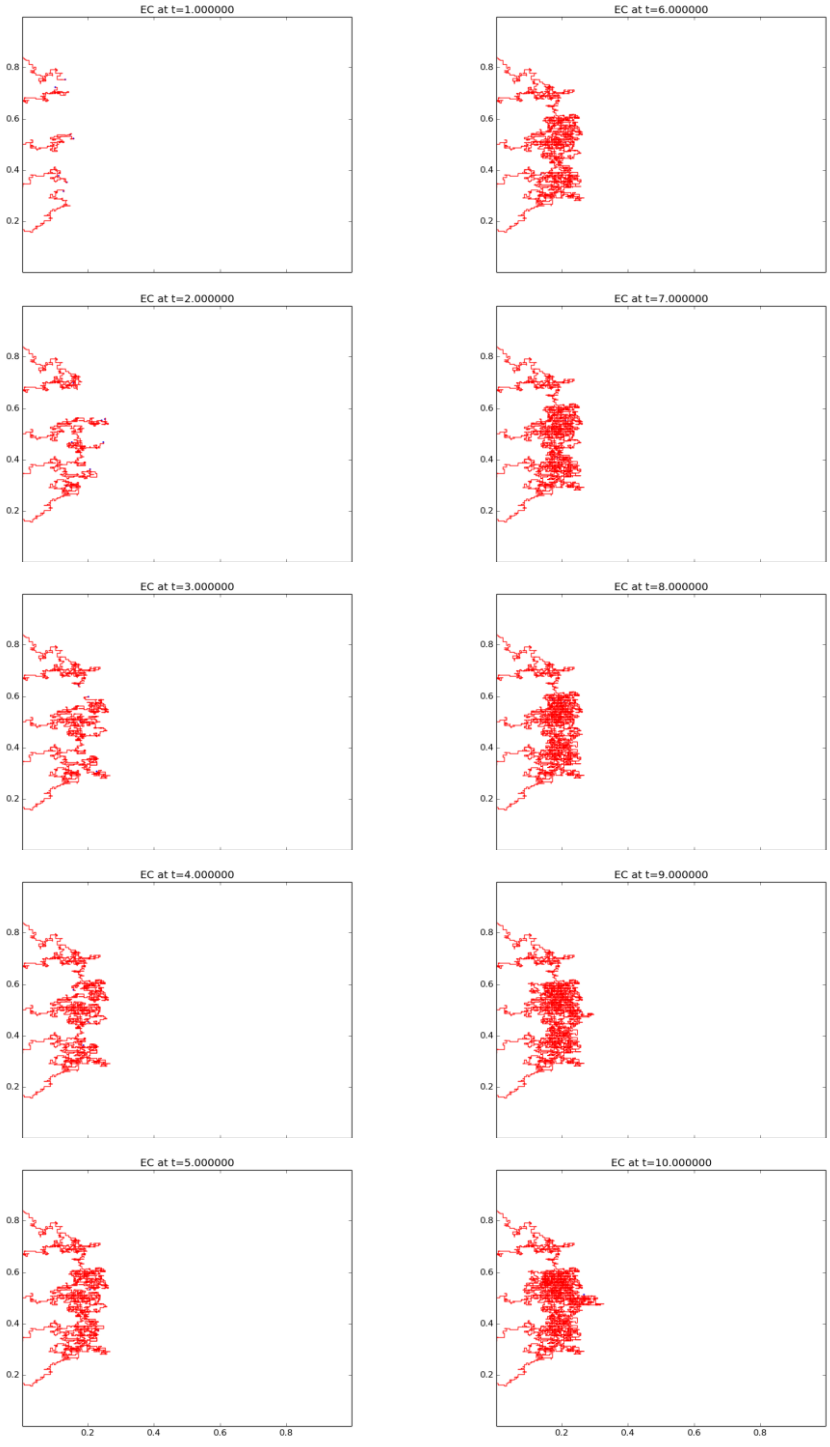

Continue to next page.

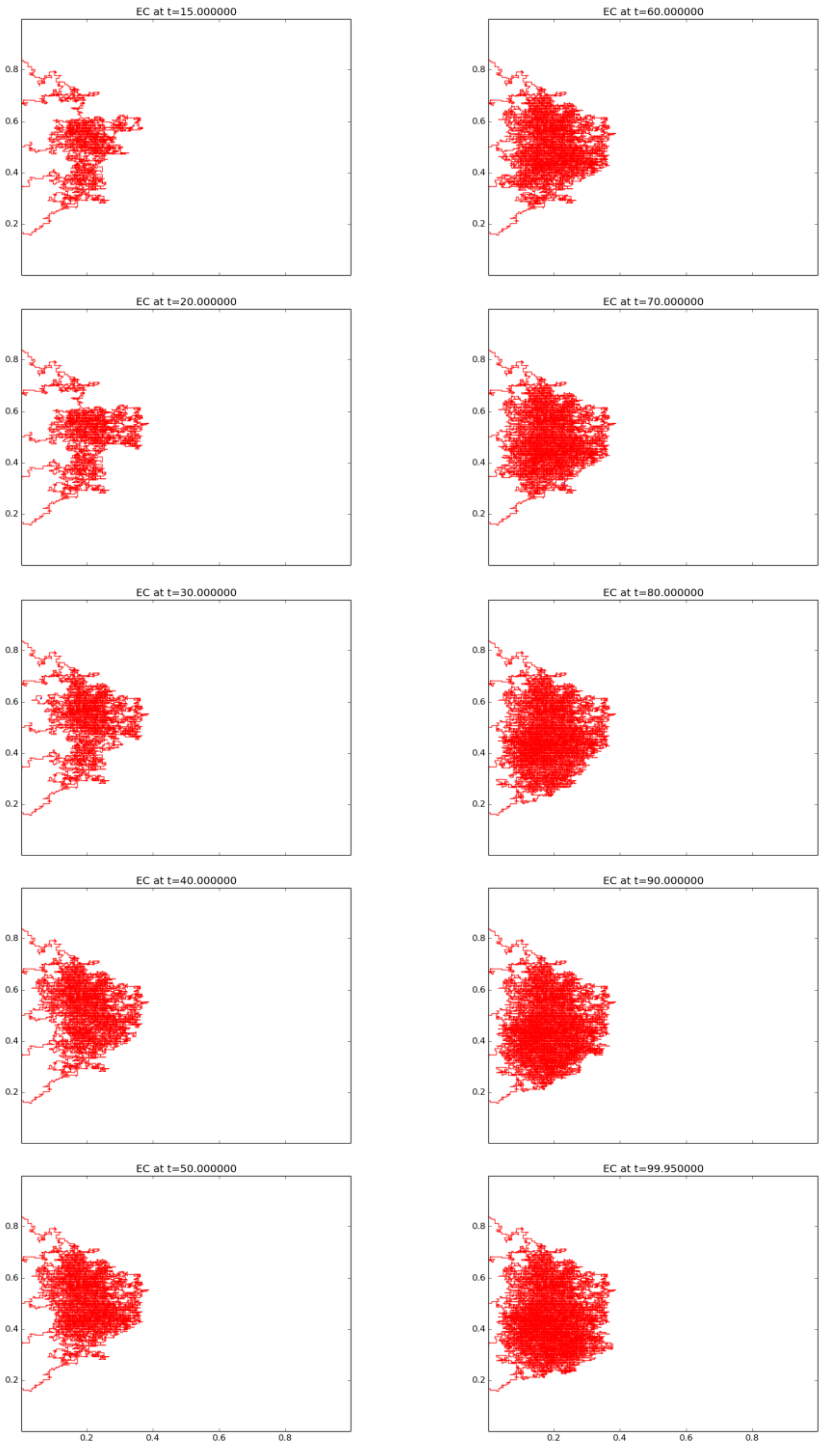

Figure 35. Growth of blood vessel network on C2 and F2 initial profile with both chemotaxis and haptotaxis and in the absence of fibronectin production rate by tip cell ($\beta_1 = 0$).

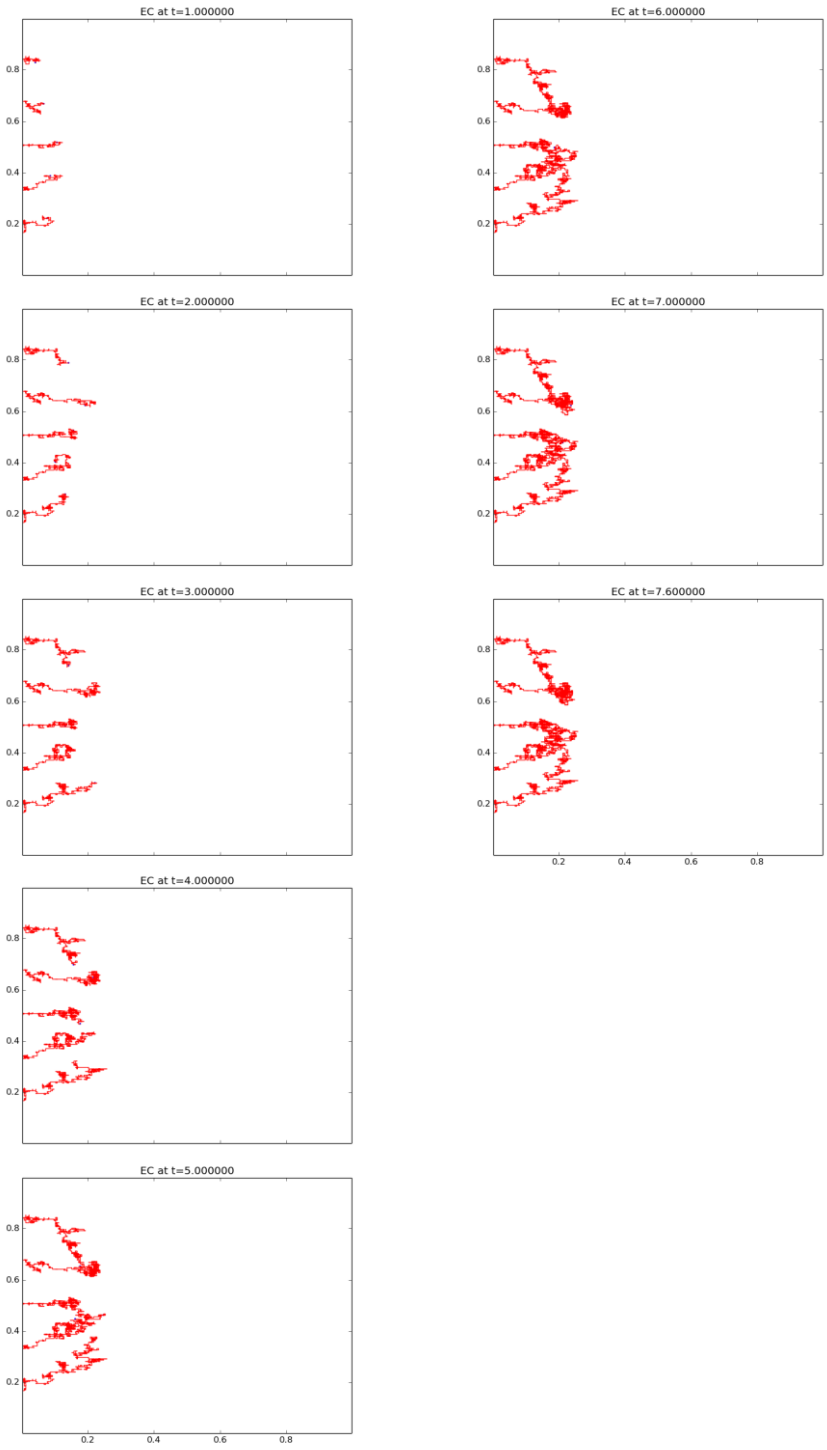

Figure 36. Growth of blood vessel network on C2 and F2 initial profile with both chemotaxis and haptotaxis and in the absence of fibronectin uptake rate by tip cell ($\eta_2 = 0$).

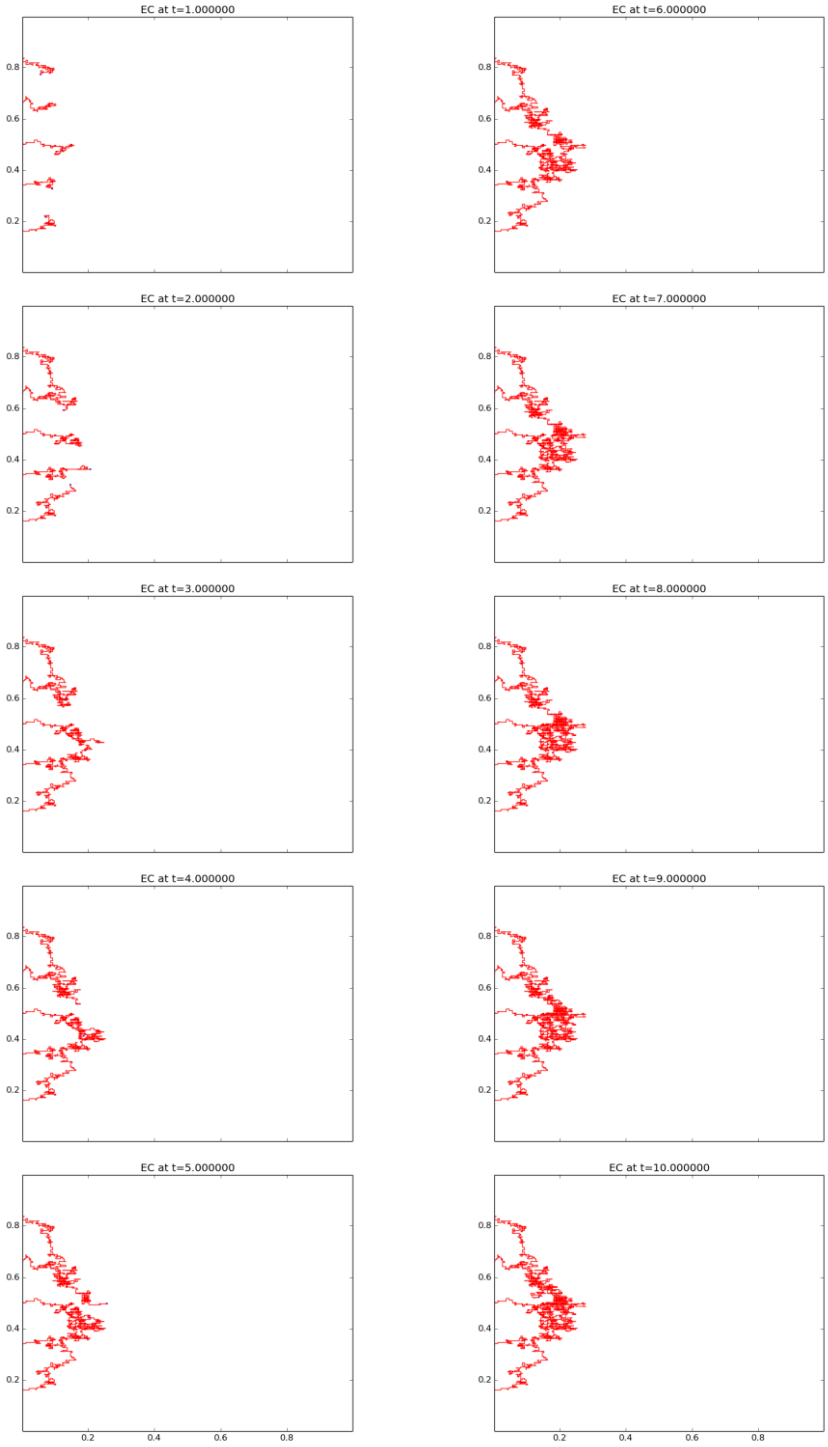

Continue to next page.

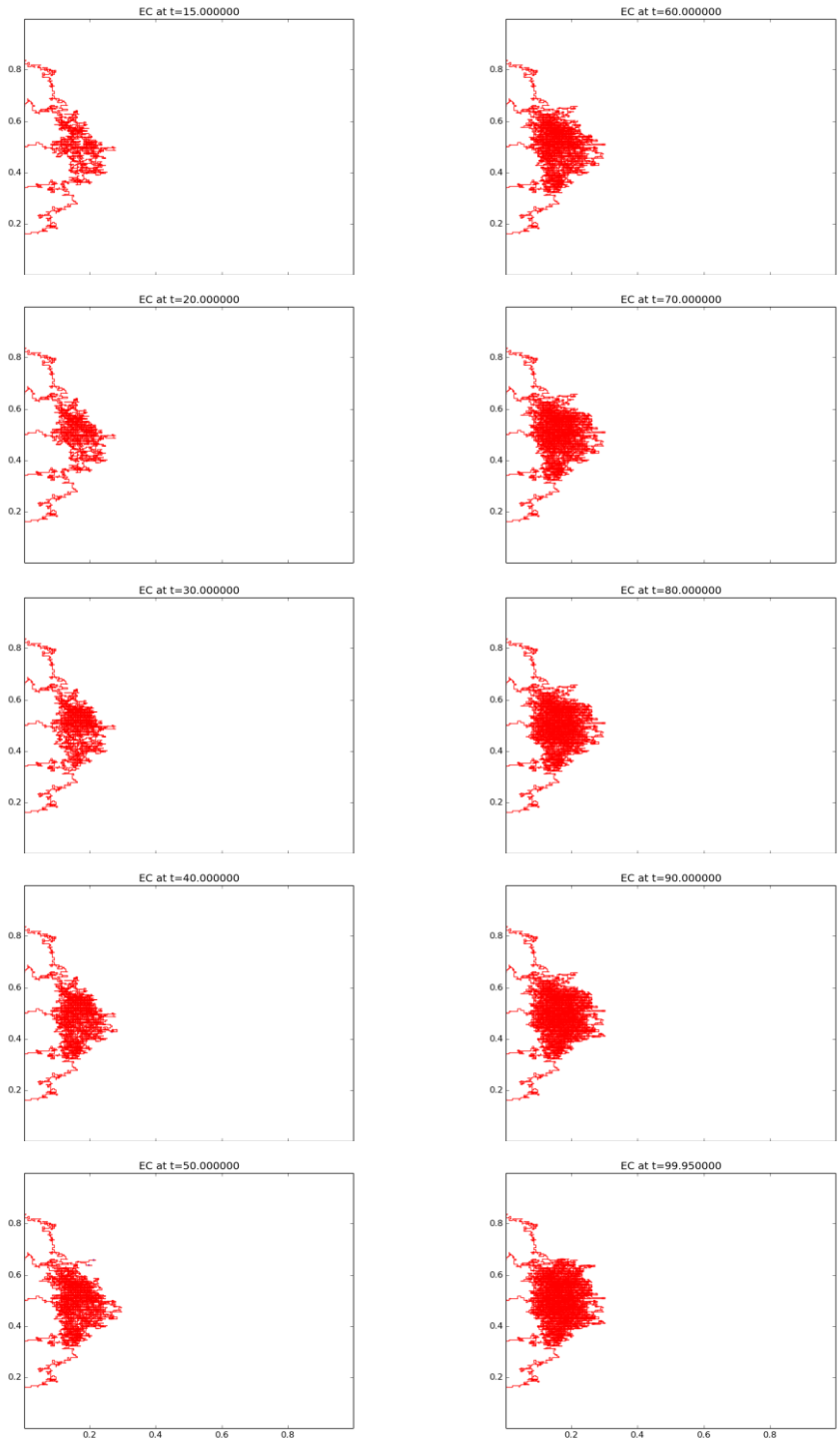

Figure 37. Growth of blood vessel network on C2 and F2 initial profile with both chemotaxis and haptotaxis and in the absence of fibronectin uptake rate by tip cell ($\eta_2 = 0$) and fibronectin production by tip cell ($\beta_1 = 0$).

Simulation Results with chemotaxis on C1 and C2 profile and haptotaxis on F2 profile in change of chemotaxis saturation factor (α_n)

Refer to Figure 30 and Figure 31 as for comparison.

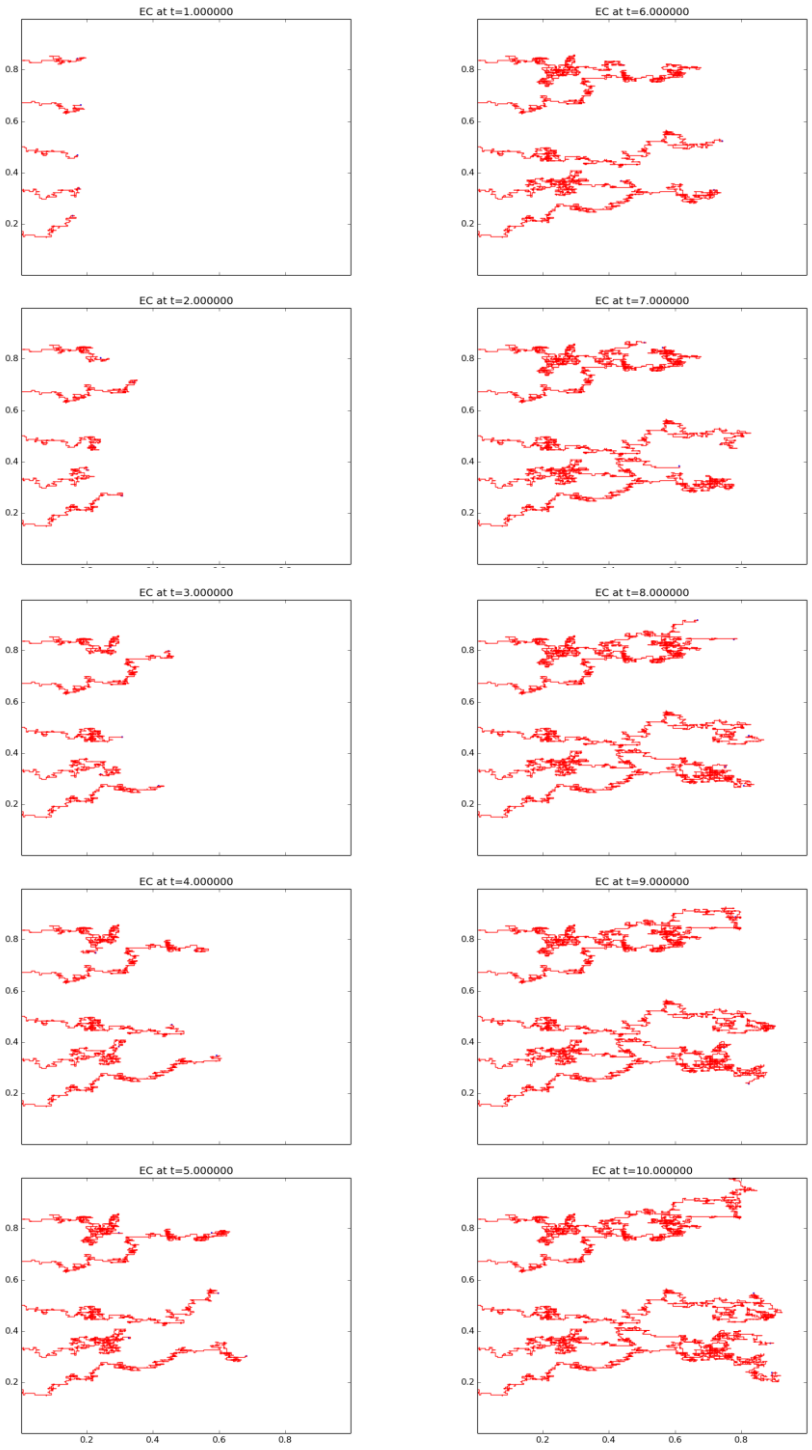

Continue to next page.

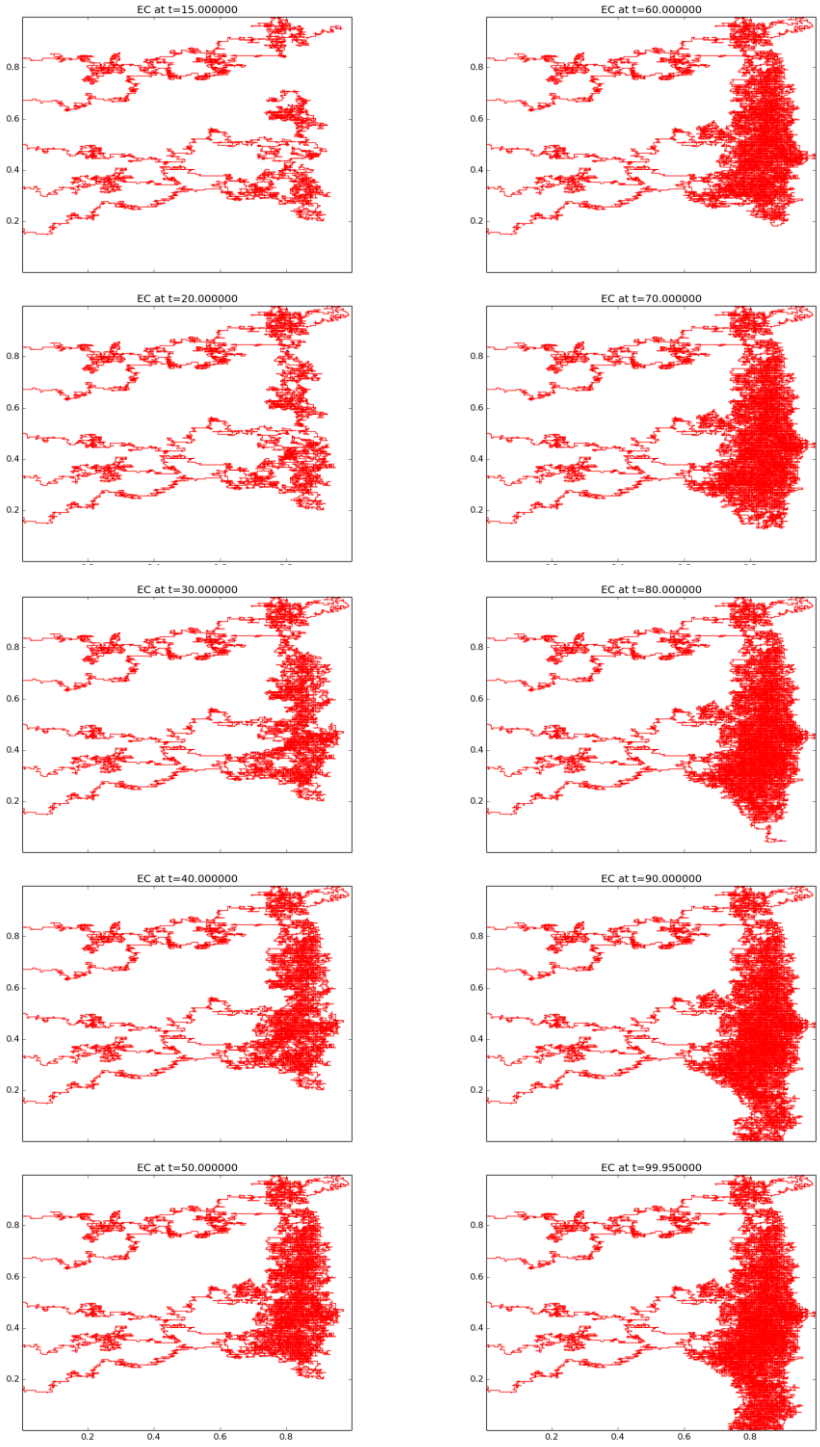

Figure 38. Growth of blood vessel network on C1 and F2 initial profile with both chemotaxis and haptotaxis and in the absence of chemotaxis saturation factor ($\alpha_n = 0$).

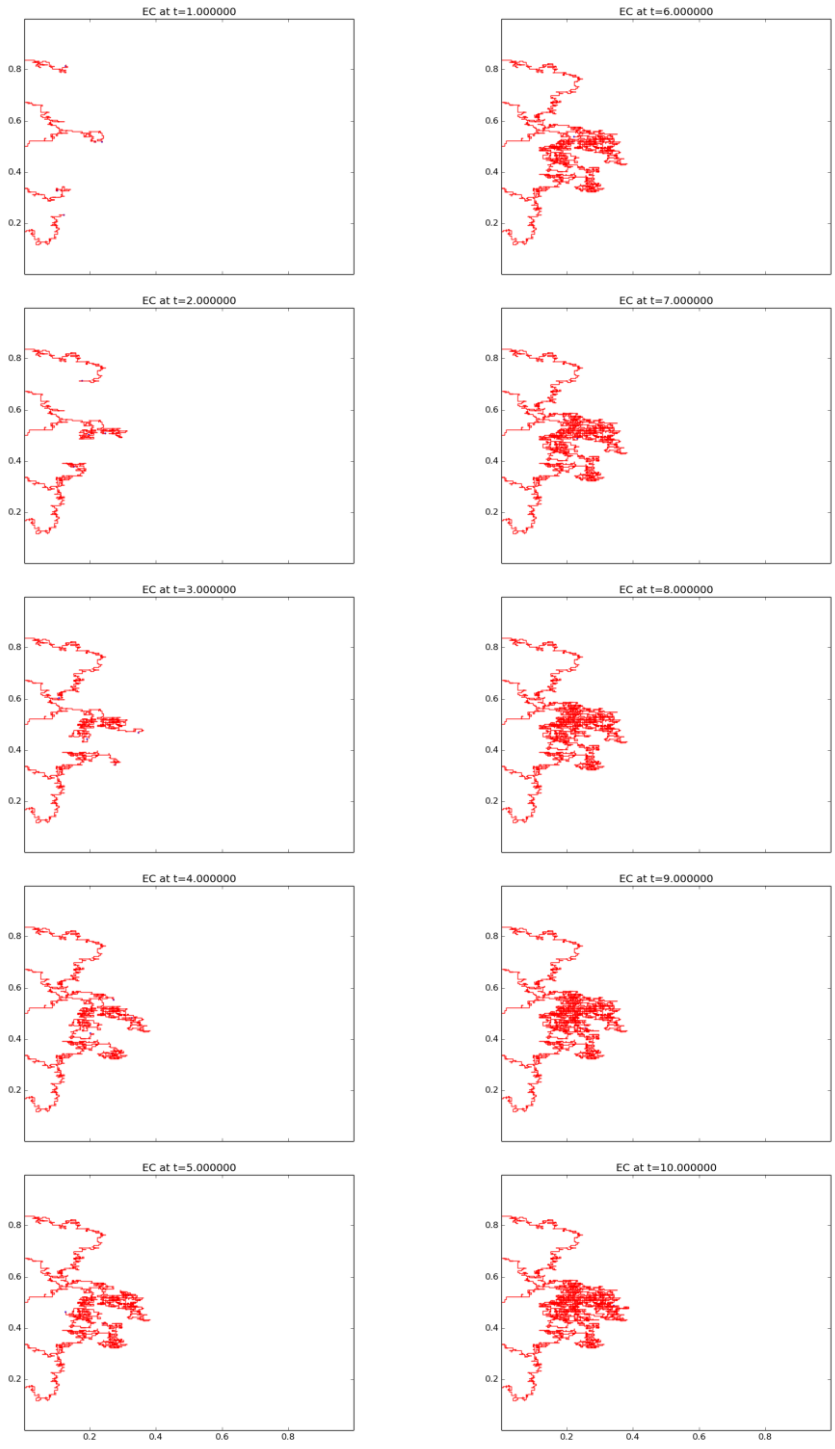

Continue to next page.

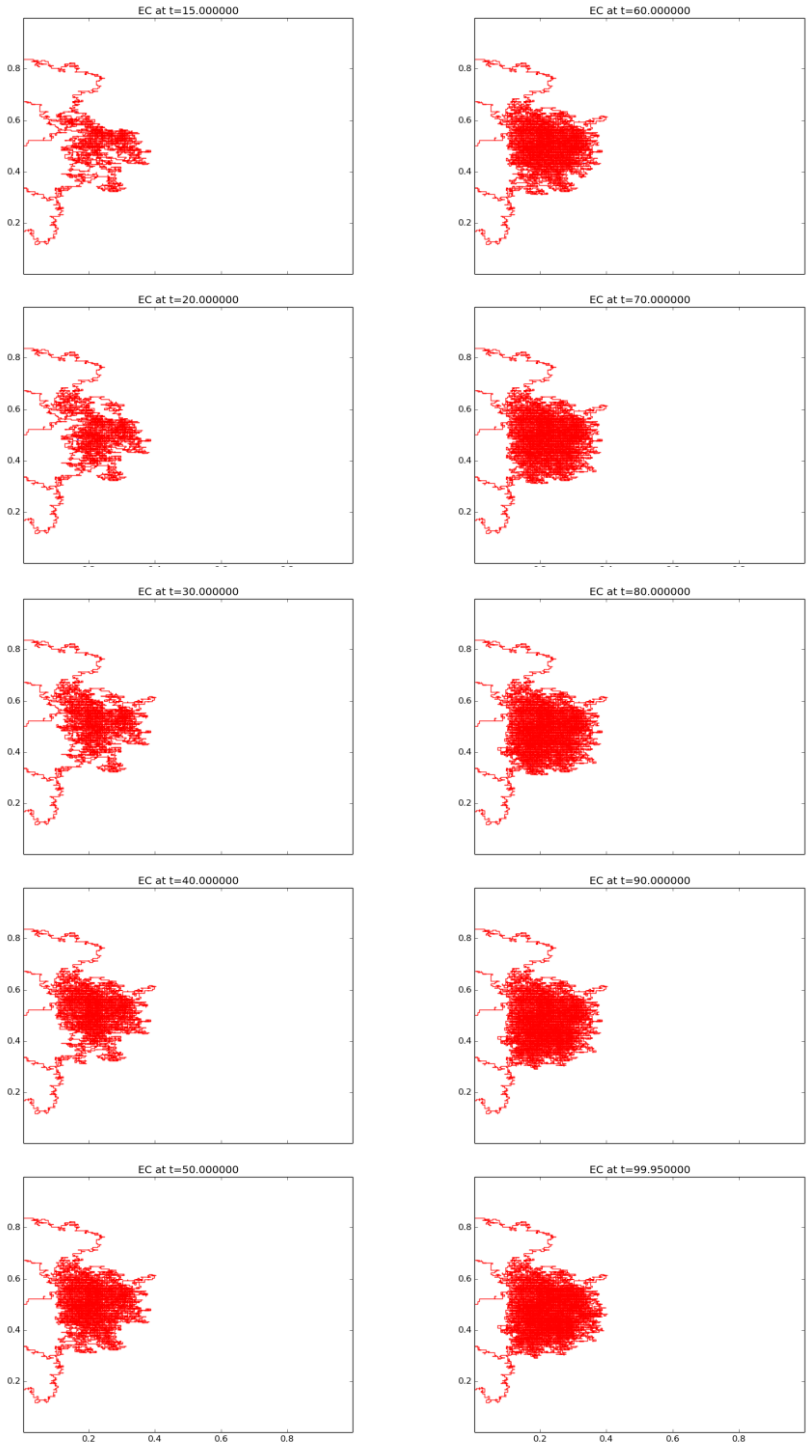

Figure 39. Growth of blood vessel network on C2 and F2 initial profile with both chemotaxis and haptotaxis and in the absence of chemotaxis saturation factor ($\alpha_n = 0$).

Concluding Remarks

The simulation results revealed some important roles of VEGF and fibronectin in the tip cell movements and pattern formation of vessel networks. The main findings are summarized below:

1. In the absence of haptotaxis, the tip cells migrate directly toward the tumor cell with little lateral movement.
2. In the presence of haptotaxis and an initial fibronectin gradient, the tip cells initially move toward the tumor cell. At some distances from the parent vessel, they begin moving backward toward the parent vessel.
3. The VEGF gradient promotes the direct movement of tip cells toward the tumor cell.
4. In the absence of an initial fibronectin gradient, the vessel network resembles that generated without haptotaxis.
5. The fibronectin gradient promotes the lateral movement of tip cells, and inhibits their movement toward the tumor.

References

Anderson, A. R. A. and M.A.J. Chaplain (1998). Continuous and Discrete Mathematical Models of Tumor-induced Angiogenesis. Bull. Math. Bio. 60, 857-900.

Atkins, P., et al. (2011). Physical Chemistry for the Life Sciences, 2nd edition. Oxford Univ. Press.

Carter, S. B. (1967). Haptotaxis and the mechanism of cell motility. Nature 213, 256-260.

Chang, Raymond. (1997). Chemistry. McGraw-Hill, Sixth Edition, P:560-584.

Clark, R. A. F, H. J. Winn, H. F. Dvorak and R. B. Colvin (1983). Fibronectin beneath reepitheliazing epidermis in vivo: sources and significance. J. Invest. Dermatol. 80, 26-30.

Folkman, J. and M. Klagsbrun (1987). Angiogenic factors. Science 235, 442-447.

Gillespie, D. T. (1976). A General Method for Numerically Simulating the Stochastic Time Evolution of Coupled Chemical Reactions. J. Com. Physics. 22, 403-434.

Hoshino, D., Koshikawa, N., Suzuki, T., et al. (2012). Establishment and validation of computational model for MT1-MMP dependent ECM degradation and intervention strategies. PLos Comp. Biol.. 8: e1002479.

Hynes, R.O. (1990). Fibronectin, Springer-Verlag: New York.

Itano, K. and Suzuki, T. (2016). ある N 分子パスウェイネットワークの数理モデリングと数学的解析. 日本応用数理学会論文誌. Vol. 26(1), 44-83.

Johansson, S., S. Gustafson and H. Pertoft (1987). Identification of fibronectin receptor specific for rat liver endothelial cells. Exp. Cell Res. 172, 425-431.

Kawasaki, S., Minerva, D. and Suzuki, T. Extracting Solvable Units of variables in Nonlinear ODEs of ECM Degradation Pathway Network. Submitted to JDDE, Feb 15.

Lapidus, I. R. and R. Schiller (1976). Model for the chemotactic response of a bacterial population. Biophys. J. 16, 779-789.

M. Aubert, et al. (2011). A continuum Mathematical Model of the Deveoping Murine Retinal Vasculaure. Springer, Bull Math Biol (73), 2430-2451.

Minerva, D. (2013). Simulation and Pathway Analysis of MMP2 Activation By MT1-MMP In The Early Stage Of Cancer Cell Invasion. Master Thesis.

Muthukkaruppan, V. R., L. Kubai and R. Auerbach (1982). Tumor-induced neovascularization in the mouse eye. J. Natl. Cancer Inst. 69, 699-705.

Paweletz, N. and M. Knierim (1989). Tumor-related angiogenesis. Crit. Rev. Oncol. Hematol. 9, 197-242.

Sato, H., Takino, T., Okada, Y., et al. (1994). A matrix metalloproteinase expressed on the surface of invasive tumour cells. Nature. 370, 61-65.

Sholley, M. M., G. P. Ferguson, H. R. Seibel, J. L. Montour and J.D. Wilson (1984). Mechanism of neovascularization. Vascular sprouting can occur without proliferation of endothelial cells. Lab. Invest. 51, 624-634.

Stokes, C.L., M. A. Rupnick, S. K. Williams and D. A. Lauffenburger (1990). Chemotaxis of human microvessel endothelial cells in response to acidic fibroblast growth factor. Lab. Invest. 63, 657-668.

List of Publications & Conferences

Publications

D. Minerva, S. Kawasaki, and T. Suzuki. Pathway network analysis and an application to the ODE model of MMP2 activation in the early stage of cancer cell invasion. International Symposium on BioMathematics (SYMOMATH), Malang, Indonesia, 2014. SYMPOSIUM ON BIOMATHEMATICS (SYMOMATH 2014). AIP Publishing LLC (Vol.1651), P:99-104 (2015).

S. Kawasaki, D. Minerva, and T. Suzuki. Extracting Solvable Units of variables in Nonlinear ODEs of ECM Degradation Pathway Network. Submitted to JDDE, February 2015.

Conferences

Poster Presentation

D. Minerva and T. Suzuki. Hybrid Simulation of Mural Cell Attachment in Angiogenesis. 平成 27 年未来研究イニシアティブ・グループ支援事業. Osaka University, Osaka, Japan, March 2016.

D. Minerva, S. Kawasaki, and T. Suzuki. Pathway Network Analysis of MMP2 Activation Model in the Early Stage of Cancer Cell Invasion. HeKKSaGOn Summer School, Institute of Mathematics, University of Gottingen, Germany, September 2014.

Oral Presentation

D. Minerva and T. Suzuki. Hybrid Simulation of Tumor-Induced Angiogenesis Model. The First JSPS Core to Core Seminar: Establishing International Research Network of Mathematical Oncology, Bosco Villa, Nara, Japan, March 2016.

D. Minerva, S. Kawasaki, and T. Suzuki. Pathway Network Analysis of MT1-MMP Model. Invited Speaker on Mathematics Colloquium, Mathematics Department, Gajah Mada University, Indonesia, August 2015.

D. Minerva, C. Lopez, and T. Suzuki. MMP2 Activation Model in the Early Stage of Cancer Cell Invasion". Invited Speaker on monthly meeting Cancer Biology Department, Vanderbilt University, United of States: as a part of final report for internship program, February 2015.

D. Minerva, S. Kawasaki, and T. Suzuki. Pathway Network Analysis of MT1-MMP Model. The 7-th SEAMS-UGM 2015 International: Conference on Mathematics and Its Applications, Gajah Mada University, Indonesia, August 2015.

D. Minerva, S. Kawasaki, and T. Suzuki. Pathway Network Analysis of MMP2 Activation Model in the Early Stage of Cancer Cell Invasion. Practice of Mathematical Medicine - Autumn School by Japanese and French Mathematicians, Osaka University, Osaka, Japan, October 2014.

D. Minerva, S. Kawasaki, and T. Suzuki. Pathway Network Analysis and an Application to the ODE Model of MMP2 Activation in the Early Stage of Cancer Cell Invasion. International Symposium on BioMathematics (SYMOMATH), Malang, Indonesia, September 2014.

D. Minerva, S. Kawasaki, and T. Suzuki. Pathway Network Analysis of MMP2 Activation Model in the Early Stage of Cancer Cell Invasion. Mathematical Medicine Workshop, Osaka, Japan, July 2014.

D. Minerva, S. Kawasaki, and T. Suzuki. Pathway Network Analysis of MMP2 Activation Model in the Early Stage of Cancer Cell Invasion. JSMB Satelite Meeting, Osaka, Japan, July 2014.

D. Minerva, S. Kawasaki, and T. Suzuki. Pathway Analysis of Activating MMP2 by MT1-MMP. 「応用トポロジーとシステムバイオロジー：数理医学の新たな挑戦」統計数理研究所数学協働プログラム (Application on Topology and System of Biologi Workshop), Osaka University, Osaka, Japan, February 2012.